Received: 1 January 2019 | Accepted: 13 February 2019

DOI: 10.1002/jccs.201900001

INVITED PAPER

JOURNAL OF THE CHINESE CHEMICAL SOCIETY

A review of transition metal-based bifunctional oxygen electrocatalysts

Kassa B. Ibrahim[1] | Meng-Che Tsai[2] | Soressa A. Chala[2] | Mulatu K. Berihun[2] | Amaha W. Kahsay[2] | Taame A. Berhe[1] | Wei-Nien Su[1] | Bing-Joe Hwang[2,3]

[1]Nano-Electrochemistry Laboratory, Graduate Institute of Applied Science and Technology, National Taiwan University of Science and Technology, Taipei, Taiwan

[2]Nano-Electrochemistry Laboratory, Department of Chemical Engineering, National Taiwan University of Science and Technology, Taipei, Taiwan

[3]National Synchrotron Radiation Research Center, Hsin-Chu, Taiwan

Correspondence
Bing-Joe Hwang and Wei-Nien Su, National Taiwan University of Science and Technology, 43 Keelung Road, Section 4, Taipei 106, Taiwan.
Email: bjh@mail.ntust.edu.tw; wsu@mail.ntust.edu.tw

Funding information
Ministry of Science and Technology, Taiwan, Grant/Award Number: 106-2923- E 011-005, 105-3113-E-011-001, 105-ET-E-; Academia Sinica, Taiwan, Grant/Award Number: AS-KPQ-106-DDPP; Ministry of Education, Grant/Award Number: 100H451401; Ministry of Economic Affairs, Grant/Award Number: 101-EC-17-A-08-S1-183; Ministry of Science and Technology, Grant/Award Numbers: 103-2923-E-011-004-MY3, 104-2911-I-011-505-MY2, 105-3113-E-011-001

Abstract

Electrochemical energy storage and conversion devices play a key role in the development of clean, sustainable, and efficient energy systems to meet the sustainable growth of our society. However, challenging issues including the sluggish kinetics of oxygen electrode reactions involving the oxygen reduction reaction (ORR) and the oxygen evolution reaction (OER) are present, limiting the implementation of devices such as metal-air batteries, water electrolyzers, and regenerative fuel cells. In this review, various monometallic and bimetallic transition metal oxides (TMOs) and hydroxides are summarized in terms of their application for ORR/OER, in which the merits and demerits of various precious metal and carbon-based metal oxide materials are discussed, with requirements for better electrocatalysts and catalyst support being introduced as well. Following this, different approaches to improve catalytic activity such as the introduction of doping and defects, the manipulation of crystal facets, and the engineering of supports, compositions, and morphologies are summarized in which TMOs with improved ORR/OER catalytic activities can be synthesized, further improving the speed, stability, and polarization of electrochemical energy storage and conversion devices. Finally, perspectives into the improvement of performance and the better understanding of ORR/OER mechanisms for bifunctional electrocatalysts using in situ spectroscopic techniques and density functional theory calculations are also discussed.

KEYWORDS

bifunctional, electrocatalysts, engineering, oxygen evolution reaction, oxygen reduction reaction, transition metals

1 | INTRODUCTION TO OXYGEN ELECTROCATALYTIC REACTIONS

Currently, society is experiencing rapid development of earth-abundant energy alternatives for use in electrochemical storage devices and efficient energy conversion systems to substitute fossil fuels as a result of the associated negative consequences such as global warming and depletion of petroleum resources, as well as increasing demands for energy.[1] This is because electrochemical power resources are one of the best solutions to mitigate fossil fuel-related problems, in which renewable energy can be produced from wind, thermal, or solar sources and can be stored in metal-air batteries (MABs), fuel cells (FCs), and electrolytic cells.

Here, regenerative fuel cells (RFCs) and water-splitting systems[2–6] possess great potential for clean energy applications; such as the "hydrogen economy," to be utilized in large-scale power applications and electric vehicles. Furthermore, rechargeable MABs such as Fe-air, Zn-air, and Li-air batteries, despite possessing kinetically sluggish reactions including oxygen evolution reaction (OER) during charging at the anode and oxygen reduction reaction (ORR) during discharging at the cathode,[7–10] are being intensively studied due to tremendously high energy densities.

ORR and OER are important processes in renewable energy devices[11] and insufficient activities can lead to insufficient energy efficiencies and delayed commercialization.[12] Therefore, the rational development of bifunctional (OER and ORR) catalysts with superior activity, high earth-abundancy, and good stability to address these issues is crucial for the commercialization of renewable energy conversion and storage devices.[13,14] In the past, precious metal catalysts such as Pt/C, Ir/C, and Ru/C have been designed as efficient ORR and OER electrocatalysts; however, these electrocatalysts possess several issues, such as limited natural abundance, high rates of metal sintering, high rates of catalyst detachment from supports,[15–17] and poor bifunctional activity. All these limit practical applications.[18–20] To address this, researchers have reported the use of carbon as a support material for precious metal catalysts due to its ability to provide high mechanical strengths,[21–24] large surface areas, and excellent electrical conductivities[25] toward the oxygen electrochemical process.[26] Nevertheless, even with these carbon supports, stability remains a detrimental issue.[27]

As for nonprecious transition metal oxides (TMOs), they possess several prominent advantages as potential catalysts, including their manifold compositions, multiple valence states, environmental friendliness, high durability, varying structures, and high abundance. Similarly, layered double hydroxides (LDHs) and sulfides[3,28–34] are also considered to be potential replacements for precious metal materials in alkaline electrolytes.[35] However, despite these advantages, nonprecious TM catalysts also possess several disadvantages, including poor electrical conductivity and limited surface area. Therefore, the engineering of morphology, the introduction of doping and defects, as well as the modification of crystal facets and the coupling with conductive materials[36–39] are all potential solutions to overcome these limitations.[40]

1.1 | Oxygen electrocatalytic reactions

The primary electrochemical reactions catalyzed by bifunctionally active catalysts are the OER and the ORR and the role of bifunctional catalysts is crucial for the practical operation of MABs to overcome the intrinsically slow kinetics of OER and ORR. In addition, OER and ORR proceed through different reaction pathways depending on the electrolyte (summarized in Table 1) in which Liu and coworkers[41] reported that the ORR mechanism involves the diffusion and subsequent adsorption of oxygen molecules onto catalyst surfaces, in which electrons are drawn from the anode and transferred to the adsorbed oxygen to weaken and break the oxygen double bond, subsequently removing OH ions from the catalyst surface into the alkaline electrolyte. Unlike the ORR mechanism, the OER mechanism is more difficult to describe because of the involvement of a series of complex electrochemical reactions with multistep electron-transfer processes. Therefore, to allow for a better understanding of the content discussed in this review, detailed mechanisms of the ORR and OER processes are presented to an appropriate extent below.

1.2 | Oxygen evolution reaction

Efforts to design active and stable electrocatalysts to improve OER kinetics under alkaline electrolytes have been broadly studied for the past several decades, such as state-of-the-art RuO_2 and IrO_2 catalysts for OER under alkaline and acidic electrolytes[42,43] in which IrO_2 is more stable than RuO_2, and can sustain higher anodic potentials in both acidic and alkaline electrolytes.[44] However, these electrocatalysts are expensive and display high degrees of dissolution as well as the formation of unstable RuO_4 and IrO_3 intermediates at high anodic potentials, limiting their application.[45] OER is a complex process that involves the interaction between solid catalysts, electrolytes, gas and liquid phase reactants, and products[46] in which chemical reactions mainly occur at the catalyst/electrolyte interface. Unfortunately, there is a lack of an in-depth understanding of the reaction interface of OER[47] arising mainly from two experimental limitations. First, the interface for catalytic reactions is generally buried between the solid and liquid phases, and is difficult to be accessed and detected using conventional spectroscopic techniques.[48] Second, active species are usually mixed with binders and conductive carbon additives, which hinder the accurate investigation of electrochemical interfaces using traditional measurement techniques.[48,49]

Because the OER is a surface reaction, its mechanisms vary depending on the geometry of the metal cation sites on the catalyst surface.[50] Furthermore, the multivalence state characteristics of TM ions are also important for OER because reactions can be induced by the interaction between the oxygen intermediate and the metal ions, resulting in the formation of bonds through valence state changes. Here, the geometric sites of the metal ions change the adsorption energy of O_2 species and determine the kinetics of OER, and

TABLE 1 OER and ORR pathways under acidic and alkaline media

Electrolyte	OER reactions	ORR reactions
Acidic electrolyte	$2H_2O \rightarrow O_2 + 4H^+ + 4e^-$	$O_2 + 4H^+ + 4e^- \rightarrow H_2O$ $O_2 + 2H^+ + 2e^- \rightarrow H_2O_2$ $H_2O_2 + 2H^+ + 2e^- \rightarrow 2H_2O$
Alkaline electrolyte	$4OH^- \rightarrow O_2 + 2H_2O + 4e^-$	$O_2 + H_2O + 4e^- \rightarrow 4OH^-$ $O_2 + H_2O + 2e^- \rightarrow HO_2^- + OH^-$ $HO_2^- + 2H_2O + 2e^- \rightarrow 3OH^-$

good OER catalysts possess lower O—O bond formation energies from oxy-hydroxide groups.[50] As for the OER mechanism of TMO catalysts under alkaline electrolytes, M-OH species are first adsorbed and transform into M-O species through oxidation at the metal sites to which they are coordinated. Following this, the mechanism can proceed through either the coupling of two neighboring M-O species to form O═O bonds or the nucleophilic attack of water by the M-O species to form M-OOH species. These formed M-OOH species can subsequently be oxidized to form M-OO species that are replaced by water in the subsequent process, allowing for the release of O_2 (Figure 1).[53,54] Here, researchers have proposed that the rate-determining step (RDS) for OER is either the peroxide formation step or the step involving O_2 evolution from the peroxide.[4,55] However, the actual RDS in the OER mechanism remains elusive. Therefore, further investigations using in situ spectroscopic techniques or density functional theory (DFT) calculations are required.

As for Pt catalysts for OER under alkaline conditions (pH = 13.9), Crumlin and coworkers[51] proposed a more complete mechanism by combining the literature data with detailed steady-state dynamic information and reported that the formation of the Pt^{δ}–OH_{ads} phase can be promoted through the nucleophilic attack of hydroxide ions on metal Pt surfaces followed by the rapid electron transfer to a metastable configuration in which OH^- is chemisorbed on "activated" platinum sites (Pt^{δ}) (if Pt oxidation reactions under alkaline conditions and high overpotentials were ignored, the OER mechanism can be represented by Figure 1b).[56,57] Because this high oxidation state of platinum is energetically unfavorable and, therefore, unstable, it is reduced by

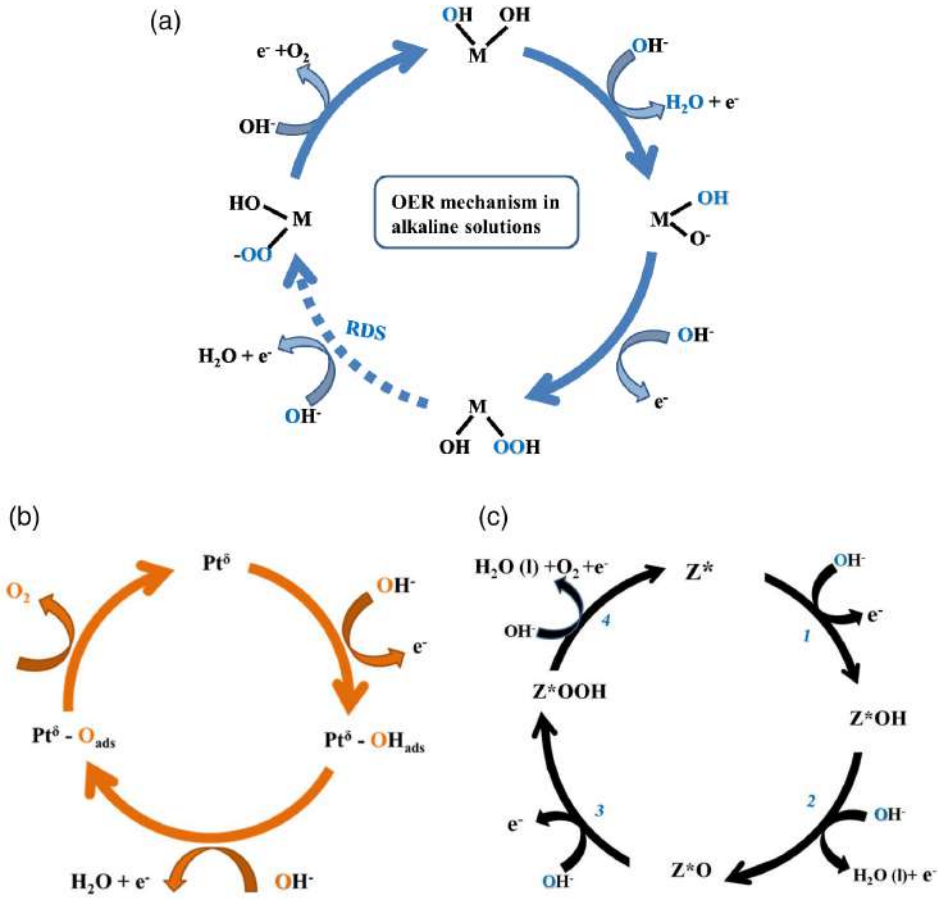

FIGURE 1 Proposed oxygen evolution reaction (OER) mechanisms for various oxygen electrocatalysts under alkaline conditions.
(a) Transition metal oxide,[4] (b) Pt,[51] and (c) metal-free catalyst[52]

electron transfer from the hydroxide ions in which platinum (IV) reduces platinum (II), resulting in two hydroxide radicals that can recombine into molecules for the oxygen generation of two oxygen radicals. As a result, Pt catalysts for oxygen evolution in electrolysis reactions in alkaline media exhibit high overpotentials and low energy efficiencies.

The proposed mechanisms of metal-free and carbon-based OER under alkaline conditions are presented in Equations (1)–(4), in which * represents the active site and OH^*, O^*, and OOH^* are the adsorbed intermediates (reaction pathways are schematically summarized in Figure 1c).[52]

$$OH^- + * \rightarrow OH^* + e^- \quad (1)$$

$$OH^* + OH^- \rightarrow O^* + H_2O(l) + e^- \quad (2)$$

$$O^* + OH^- \rightarrow OOH^* + e^- \quad (3)$$

$$OOH^* + OH^- \rightarrow * + O_2(g) + H_2O(l) + e^- \quad (4)$$

One main goal of developing bifunctional oxygen catalysts is to apply them in RFCs and rechargeable air electrodes for secondary MABs, whereby extensive efforts have been dedicated to the investigation of OER active metal oxide catalysts (e.g., oxides of Fe,[58] Mn,[59,60] Ni,[61] and Co[62]) and various layer structures.[63] This is because TM-based oxides are inexpensive, easily synthesized, and environmentally benign. Furthermore, TM-based oxides are stable in alkaline media and display moderate conductivities, making them promising candidates as OER electrocatalysts. Furthermore, these catalysts can be divided into different classifications based on their composition (monometallic or bimetallic) and will be discussed in detail in Section 3.

1.3 | Oxygen reduction reaction

The electrochemical ORR is the cathodic reaction of MABs and FCs. The reaction is kinetically slow[64] due to the extraordinarily strong O═O bond (498 kJ/ mol), which is too strong to be broken electrochemically. Furthermore, people are still engaged in a quest for economically affordable ORR catalysts alternative to Pt.[65] However, researchers have suggested that TM catalysts are favorable for ORR in alkaline solutions.

Depending on the oxygen adsorption mode and dissociation barrier of Pt-based or metal oxide catalyst surfaces, ORR reactions can proceed through a dissociative or associative mechanism.[66,68] In addition, the different adsorption modes of ORR reactions include the adsorption of end-on O_2, which leads to a direct four-electron pathway without the formation of peroxide, and the adsorption of bidentate O_2 (two O atoms coordinate with the metal), which leads to a two-electron pathway with the formation of peroxide. Here, four-electron pathway reactions are dominant on Pt surfaces[69] with the fraction of two-electron pathway reactions increasing on nonprecious TMO and carbon material surfaces.[70] Because of this, it is essential to enhance the four-electron pathway reactions on nonprecious transitional metal surfaces through various approaches.

Proposed ORR mechanisms and pathways follow different rationales on different metal surfaces in which the surface cations of TMOs are coordinated with the oxygen of H_2O to fulfill full oxygen coordination (Figure 2a) so that H_2O hydrogen atoms become distributed over the catalyst surface. Furthermore, to create hydroxide ions, the protonation of oxygen surfaces is charge-compensated through the reduction of the metal surface. Here, the metal hydroxide (M-OH) surface can further interact with O_2 that is adsorbed on the oxide surface either in a side-on or end-on configuration. As for the RDS in this ORR mechanism, it can either be the displacement or regeneration of the OH surface.[4,71] Another criterion that determines reaction kinetics is the adsorption energy of OOH* intermediates in which a relatively strong OOH* adsorption energy can facilitate the $4e^-$ pathway and a relatively weak OOH* adsorption will lead to the $2e^-$ pathway.[72]

The ORR for Pt catalysts in alkaline media normally takes a dissociative pathway due to the strong initial O_2 adsorption. Here, ORR can proceed through a two-step $2e^-$ pathway with the formation of H_2O_2 (in acidic media) or HO_2^- (in alkaline media) as intermediate species, or through a more efficient $4e^-$ process with the direct formation of H_2O (in acidic media) or OH^- (in alkaline media).[73] Here, the selectivity toward the $2e^-$ or $4e^-$ pathway primarily depends on the adsorption energy of the intermediates and the reaction barrier on the corresponding surface. This theoretical proposal is also consistent with experimental evidence, because Pt-based catalysts always exhibit selectivity for the $4e^-$ pathway without the desorption of reaction intermediates (such as peroxide) from the surface according to the following reaction steps (Equations (5)–(8), also depicted in Figure 2b):

$$O_2 + e^- \rightarrow (O_2{}^- -)_{ads}, \quad (5)$$

$$(O_2{}^- -)_{ads} + H_2O + e^- \rightarrow (HO_2 -)_{ads} + OH^- \quad (6)$$

$$(HO_2 -)_{ads} + H_2O + e^- \rightarrow (HO -)_{ads} + 2OH^- \quad (7)$$

$$(HO)_{ads} + e^- \rightarrow OH^- \quad (8)$$

As for metal-free electrocatalysts, ORR can proceed either through a $2e^-$ or $4e^-$ pathway depending on the

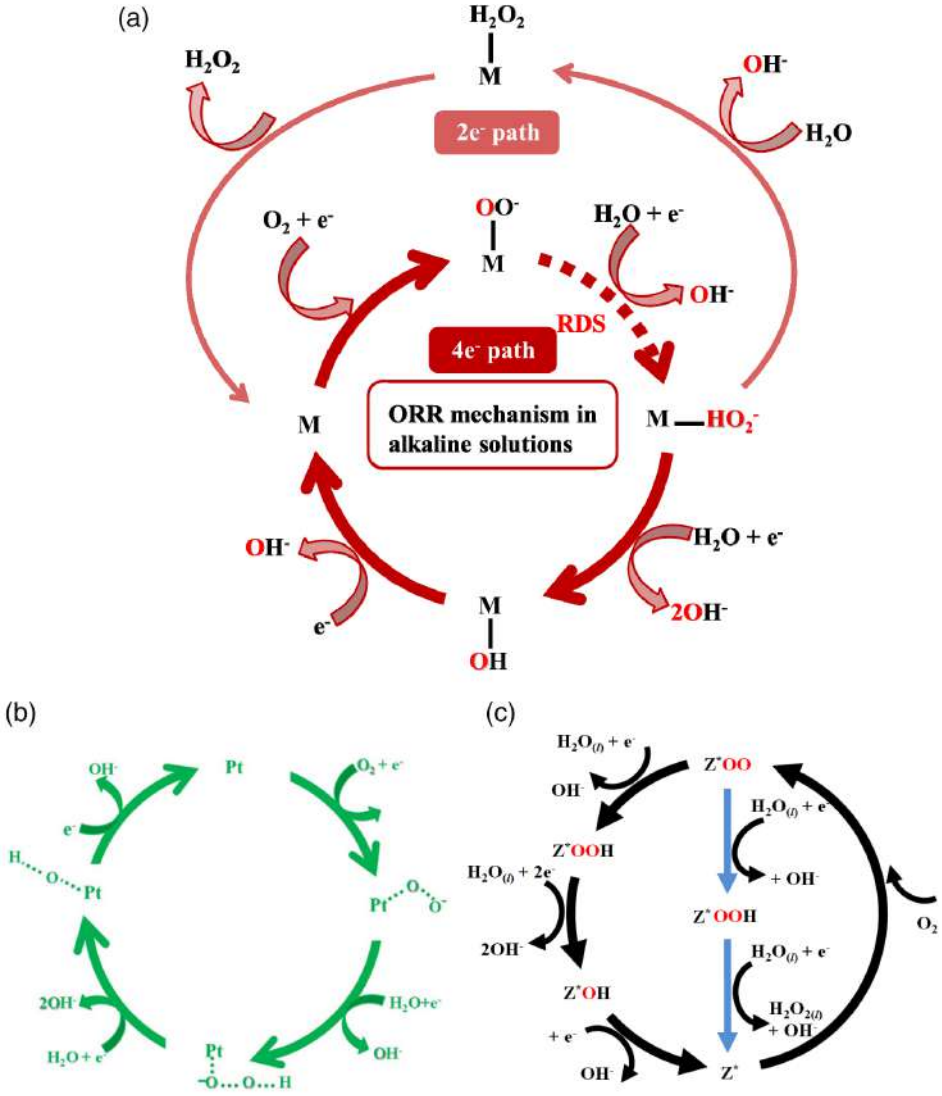

FIGURE 2 Proposed oxygen reduction reaction (ORR) mechanisms of various oxygen electrocatalysts in alkaline media: (a) transition metal oxide, (b) Pt, and (c) metal-free catalysts. Here, bold black arrows indicate the $4e^-$ pathway, thin blue arrows indicate the $2e^-$ pathway with corresponding elementary reactions, Z* represents the active sites

relative stability of the O^* and OOH^* intermediates generated after the adsorption of O_2 on the catalyst. Here, the intermediate product of O^* is present in both pathways and is the major difference compared with the ORR mechanisms of metal-based electrocatalysts (Pt and TM-based oxides). In alkaline media, ORR using metal-free electrocatalysts can proceed through a $2e^-$ pathway as represented by Equations (9) and (10),[52]

$$O_2{}^* + H_2O(l) + 2e^- \rightarrow O^* + 2OH^- \quad (9)$$

$$O^* + 2OH^- + H_2O(l) + 2e^- \rightarrow 4OH^- \quad (10)$$

or it can proceed through a $4e^-$ pathway as represented in Equations (11)–(14).

$$O_2{}^* + H_2O(l) + e^- \rightarrow OOH^* + OH^- \quad (11)$$

$$OOH^* + e^- \rightarrow O^* + OH^- \quad (12)$$

$$O^* + H_2O(l) + e^- \rightarrow OH^* + OH^- \quad (13)$$

$$OH^* + e^- \rightarrow * + OH^- \quad (14)$$

The reaction schematics for metal-free electrocatalysts are also illustrated in Figure 2c.

Although reviews on TM-based bifunctional electrocatalysts are emerging, the focus of this review will be to provide up-to-date appraisals of TM-based bifunctional electrocatalysts under aqueous alkaline media and potential application as oxygen electrocatalysts. As for readers who are interested in ORR in acidic media, several extensive reviews and books have been published as a reference. [74–76] To avoid duplications with existing review literature, our review will start with the background of bifunctional electrocatalysts followed by a general overview.

In this review, recent advancements of nonprecious TM-based electrocatalysts as well as the basic criteria and selection requirements of desirable electrocatalysts are presented. In addition, recent progress of TM-based bifunctional electrocatalysts and key factors used to determine the ORR/OER of catalysts are summarized, including the basic requirements of better electrocatalysts and supports. Furthermore, this review will focus on current activity and performance optimization strategies ranging from engineering approaches such as the introduction of doping and defects to the modification of crystal facets, compositions, morphologies, and synergetic supports.

2 | OVERVIEW OF BIFUNCTIONAL ELECTROCATALYSTS

Increasingly advanced high-performance materials for MABs, water electrolyzers, and FC devices are appealing because they are environmentally friendly and possess high energy densities. However, sluggish kinetics remain a major challenge in their utilization. In the past, Pt-based catalysts were considered to be the best electrocatalysts to minimize these challenges.[77–79] These Pt-based materials suffer drawbacks such as scarcity and vulnerability to poisoning by small molecules such as CO and H_2S making them unsuitable for OER, restricting the development of bifunctional electrochemical devices. Therefore, the design and synthesis of nonprecious bifunctional electrocatalysts are crucial for the utilization of renewable energy sources.

Recently, 3D TM materials have attracted increasing attention for application in ORR and OER electrocatalysts in alkaline media.[59,80] This is because compared with precious metal catalysts, TM catalysts are less expensive, geographically ubiquitous, more abundant, and less susceptible to poisoning. However, TM compounds also possess limited surface area, poor electronic conductivity, and unsatisfactory activity in which the electrocatalytic activity of TM catalysts is affected by the site activity and site population, which depend on the intrinsic properties (nature of the metal, crystal structure, crystal size, crystallinity, morphology and composition engineering, surface area, facet engineering, defect engineering, doping engineering, and support engineering)[68] and extrinsic properties (synthesis methods, temperature, type of electrolyte, type of electrode, and concentration of electrolyte [Figure 3]) of the catalyst. Here, intrinsic properties can be tuned through various approaches and the details are presented in Section 4. As for the extrinsic properties, improvements require the addition of other materials or through geometric structures, such as the preparation of interfaces with another solid material, liquid, or gas to influence the host catalyst.[68]

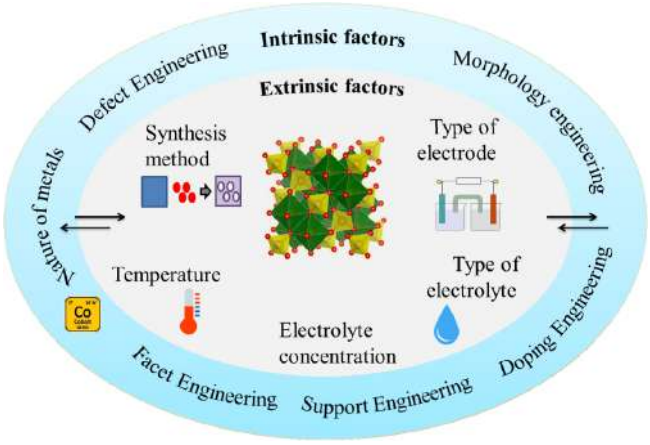

FIGURE 3 Summary of extrinsic and intrinsic factors that affect the performance of electrocatalysts

2.1 | Requirements of optimal electrocatalysts

Potential bifunctional electrocatalysts need to possess properties such as a small energy barrier between the involved chemicals and the charge transfer steps to minimize overall overpotential (Figure 4), optimal bond strength between the metal cation and the oxygen/hydroxide species to provide high site activity,[81,82] and a high surface area with proper electrode porosity to maximize the accessibility of site populations.[83] Here, to achieve high site activity and site population, defective structures with low formation energies of proper defects or even amorphous materials may be required. In addition, supports with high electrical conductivities can maximize accessible site populations through the coupling effect, especially in thick porous layers.[84,85]

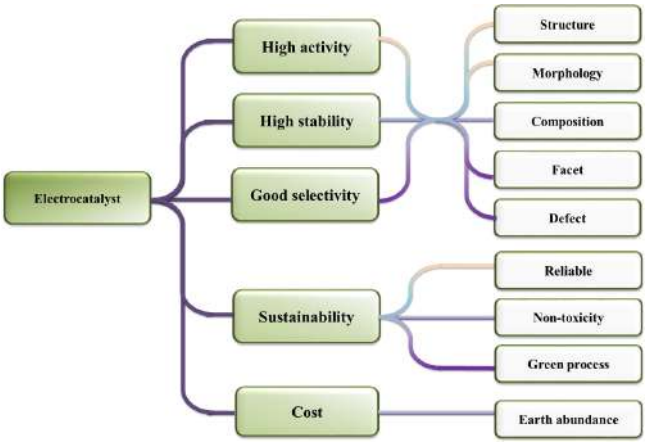

FIGURE 4 General criteria for optimal electrocatalysts

Detailed discussions of these factors can be found in Section 4.

2.2 | Requirements of optimal catalyst supports

The interaction between catalysts and oxide supports is of great importance in heterogeneous catalysts and electrocatalysts in which carbon-based support materials are considered to be the best candidate. However, these support materials are susceptible to carbon corrosion, which can lead to the detachment and aggregation of metal catalysts from the support at higher potentials, leading to poor durability limiting their application.[86] To minimize this, TM alloy supports have been studied and have shown promising performances, but the occurrence of support material leaching from catalyst surfaces is still a major problem.[87–89] Therefore, doped metal oxides have been reported by researchers to resolve these challenges and have demonstrated relatively better durability and stability as support materials.[90] Furthermore, because the conductivity of TM electrocatalysts is insufficient for electron transfer during electrochemical operations, researchers have reported that defect metal oxide supports such as Ti_nO_{2n-1} ($4 < n < 10$), WO_{3-x}, and MoO_x can be used to improve conductivity[91] through the synergetic effects between the catalyst and oxide support. Concurrently, support materials should possess high surface areas through the engineering of morphology and the design of geometry on which catalysts can be easily dispersed and highly utilized.[92] Overall speaking, an optimal electrocatalyst supports should possess basic properties such as high stability, large surface area, and good synergetic interaction with catalysts (summarized in Figure 5).

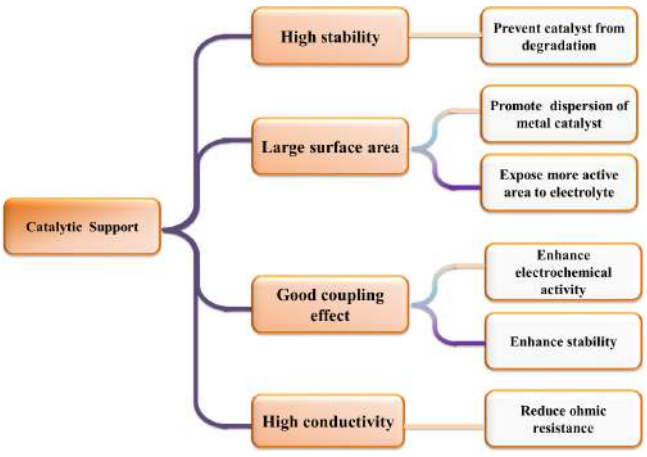

FIGURE 5 Summary of the requirements of optimal catalyst supports

3 | ADVANCEMENTS OF TM-BASED ELECTROCATALYSTS

Nonprecious TM-based OER and ORR electrocatalysts have been investigated for application in energy conversion and storage devices and researchers have reported that oxides, sulfides, hydroxides, and carbides of TMs are the most promising candidates as bifunctional electrocatalysts, which have gained increasing attention due to promising activities and satisfactory stabilities in alkaline solutions. In addition, raw precursors of these catalysts are abundant and inexpensive, making them optimal alternatives of precious metal electrocatalysts. In this section, the performance of various Co, Ni, Fe, and Mn-based electrocatalysts and the various approaches used to enhance their performance will be thoroughly reviewed, with a focus on the recent progress of TMOs.

3.1 | Transition metal oxides

3.1.1 | Ni, Co, Fe , and Mn monometallic oxides

Typical metal oxides (Ni, Fe, Co, and Mn) are candidates for bifunctional electrocatalysts due to promising intrinsic activities and good stabilities.[93,94] However, limited surface areas, poor electronic conductivities (insulators by nature), and sluggish ORR kinetics due to large band gaps limit their usage. To resolve these issues, viable strategies include the modification of catalytic activities through doping and decoration, as well as the engineering of morphologies to create extra active sites on oxide surfaces have been reported.[95,96]

In metal oxide-based electrocatalysts, the catalyst crystalline nature, crystal plane, and geometry play crucial roles in site activity and site population, and are responsible for the corresponding electrocatalytic activity. In metal oxides such as NiO,[97] Mn_3O_4,[98] and Co_3O_4,[99] the coexistence of multiple oxidation states ($Mn^{2+}/Mn^{3+}$and Co^{3+}/Co^{2+}) can enhance bifunctional electrocatalytic performance.[3,5,39,100] Here, the performance of metal oxides (Co_3O_4, NiO, Fe_2O_3/Fe_3O_4, and MnO_2) depends on the morphology of the material, (nanoflower, nanoparticle [NP], nanocube, nanosheet, nanorod, and nanotube), including the M-valence states, the crystalline phases, and the varying structures (micro/-nanostructure). For example, Sun and coworkers[67,101,102] prepared Co_3O_4 nanorods and nanocubes comprised mainly of exposed {110} and {100} facets and investigated the facet-dependent electrocatalytic activity toward OER based on the characterized crystalline structures and surface features (Figure 6a). Here, the researchers reported that the Co_3O_4 nanorods with mainly exposed {110} facets exhibited higher electrocatalytic OER activities than Co_3O_4 nanocubes with mainly exposed {100} facets in alkaline solutions

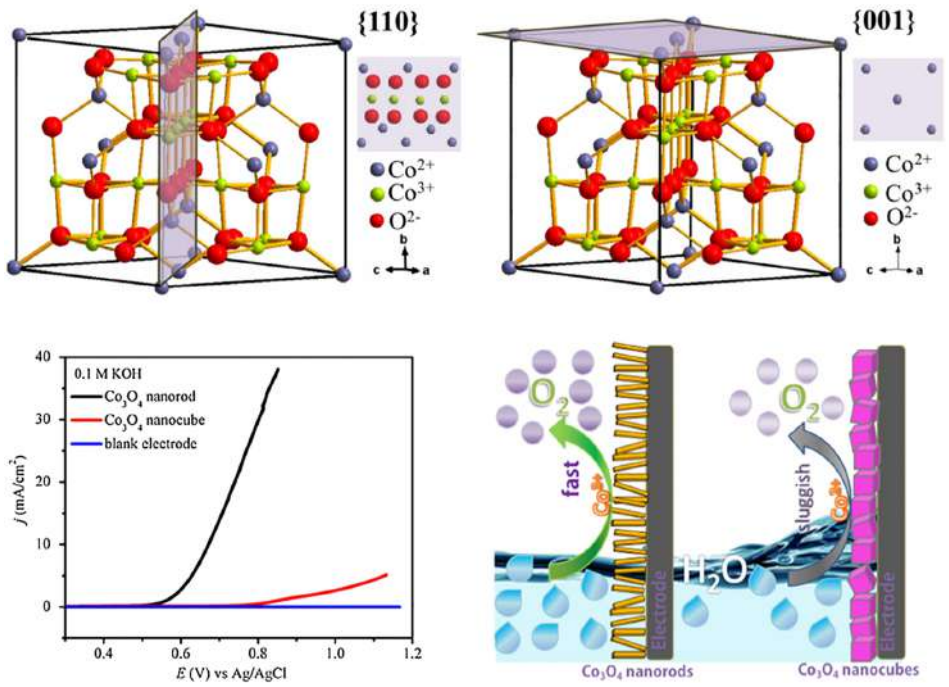

FIGURE 6 (a) Crystal and surface atomic configurations for the Co_3O_4 (i) {110} and (ii) {001} planes. (b) Polarization curves for Co_3O_4 with different nanostructures in 1 M KOH. (c) Schematic illustration of water oxidation on Co_3O_4 nanorods and Co_3O_4 nanocubes[67]

(Figure 6b,c) and attributed this enhanced activity to the synergistic effects of the facet and morphology.[67].

In another study, Liu and coworkers[103] investigated the effects of different crystal facets on Co_3O_4 bifunctional electrocatalysts for rechargeable MABs through the experimental and theoretical study of the octahedral and cubic forms of Co_3O_4. It is found that Co_3O_4 with an octahedron geometry demonstrated much higher cycling performances, better specific capacities, and higher rate capabilities than cubic Co_3O_4 and attributed this to the fact that the octahedron Co_3O_4 geometry can provide more Co^{2+} on the coordinated planes of the catalyst surface, providing more active sites for OER and ORR. In addition, DFT calculations conducted in this study revealed that the octahedron Co_3O_4 possessed a smaller O_2 desorption activation barrier for OER than cubic Co_3O_4, which plays an important role in refreshing catalyst active sites, and therefore, further allowing the exposed Co_3O_4 octahedron (111) to provide more active sites to enhance ORR and OER. In the case of ORR, the researchers in this study reported that surface Co^{2+} possesses better catalytic activities than Co^{3+} in which Co^{2+} tends to transfer electrons to absorbed O_2 molecules and weaken or assist in the breaking of O—O bonds during ORR in which Co^{2+} is subsequently oxidized to Co^{3+} intermediate products. Despite the promising findings and the proper identification of active sites in this study, the site population and fading degradation mechanism under OER and ORR were not clearly defined. Furthermore, Tung et al. applied an in situ grazing-angle X-ray diffraction (XRD) approach in a liquid environment to investigate the phase transformation of the Co_3O_4@CoO single-crystal nanocube. It is interesting to note that β-CoOOH forms first and σ-CooH later as the applied voltage increases. The thin CoO shell works as an adaptive layer to ease off the strain in the nanocrystal substrates when the active phases are formed, thus to prolong the durability of the electrocatalyst.[104]

Similar to Co_3O_4, MnO_x is promising for application as ORR and OER electrocatalysts and possess advantages such as high abundancy, nontoxicity, low costs, and eco-friendliness.[105,106] In addition, the MnO_x family possesses over 30 different crystal structures and variable valences of Mn centers in different polymorphs. As a result of its multiple valence states and the ability to form different crystallographic structures, MnO_x-based electrocatalysts have been extensively used as ORR catalysts.[7] Here, the presence of variable oxidation states and the ease of engineering for crystallographic structures result in the formation of different oxides of manganese such as (α, β, γ) MnO, Mn_3O_4, Mn_2O_3, MnOOH, Mn_5O_8, and MnO_2 (Mn_5O_8 < Mn_3O_4 < Mn_2O_3 < MnOOH in ORR activity).[107] Researchers have reported that β-MnO_2 is the most stable and best ORR catalyst in alkaline media, suggesting that morphology (nanosphere, nanowire, and microparticles) and crystallographic structure (α- > β- > γ-MnO_2) can play an important role in site activity, site population, and stability of Mn-based oxides.[105,108–111] Furthermore, researchers have reported that Mn^{3+} in the octahedral coordination possesses higher specific activities than Mn^{2+} or Mn^{4+} and that the inclusion of Mn^{4+} can improve charge transfer to adsorbed oxygen and promote activity. In addition, the presence of Mn^{3+} with some Mn^{4+} in perovskite structures can help to achieve highly specific ORR activities in basic solutions.[112]

Here, the ORR activity for the different phases of MnO_x depends on the structure and valance state of Mn. And, as a result, their catalytic activities are reported in the order of α- > β- > γ-MnO_2,[105] β-MnO_2 > Mn_3O_4 > Mn_2O_3,[109] and MnOOH > Mn_2O_3 > Mn_3O_4 > Mn_5O_8.[110] Despite this, previous studies on the mechanistic aspects of MnO_x-based alkaline air electrodes[111,113] have revealed that MnO_2 possesses prominent ORR activities,[114] suggesting that the identification of the optimal active and stable crystallographic phase (α, β, γ) of MnO_x is still lacking.

3.1.2 | Copper oxides

Copper oxides (CuO_x) can also behave as suitable non-precious metal electrocatalysts for ORR due to variable oxidation states, high chemical stability, and large surface areas. However, relatively poor conductivities as well as low catalytic activities limit widespread application.[115] To resolve this, researchers have reported that the mixing of CuO_x with carbonaceous materials is an effective solution to enhance the electrocatalytic properties.[116] Because Cu^{2+} ions can act as active sites for ORR and OER and possess great affinity toward the formation of stable complexes with N-based ligands,[117] the combination of CuO and N-rGO can produce nanocomposites (i.e., CuO/N-rGO) with tremendous ORR activity. In particular, CuO/N-rGO nanocomposites can rapidly reduce HOO-intermediates to achieve high current densities and more positive onset potentials with a 4-electron pathway during the reaction in which synergic effects arising from the Cu—N interaction can improve the ORR performance of the nanocomposite.[115] Similarly, a composite of Nd and Cu oxide ($NdCuO_x$) on conductive carbon support was also reported as a promising ORR electrocatalyst.[118] In another study, Hong et al.[119] investigated the dispersion of CuO onto $La_{0.6}Sr_{0.4}Co_{0.2}Fe_{0.8}O_{3-x}$ (LSCF; a representative solid oxide fuel cell (SOFC) electrocatalyst) as a synergistic catalyst for ORR and reported that the resulting catalyst produced greatly accelerated ORR kinetics by a factor of up to 4 as obtained by electrical conductivity relaxation measurements. Despite these promising performances, functional copper-based bifunctional electrocatalysts require combination with other TMs. For example, Serov et al.[120] reported a $CuCo_2O_4$ bifunctional catalyst that demonstrated high activities for both ORR and OER, with onset potentials of 0.8 and 1.51 V, respectively.

3.1.3 | Molybdenum oxides

Numerous TMOs possessing similar crystal structures to rutile TiO_2 are highly conductive in ORR. Among these TMOs, molybdenum oxides (MoO_x) possess different Magnéli phases including MoO_2, MoO_3, Mo_4O_{11}, Mo_8O_{23}, and Mo_9O_{26} in molybdenum-oxygen systems, all of which affect crystal orientation and chemical composition, and, therefore, corresponding electrochemistry and catalytic activity. All Magnéli phases of MoO_x are also moderately conductive and stable in acidic solutions except MoO_3.[121] In addition, most of these Magnéli phases can be grown into large single crystals to investigate the effects of orientation. Furthermore, Chandrasekaran et al.[122] recently reported that molybdenum oxide-based compounds with different structures and properties can demonstrate excellent OER and ORR activities; attracting considerable interest in the field of materials research. There are few studies into the use of MoO_3 as catalysts or catalyst supports. Among them, Liu et al.[123] prepared a Pt-MoO_3 catalyst with the aim of eliminating the harmful effects of SO_2 on the performance of Pt NPs for ORR and reported that the presence of MoO_3 can weaken the S–Pt bond and reduce the adsorption energy of SO_2, resulting in higher ORR activities.

Metal molybdates have also been proposed to be excellent candidates in electrochemical energy conversion and storage systems such as water-splitting devices and lithium-ion batteries as a result of their rapid and efficient redox activity arising from their exceptional stability in alkaline solutions. In terms of crystallography, MoO_3 exists in three phases, including orthorhombic α-MoO_3, monoclinic β-MoO_3, and hexagonal H-MoO_3 in which the hexagonal H-MoO_3 system is a metastable phase that is composed of zigzag chains of octahedral [MoO_6] as building blocks through adjacent oxygen atoms. Compared with α and β crystal structures, hexagonal MoO_3 retains numerous interesting properties. However, to date, there have been no reports of multifunctional catalysts based on hexagonal molybdenum oxide-embedded graphene materials for ORR and OER. Alternatively, binary metal oxides and mixed metal oxides such as $NiMoO_4$[124] and $CoMoO_4$[125] have been recently studied due to their considerable ORR and OER activities, in which researchers have deemed $CoMoO_4$ as a highly promising ORR catalyst due to its low cost, abundance, low toxicity, and durability.

3.1.4 | Bimetallic oxides

NiCo oxides

Oxides of Co[93,126] and Ni[127] have been demonstrated to be promising OER electrocatalysts and have shown moderate activities as bifunctional catalysts in alkaline electrolytes. However, their ORR activities are unsatisfactory due to sluggish kinetics and require effective catalysts to facilitate the direct $4e^-$ pathway mechanism. Recently, researchers have focused on the development of bifunctional catalysts through the formation of bimetallic oxides of Ni and Co

based on the fact that in bimetallic systems, the incorporation of secondary atoms to multivalent TMs such as Mn, Co, and Fe can improve ORR activity and stability,[128,129] in which there is general consensus that $NiCo_2O_4$ possesses the best ORR activity among all mixed nickel and cobalt oxides.[130,131] As for the study of OER in Co_3O_4 electrocatalysts, water oxidation activity can be generally ascribed to the presence of Co^{4+}, which originates from the CoO_2/CoOOH redox couple right before the onset of the OER. Based on this, Co in NiCo oxide-based electrocatalysts such as $NiCo_2O_4$@MnO_x,[132] NiO/$NiCo_2O_4$,[133] NiCo@$NiCoO_x$,[134] $NiCo_2O_4$,[135] Ni-Co nanowire,[136] $Ni_xCo_{3-x}O_{4-y}$,[137] hollow mesoporous $NiCo_2O_4$,[138] and Ni/NiO/$NiCo_2O_4$[139] can weaken O—H bonds in absorbed OH through affinity to O atoms. In addition, the Ni counterpart of these catalysts can help to dissociate protic H through affinity to H atoms, leading to the synergistic enhancement of O—H bond breakage.

Co^{3+} cations, possessing a higher oxidation state, are considered to be the active sites for ORR activity in NiCo oxide-based electrocatalysts. This is because Co^{3+} cations can be used as donor–acceptor reduction sites to catalyze ORR through the capture of electrons in electrodes and release of electrons in electrolyte solutions. In addition, the addition of Co can change Ni-centered bond distances (such as Ni-O and Ni-M [M: Fe, Ni, and/or Co]) resulting from the substitution of Ni^{2+} with the higher oxidation state of Co^{3+}. In general, the valance state and morphology of nickel-cobalt oxides prepared through the electrodeposition method (Figure 7a) have significant effects on the site activity and site population of bifunctional ORR/OER electrocatalysts.

The attractive ORR/OER properties of $NiCo_2O_4$ include intrinsically high activity, easy availability, and good corrosion resistance, but the electrocatalytic capability of $NiCo_2O_4$ is hindered by its bulky morphology, which negatively affects site population, electrical conductivity, and electron transfer rate. Here, the tuning of compositions/structures, the creation of defects, the design of morphologies, the control of valence states, the growth on conductive substrates, and the coupling with conductive supports are all methods used by researchers to enhance activity in electrocatalysts. Among these methods, the coupling effect can play an enormous role in the modification of electronic structure and conductivity of an electrocatalyst, in which enhanced OER and ORR activities can arise from the as-synthesized materials due to the synergetic effect between Co and Ni (Figure 7b,c). Furthermore, the active sites for OER activity of multivalent Co (Co^{2+}, Co^{3+}, or Co^{4+}) are still unclear, and although different research groups have suggested that different surface states, such as Co^{2+},[50] Co^{3+},[140] or Co^{4+}[141] can potentially be the OER active sites, reaction mechanisms as well as the active surface of Co require further investigation. Researchers have reported that in the normal spinel crystal structure of Co_3O_4 with a close-packed face-centered cubic configuration in which Co^{2+} ions occupy the tetrahedral A sites and Co^{3+} ions occupy the octahedral B sites,[142] exposed active sites associated with cations possessing higher oxidation states (Co^{3+} ions) can

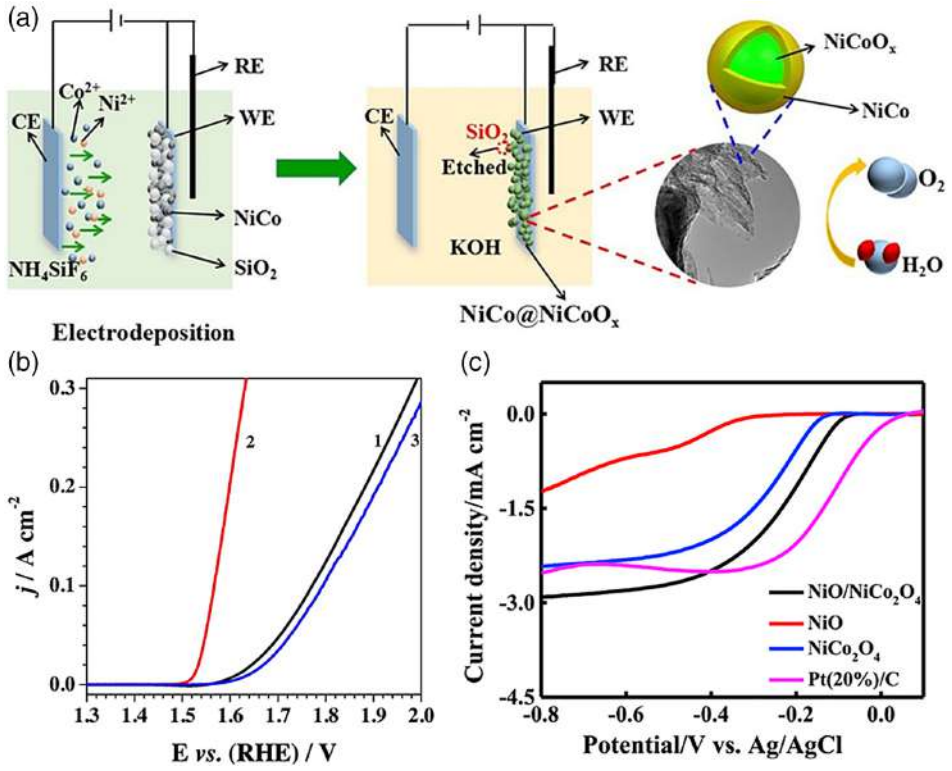

FIGURE 7 (a) Schematic illustration of the preparation of NiCo@$NiCoO_x$.[134] (b) Polarization curves of (1) pristine $NiCoO_x$, (2) NiCo@$NiCoO_x$ core–shell, and (3) Ti/IrO_2 electrodes.[134] (c) Polarization curves of NiO/$NiCo_2O_4$ nanotubes and NiO nanofibers [133]

play a dominant role as ORR active sites.[80] Moreover, there are limited studies on the site populations of NiCo-based oxides. Additionally, although the stability of NiCo oxide-based electrocatalysts for OER and ORR in different environments has been reported, there have been no reports on the stability of these catalysts in bifunctional environments, nor has there been any reports on the fading degradation mechanism of these oxides.

CoFe oxides

Cobalt ferrite oxides ($M_xCo_{3-x}O_4$) are Co-containing and Fe-containing spinel structures, which can be represented as $(Fe^{3+})[Co^{2+}Fe^{3+}]_2O_4$ with tetrahedral and octahedral geometries in which Fe^{3+} occupies 1/8 of the tetrahedral site and Co^{2+} and Fe^{3+} occupy 1/2 of the octahedral site. These spinel structures possess good electrical conductivities due to the electron hopping between valence states of the cations at the octahedral site. Based on its unique structural and chemical stability, $CoFe_2O_4$[143] has received great attention as an effective catalyst for ORR and OER.[144]

TM composites of Fe and Co are one of the best representatives of bimetallic systems due to their low costs and the ability to perform well in both alkaline and acidic electrolytes. Furthermore, these composites can provide better performances as compared with monometallic counterparts for OER.[48] However, numerous experimental and computational studies have confirmed the fact that these TMOs and associated metal-dopants are vital for OER catalysts,[125] factors such as the role of the secondary metal (i.e., Fe) in catalysis remain unclear in which researchers have yet to determine whether these secondary metals activate the catalyst sites or whether they are the "active sites." Here, several studies have reported that Fe is an active site for OER[145–148] whereas other studies have reported that the role of Fe is to improve the conductivity of the electrode[149,150] or that Fe acts as an electron promoter[84] to enable high catalytic activities.

Hung et al. delicately used X-ray absorption techniques to explore this issue by deliberately varying the iron dopant amount in cobalt oxide. It is found that Fe occupies the octahedral sites ($Fe^{3+}_{(Oh)}$) and confines Co to the tetrahedral site ($Co^{2+}_{(Td)}$). Further increasing the composition of Fe ions would occupy the tetrahedral sites to decrease the amount of $Co^{2+}_{(Td)}$ and worsen the OER activity.[50] It is suggested that $Fe^{3+}_{(Oh)}$ has an effect to confine cobalt ions to the tetrahedral site to restrain the multipath transfer of cobalt ions during the structural transformation between spinel and oxyhydroxide. Thus, $Fe^{3+}_{(Oh)}$ keeps promoting the catalytic behavior of $Co^{2+}_{(Td)}$ ions.[50]

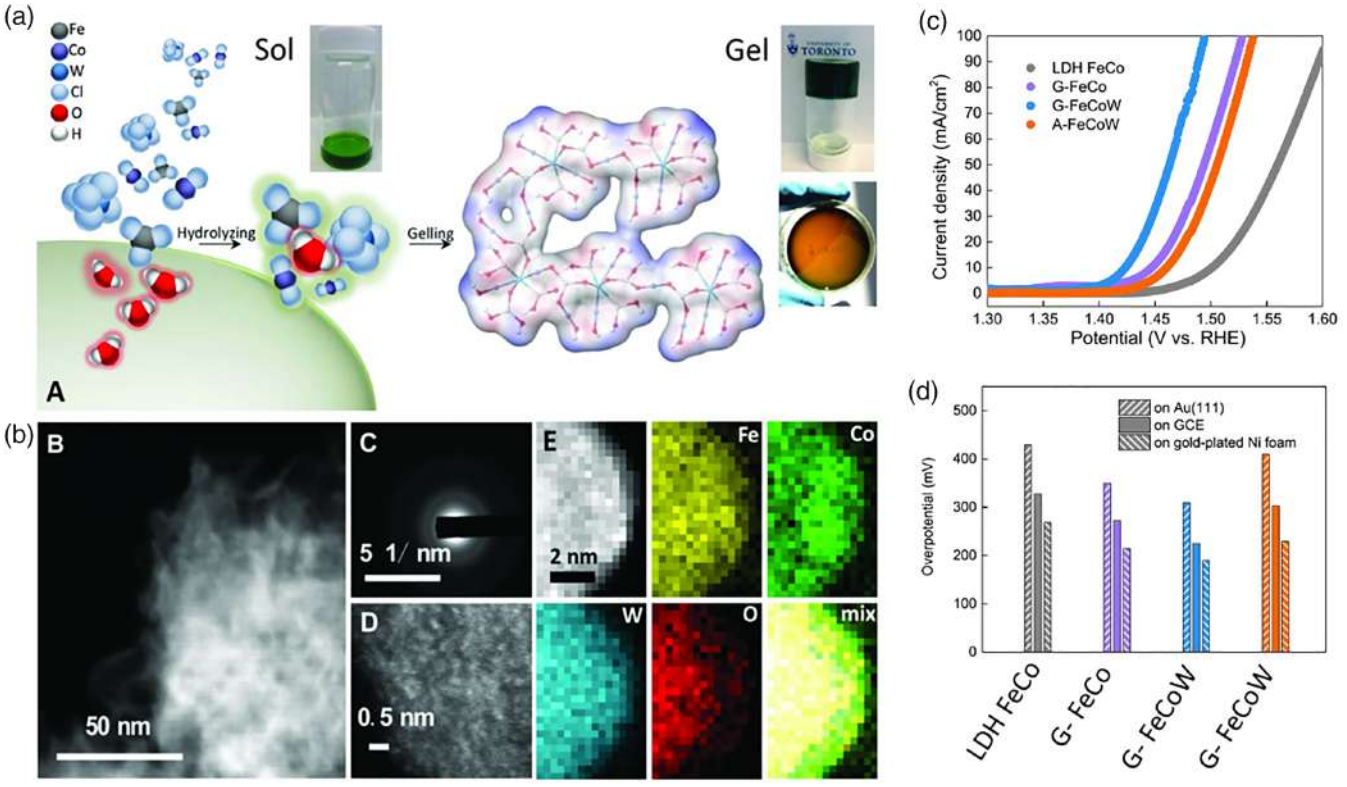

FIGURE 8 (a) Schematic illustration of the synthesis of ternary (oxy) hydroxide catalysts. (b) TEM image, atomic-resolution TEM image, and EDX of G-FeCoW. (c) Polarization curves of catalysts loaded onto Au-plated Ni foam. (d) Overpotentials obtained for OER at 10 mA/cm tested on Au, GCE and Au-plated Ni foam electrodes[151]

Fe also plays an important role in optimizing OH adsorption energies on transitional metal-based oxide electrocatalysts. Zhang et al. designed ternary spinel type electrocatalysts including annealed FeCoW, gelled FeCo, FeCo LDH, and gelled FeCoW and reported that among these catalysts, the gelled FeCoW displayed the lowest overpotential (0.191 V @ 10 mA/cm) and the highest OER activity with optimized OH adsorption energies (Figure 8).[151] In addition, the researchers also reported that gelled FeCoW demonstrated long-term stability with no evident degradation after 500 hr. Here, the researchers suggested that the lowest overpotential, the best OER activity, and the long-term durability of the gelled FeCoW can be attributed to the synergistic effects between the three transition metals, which can create beneficial coordination environments and electronic structures. Despite these promising performances, the maintenance and control of coexisting components (composition) as well as the particle size and morphology of the different metals is especially challenging in binary or ternary TM-based catalysts. Therefore, it is essential to elucidate the effects of the introduction of metals and its role in electrocatalysts using spectroscopic techniques such as XRD to determine shifts in angle or changes in structure for nanocrystals, and with in situ Raman, XAS, and X-ray photoelectron spectroscopy (XPS) to obtain qualitative identifications.

NiFe oxides

Currently, different alloys, oxides, and hydroxides of Ni and Fe are thought to be promising OER electrocatalysts as a result of their intrinsically high activity and corrosion-resistant nature.[152,153] Highly crystalline NiFe oxides can be formed through the high-temperature annealing of NiFe alloy,[154] in which the ratio of the two metals and the multivalence state of the metals (Ni^{2+}/Ni^{3+} and Fe^{2+}/Fe^{3+}) in $NiFe_2O_4$ spinel materials are major factors determining OER activity.[155] In addition, $NiFe_2O_4$[156] has also been reported to demonstrate good OER catalytic activity due to factors such as the outstanding OER activity of Ni-based oxides and the role of Fe in tuning the electronic structure of NiO_x compounds. Moreover, the introduction of conductive substrates into $NiFe_2O_4$ can also reportedly improve electrochemical performances through the increase of electronic conductivity. However, the main challenge of these materials is to identify the exact active sites and to quantify site populations.

In one example, Yan et al.[157] recently synthesized a novel 3D $FeNi_3/NiFeO_x$ nanohybrid material as a bifunctional catalyst for efficient overall water electrolysis and reported a relatively small OER overpotential of ~240 mV. Here, the researchers suggested that the defect-rich $FeNi_3/NiFeO_x$ can be a promising electrocatalyst for cathodes and anodes in alkaline electrolyzers due to its abundancy, cost-effectiveness, and activity as a bifunctional catalyst. Furthermore, the researchers reported that Ni is the active site and that Fe and $NiFeO_x$ can improve the conductivity and electronic structure of Ni in this composite material, therefore suggesting that the higher OER activity (Figure 9a) of the $FeNi_3/NiFeO_x$ series is due to the synergistic effects between

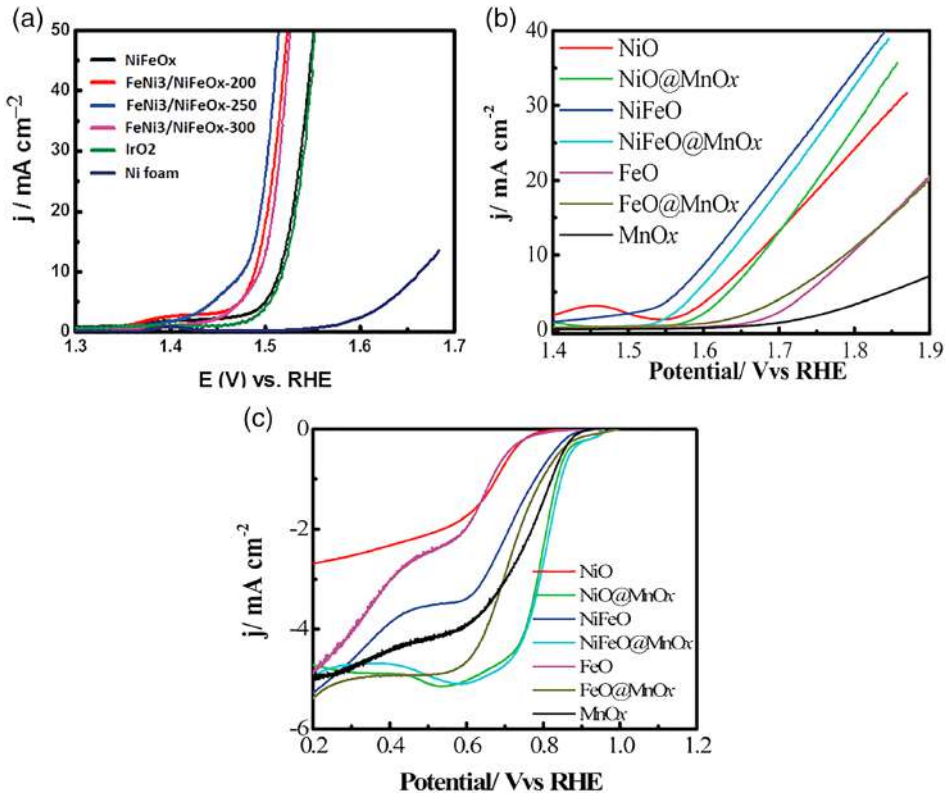

FIGURE 9 (a) OER polarization curves of IrO_2, $NiFeO_x$, and $FeNi_3/NiFeO_x$ series.[157] (b) OER polarization curves of $NiFeO@MnO_x$ catalysts. (c) ORR polarization curves of metal oxide and metal oxide@MnO_x catalysts[158]

$FeNi_3$ and $NiFeO_x$, as well as to the larger ECSA and more exposed surface defects of $NiFeO_x$.

Following this concept, Cheng et al.[158] developed a new synthesis approach based on ultrafine TMO NPs cores such as NiO, FeNiO, and FeO embedded into an amorphous MnO_x shell for reversible OER and ORR catalyses. Here, a nanostructured confinement strategy was used to synthesize an efficient core–shell structure, in which the shell and core of the material can serve as effective catalysts for OER and ORR, respectively. In addition, the amorphous MnO_x shell can simultaneously provide outstanding structural confinement of the embedded metal-oxide cores. To evaluate the overall activity of the resulting oxygen electrocatalyst for reversible OER and ORR, the researchers quantified the potential gaps (the difference between ORR and OER potentials @ −3 and 10 mA/cm) and reported that the $NiFeO@MnO_x$ demonstrated a potential gap of 0.788 V, which was smaller than the overall overpotential for $NiO@MnO_x$ (0.835 V) and $FeO@MnO_x$ (1.038 V). Here, the researchers suggested that the high OER/ORR activity of the core–shell structure was significantly enhanced by the synergistic interaction between the core and shell (Figure 9b, c). In general, the active site theory of ORR and OER results from the perspective of electronic configuration, surface morphology, and bulk structure of catalysts. Nevertheless, site populations and fading degradation mechanisms of NiFe oxide catalysts are unclear.

MnCo oxides

TMs with multiple valence states are also considered to be promising oxygen electrocatalysts. As previously discussed, MnO_x catalysts are prominent ORR electrocatalysts under alkaline media, and therefore, have been extensively studied for alkaline FCs and MABs.[7] Similar to other TMO families, drawbacks of MnO_x include poor electronic conductivity and limited ORR activity; and therefore, various strategies such as the design of defected MnO_x,[111,113] the blending with conductive supports such as Ag,[159] Au, and Pd[160] (in which Au > Pt > Pd), and the decoration with other metal or metal oxides (Mn_3O_4-decorated Co_3O_4 NPs[161] and Ni-doped Mn_3O_4[162]) have been proposed to enhance OER, ORR, and bifunctional activities, in which researchers reported that the optimal ORR nature of the $Mn_3^{II,III}O_4$ phase, the OER nature of the mixed $Mn^{III,IV}$ oxides, and the synergistic effect between the catalyst and support can all contribute toward outstanding ORR/ORR activities for manganese oxides.[163] Another approach used by researchers to obtain active and stable materials is to design multivalent metal spinels. This is because multivalent metal spinels; and in particular $Co_{3-x}Mn_xO_{4\pm\delta}$, are attractive nonprecious oxygen electrocatalysts.[93,164] However, the structure-property relationship of spinel metal oxides remains elusive and their catalytic performances are limited as compared with Pt-based counterparts as a result of low electrical conductivities and poor O_2 binding. Another challenge of $Co_xMn_{3-x}O_4$ is that calcination at higher temperatures or prolonged synthesis will result in catalysts with poor performances, large particle sizes, high rates of agglomeration, and small specific surface areas.

To address these issues, Cheng et al.[29] studied bifunctional $Co_xMn_{3-x}O_4$ NPs through the rapid reduction and recrystallization of amorphous MnO_2 precursors in an aqueous solution containing Co^{2+} at room temperature. Here, CoMnO-P and CoMnO-B (P and B represent NaH_2PO_2 and $NaBH_4$) are the two representative nanocrystals studied by the researchers, which possessed tetragonal and cubic spinel phases, respectively (structures in Figure 10a,b), in which synthesis was carried out using NaH_2PO_2 and $NaBH_4$ as reductants. Consequently, the researchers reported that the cubic spinel phase outperformed the tetragonal spinel phase in terms of the intrinsic ORR activity, but that the tetragonal spinel phase outperformed the cubic spinel phase in terms of the OER activity (Figure 10c,d). The researchers attributed these results to the disparate oxygen adsorption binding energies (cubic phase shows an increase in O_{ads}) of Co, as well as to the defect sites of Mn for OER and ORR.

In a later study, similar results concerning the phase and compositional effects of MnCo oxides were published by Chen and coworkers[166] in which the researchers rationally prepared Mn-Co spinel phases through structural variations, multiple oxidation states, and elusive distribution of cations. In this study, the tetragonal and cubic phases of $Co_{3-x}Mn_xO_4$ were obtained by varying the Co/Mn ratio in which low Mn proportions ($0 \leq x \leq 1.3$) resulted in the cubic spinel phase, whereas high Mn proportions ($1.9 < x \leq 3$) resulted in the tetragonal spinel phase at room temperature. In Figure 10e, the tetragonal spinel *c*-$CoMn_2$ provided better ORR and OER performances and superior catalytic durability as compared with the cubic spinel phase. Here, the researchers attributed these results to the fact that *c*-$CoMn_2$ possesses smaller particle sizes, abundant ionic defects, high specific surface area, and variable metal valences.

In another example, He et al.[166] recently designed $NiMnO_3/NiMn_2O_4$ hybrid oxides (Figure 10b) through the template synthesis method to investigate the effects of metal composition on activity using a preparation method involving the use of melon pollen as a template followed by the subsequent two-step annealing. Here, the composition of the resulting $NiMnO_3/NiMn_2O_4$ hybrid oxides varied from $NiMnO_3$, $NiMn_2O_4$, 3.11 $NiMnO_3/NiMn_2O_4$, 1.57 $NiMnO_3/NiMn_2O_4$, 0.61 $NiMnO_3/NiMn_2O_4$, to 0.42 $NiMnO_3/NiMn_2O_4$, and the researchers reported that 1.57 $NiMnO_3/NiMn_2O_4$ and 0.61 $NiMnO_3/NiMn_2O_4$ demonstrated the highest ORR and OER activity, respectively. Furthermore, the bifunctional activity of

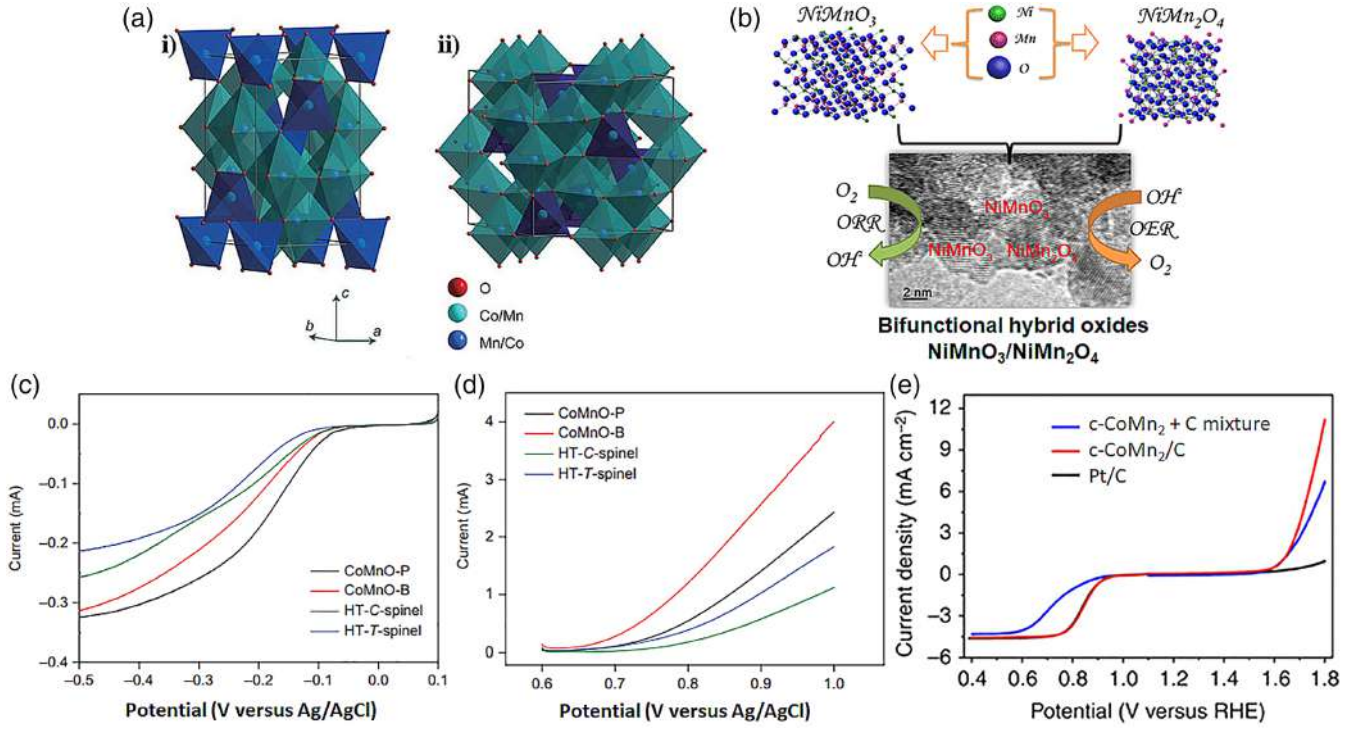

FIGURE 10 (a) Schematic illustration of (i) tetragonal and (ii) cubic CoMnO spinels.[29] (b) TEM image of $NiMnO_3/NiMn_2O_4$.[165] (c) Polarization curves of ORR using catalyst-modified RDE in O_2-saturated alkaline electrolytes.[29] (d) Polarization curves of OER using catalyst-modified RDE in O_2-saturated alkaline electrolytes.[29] (e) Evaluation of OER and ORR activities for the *c*-$CoMn_2$+C mixture, the *c*-$CoMn_2$/C hybrid, and a Pt/C catalyst[166]

these oxides was also tested and 0.61 $NiMnO_3/NiMn_2O_4$ reportedly exhibited higher activities with a minimum relative potential gap of 0.88 V. The researchers attributed this enhanced activity of the hybrid material to the synergistic effects arising from the interaction between the $NiMn_2O_4$ and $NiMnO_3$ NPs. Additionally, the researchers reported that this interaction can also modify the charge transfer between the catalyst and the active species in the electrolyte and that the surface Ni^{3+} and Mn^{3+} with small amounts of Mn^{4+} were the active sites for OER and ORR, respectively. Despite the promising findings in this study, the site population of this material was not quantified.

The activity of electrode materials toward OER and ORR depends on their electronic structure and the catalytic surface during reaction conditions is complex and dynamic. At first glance, these reactions appear simple in which reactants adsorbed from the gas or liquid phase react and subsequently desorb as products. However, these adsorbed species can also interact with oxide catalyst surfaces as well as other adsorbed species (through direct interaction and surface-mediated interaction) and change the electronic and geometric properties of the catalytic surface.[167] Therefore, the best metal oxide catalysts are often ones that bind relevant adsorbents with intermediate adsorption strengths, in which metals that possess either stronger or weaker oxygen bonding than Pt are usually poorer oxygen-reduction catalysts.[66]

The estimated catalytic activity of various metallic surfaces toward ORR can be represented by a "volcano" plot (Figure 11a) using the calculated binding energies of the oxygen intermediates *O as the activity descriptor. From these calculated binding energies, it can be seen that metal catalysts with slightly lower oxygen-binding energies than

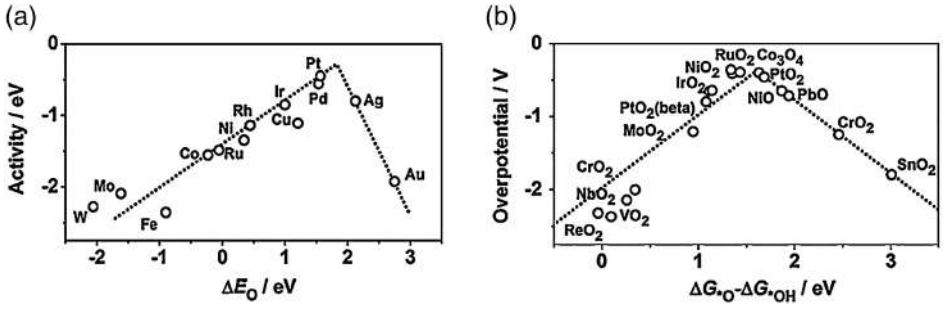

FIGURE 11 Trends in oxygen reduction activity plotted as a function of electrocatalytic activity (expressed in different terms) based on relevant calculated "activity descriptors" for (a) ORR[66] and (b) OER[168]

Pt should possess higher rates of oxygen reduction.[169] Here, DFT calculations have shown that Pt alloy catalysts with TMs such as Ni, Co, Fe, and Cr, in which Pt will segregate to the surface,[170] possess smaller oxygen-binding energies than pure Pt, and the OH-binding energies are not reduced to the same extent on these Pt catalyst surfaces. In the case of Ni metal, which binds O and OH strongly, the activity is limited by the proton transfer to the O and OH. As for Au metal, which binds O and OH weakly, although proton transfer is faster, oxygen is less stable on the surface of the catalyst than it is in the gas phase, meaning that no transfer of protons and electrons to the oxygen on the surface of the catalyst occurs at the beginning of the ORR process. Thus, weak binding leads to the rapid reduction of ORR activity as compared with strong binding.[171] Researchers have reported that Pt_3M (M = Ni, Fe, Co Ti, Sc, and Y) bimetallic alloys as Pt-based catalysts can further reduce overpotentials by increasing the oxygen adsorption energy by 0.2–0.3 eV as compared with a pure Pt catalyst.[171] In the case of Pt oxides, although they do not possess superior activities for OER, they possess optimal binding energies for key reaction intermediates. Despite the fact that Pt catalysts are near the top of the volcano-like trend for metals, they still demonstrate overpotentials of 0.3–0.4 V.[66,168,172]

In a more recent study, Man et al. used the difference between the energy states of two subsequent intermediates ($\Delta G^{O}_{HOO*} - \Delta G^{O}_{HO*}$) as a descriptor for catalytic activity for several different compounds and reported a volcano relationship (Figure 11b).[168] Here, the researchers reported that the difference of bonding strengths follows the Sabatier principle[173] in which if oxide catalyst surfaces bind oxygen too weakly, intermediates cannot easily react and potentials become limited by the oxidation of HO*. Alternatively, if oxygen bonding is too strong, intermediates and adsorbed products stabilize and potentials become limited by the formation of HOO* species. Optimal electrocatalysts should, therefore, possess medium bonding strengths for oxygen, such as in the case of RuO_2, Co_3O_4, NiO, and PtO_2. Furthermore, the actual surface of oxide catalysts also experiences oxidation and/or dissolution in highly corrosive OER environments. For example, oxides such as NbO_2, ReO_2, MoO_2, and CrO_2 are not stable for OER. However, their theoretical values can still provide guidance in the design of mixed oxides to improve activity.[174,175]

In general, it is important to emphasize that in the case of metal or oxide electrodes, although the use of calculated descriptors can predict and explain observed activity trends, this only applies for certain electrolytes in specific model environments. In addition, based on the reported data (12), the optimization of OH adsorption energies is preferable to O adsorption energies because it is likely the most abundant surface intermediate. Furthermore, this theoretical volcano-like trend between ORR catalytic activity and oxygen or/and hydroxyl adsorption energy for metal catalysts is observed in FCs.

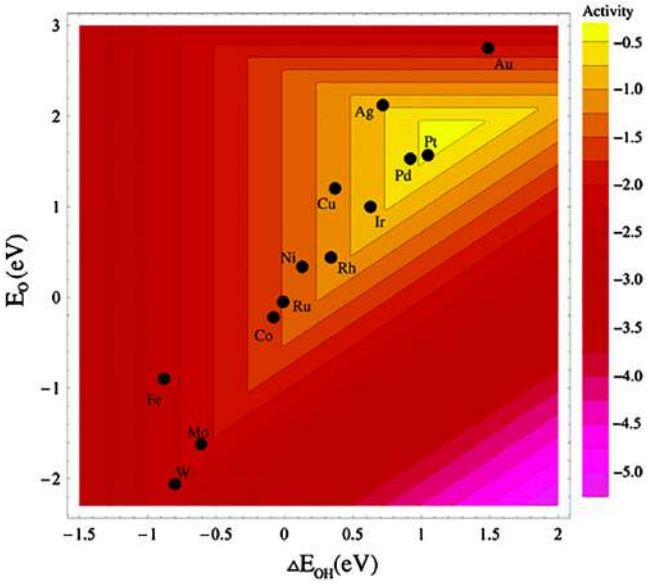

FIGURE 12 Trends in oxygen reduction activity plotted as a function of electrocatalytic activity on relevant calculated "activity descriptors" for both O and OH adsorption energies in fuel cells[66]

Overall, ideal bifunctional ORR and OER catalysts should possess properties such as (a) tolerance for wide pH range conditions, (b) operation at moderate overpotentials with high current densities, (c) long-term stability (years to decades), (d) composition of inexpensive earth-abundant materials, and (e) simple and economical preparation and fabrication methods. However, any single catalyst may never realistically possess all these qualities. Therefore, choosing appropriate catalysts based on the needs of each application is key to deciding developmental priorities for future water-splitting electrolyzers. In addition, researchers need to find a balance between the varying factors in which a balance between the efficiencies of ORR and OER is most needed. A good example of this balance is the balance between cost and efficiency. Therefore, researchers must explore a wide range of bifunctional electrocatalysts with various properties to advance the development of next generation energy conversion technologies.

3.2 | Layered double hydroxides

LDHs are typical inorganic brucite-like materials, which can be described using the general formula: $[M^{II}_{1-x}M^{III}_{x}(OH)_2]^{z+}(A^{n-})_{z/n}.yH_2O$, in which M^{II} and M^{III} are divalent (e.g., Mg^{2+}, Ni^{2+}, Co^{2+}, Zn^{2+}, or Fe^{2+}) and trivalent cations (e.g., Al^{3+}, Fe^{3+}, Cr^{3+} or Ga^{3+}) and A^{n-} is the interlayer anion compensating for the positive charge of the brucite-like layer.[176] LDHs are formed by the substitution of M^{2+}

ions with trivalent ions possessing similar radii to Mg ions. In addition, the metallic cations that make up the lamella in LDHs must present an octahedral shape with an ionic radius in the range of 0.50–0.74 Å. Recently, LDHs have been proposed as interesting alternatives for application in catalysis,[177,178] adsorption,[179] and energy storage and conversion.[180] Due to intrinsically poor conductivities and limited surface areas, the use of LDHs as catalysts in energy conversion systems is limited. To resolve these issues, researchers have proposed many different strategies, including the blending, decorating, and supporting of LDHs with defected metal oxides (Figure 13a,d), which reportedly improve stability but decrease electronic conductivity; or the mixing with conductive carbon materials (Figure 13b,c), which reportedly enhances conductivity and surface area but reduces the long-term stability of carbon due to carbon corrosion. Therefore, the optimal design of defective metal oxide supports is essential to simultaneously improve conductivity and stability.

Among these LDH materials, Ni-based catalysts such as NiFe,[48,176] NiCo,[184,185] NiMn,[186,187] NiTi,[188] NiV,[189] and NiRu[190] have all been reported to show promising OER activity. However, the lack of investigation into the ORR activities of LDHs greatly limits further application in rechargeable MABs and RFCs. Therefore, it is vital to evaluate the bifunctional performance of LDH-based materials to broaden electrochemical applications. Recently, Qian et al.[185] investigated ternary NiCoFe LDHs as ORR and OER electrocatalysts and reported that the observed outstanding ORR and OER performances (Figure 14a,b) of the O-NiCoFe LDH originate from the oxidation process, which can improve the valence state of Co. As for the challenges of the limited surface area and poor electronic conductivity of NiFeCo LDHs encountered during electrochemical measurements, Zhou et al.[191] grew NiFeCo catalysts onto N-doped graphene oxide (GO) (Figure 14c) to enhance electrical conductivity and reported that the resulting $Ni_2Co^{III}Fe$-LDH/N-GO catalyst displayed the best bifunctional activity with 0.88 and 1.41 V for ORR and OER, respectively (Figure 14d). Here, the researchers attributed this enhanced OER and ORR activity to the synergistic effects between the LDH and the conductive support in which Co^{3+} and N-doped GO can act as active sites for OER and ORR, respectively. A similar phenomenon was also reported by Duarte et al.[192] through the combination of CoMn LDHs with carbon nanotubes as efficient and effective bifunctional electrocatalysts for OER and ORR.

Despite these promising performances, carbon-supported LDH catalysts still encounter short-term durability issues due to the degradation of carbon supports at higher potentials resulting from carbon oxidation. To resolve this, Ibrahim et al.[190] introduced a new approach to synthesize highly durable and active metal oxide decorated LDHs as efficient and stable ORR catalysts and reported superior performances (Figure 14e). Here, 3D flower-like NiRu LDHs were decorated using highly conductive and robust Ti_4O_7 in which the researchers suggested that the morphological engineering of NiRu LDH into 3D FL-NiRu LDH can increase

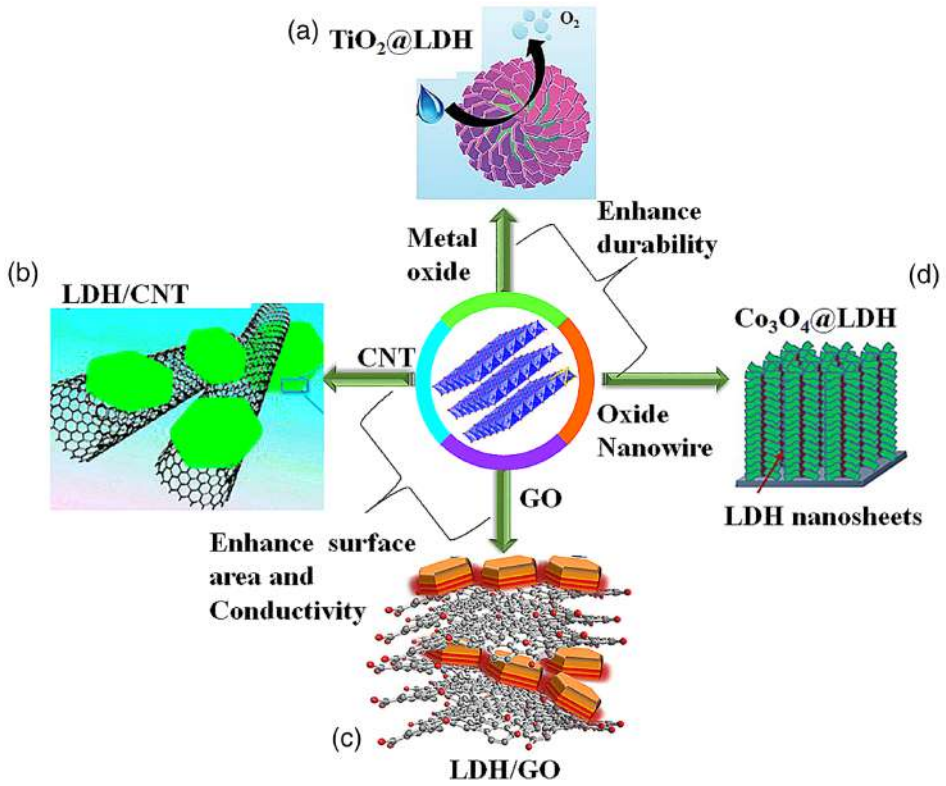

FIGURE 13 Summary of different support materials for the preparation of LDH-based catalysts: (a) TiO_2@LDH,[181] (b) LDH/CNT,[182] (c) LDH/GO,[183] and (d) Co_3O_4@LDH[180]

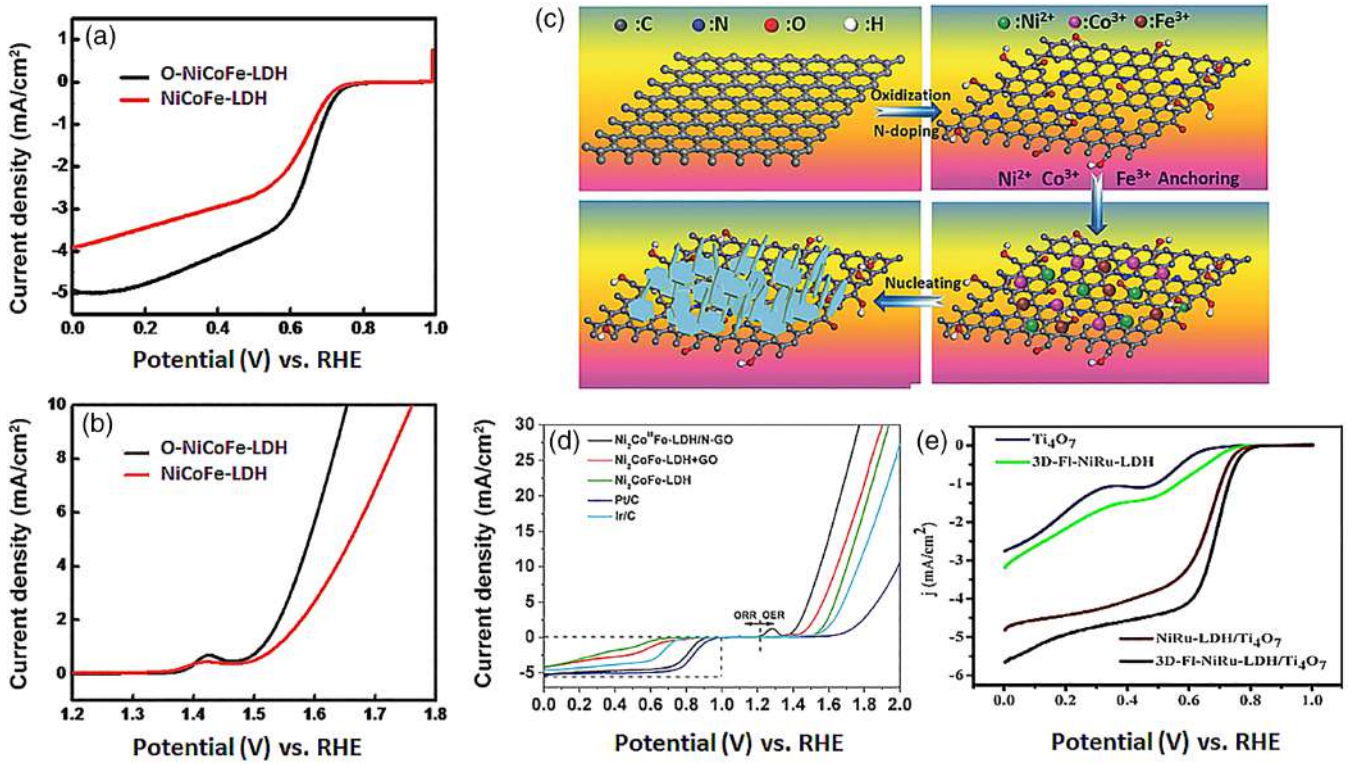

FIGURE 14 (a,b) ORR and OER polarization curves of NiCoFe-LDHs.[185] (c) Schematic of the in situ growth of LDH nanosheets on N-GO. (d) OER and ORR polarization curves of Ni_2CoFe LDH+GO, Ni_2CoFe LDH, Ir/C, and Pt/C.[191] (e) ORR polarization curves of 3D FL-NiRu LDH, Ti_4O_7, 3D-FL NiRu LDH/Ti_4O_7, and NiRu LDH/Ti_4O_7[190]

active sites and allow for easy accessiblity to electrolytes, and that the selection of a support with strong interactions to the metal can reduce NP agglomeration and allow Ti_4O_7 to boost the conductivity and durability of the LDH material. In addition, the researchers suggested that the superior performance of the resulting hybrid arises from the intrinsically high activity of the NiRu-LDH and the strong coupling effect between the LDH and the robust and conductive Ti_4O_7.

In general, the above-mentioned LDHs have demonstrated activity for ORR and OER and have shown stability at individual reaction potentials (as OER or ORR), but there are limited reports on the quantification of site populations and stability measurements in real-life conditions (bifunctional conditions). In addition, researchers have not yet reported the fading mechanisms of LDH-based materials.

3.3 | Metal sulfides, selenides, nitrides, and carbides

Metal oxides have been extensively studied as potential oxygen electrode catalysts. Due to limited conductivities of metal oxides, researchers have branched out to TM nitrides,[193] sulfides,[194–196] phosphides,[197] selenides,[198] and carbides[199] and have reported promising results for ORR and/or OER. This is because at higher oxidation states, site activity of the TMs occurs regardless of the anions they are coordinated to. In the case of transition metal carbides (TMCs), they possess good electronic conductivity, high chemical stability, and satisfactory metallic properties, and are potentially viable for ORR.[200] Due to the instability of TMCs at higher potentials, only a few studies have examined their OER properties, in which most notably, bimetallic carbide-based materials are potentially promising candidates as OER and ORR electrocatalysts due to the incorporation of secondary metals, which can manipulate the electronic structure and expose abundant site activities.[201,202] Similarly, TM sulfides such as NiS_2 and CoS_2 have also been reported to be promising ORR and OER electrocatalysts due to their electrochemically stable nature.[203,204] Here, researchers reported that the activity of these TM sulfides is dependent of the morphology and crystal structure of NiS_2,[205] and that due to the electronically insulating nature of sulfur, metal sulfides need to be blended with conductive substrates or supports to modify conductivity. As for selenides of Ni and Co, they possess similar chemical properties to sulfide and are also promising candidates for oxygen electrode catalysts. Here, Co can exist in two stable forms of Se (CoSe and $CoSe_2$), both of which possess high electrocatalytic activities for OER,[206] ORR,[163,204] and hydrogen evolution reaction (HER),[207,208] making $CoSe_x$ an interesting candidate in the field of water electrolyzers.

Furthermore, in the case of TM selenides,[209] sulfides,[67] and nitrides,[210] they are similar to mixed metal oxides and can enhance the electrocatalytic nature of compounds due to the highly electron-rich nature of the nonmetals.[211] Similar to TMOs, a major drawback for TM sulfides, selenides, and nitrides is the poor electronic conductivity.[212] To resolve this issue, researchers have reported that the coating of these TM-based catalysts (Figure 15a) with carbonaceous materials is an effective solution due to the highly conductive nature of carbon. Liu et al.[128] synthesized a catalyst possessing a composition of Co and Ni ($NiCo_2S_4$@g) and reported efficient OER and ORR activities with an overall potential of 0.98 V. Here, the researchers attributed this dramatic enhancement in bifunctional activity to the unique d-electronic configuration of Co^{3+} at the surface of the $NiCo_2S_4$. And in a later study, Dong et al.[196] introduced an easy and facile synthesis approach to grow binary Ni-Fe sulfide onto Ni-foam (15c) and reported extremely high current densities due to the highly conductive nature of Ni-foam as well as the covalent bridge between the active sulfides and the carbon as the support to provide facile pathways for electron and mass transport.

Precious metals (Pt for ORR and IrO_2 and RuO_2 for OER) have been extensively used as oxygen reaction catalysts for FCs and MABs (summarized in Table 2 and Figure 16). However, these devices are hindered by high costs, a limited abundance of noble metals, poor bifunctional activities of Pt, IrO_2, and RuO_2, as well as poor stability and unsatisfactory ORR/OER processes. To overcome these issues, researchers have applied different carbon-based materials (as a catalyst and as support), chalcogenides, metal carbides, nitrides, oxides (monometallic and bimetallic oxides), and oxide supports as catalysts. Nevertheless, although the use of carbon as the catalyst and catalyst support (Figure 16) provides advantages such as high surface area and good conductivity, it also possesses issues such as poor stability arising from carbon oxidation at relatively higher potentials, limiting the future development of such materials. To resolve this, researchers have designed TMO-based electrocatalysts that possess good stability, but still face the issue of insufficient activity due to poor conductivities and small surface areas. Therefore, an emerging strategy to minimize these issues is to dope metal into well-defined structures of oxides, spinels, and hydroxides to modify catalytic activity through the alteration of electronic structures and the creation of synergetic effects. Although this strategy does increase site activity, site population, and provide good stability, conductivities are still unsatisfactory. Furthermore, metal oxide support catalysts have recently emerged as promising candidates for bifunctional catalysts with

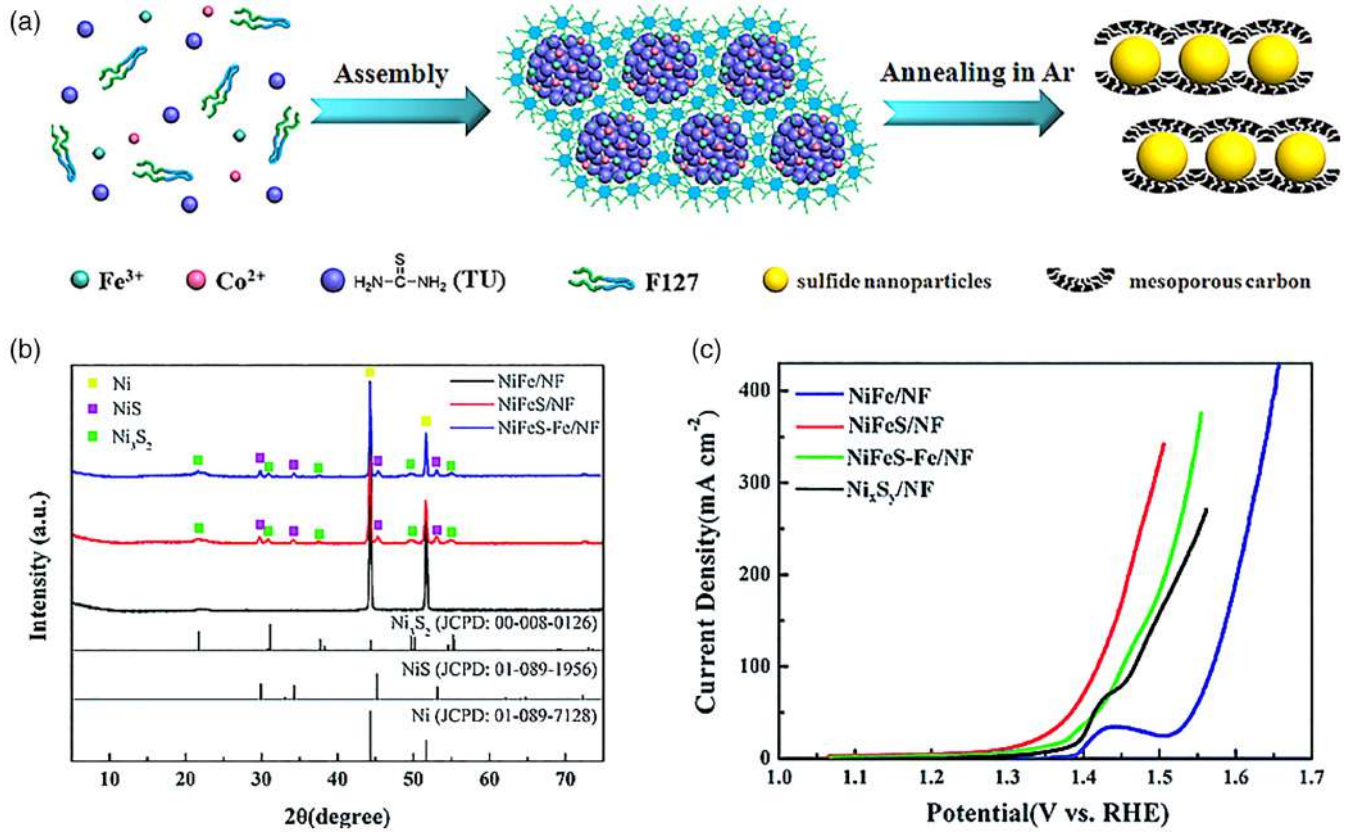

FIGURE 15 (a) Synthesis process for $Co_{1-x}Fe_xS$ using a template.[212] (b,c) XRD patterns and polarization curves of NiFeS samples measured in 1 M KOH[196]

TABLE 2 Summary of ORR/OER activity of recently reported bifunctional oxygen electrocatalysts

Bifunctional electrocatalysts	η (mV) at J = 10 mA/cm	E_{OER} (V) at J = 10 mA/cm	E_{ORR} (V) at J = −3 mA/cm	Oxygen electrode ΔE (V) = $E_{OER} - E_{ORR}$	Reference
Carbide, nitride					
Co/N-C	371	1.599	0.74	0.859	[200]
FeNi@C	280				[213]
NiFe@NC_x	320				[214]
Fe_3C@NG	361	1.591	0.811	0.780	[215]
Co/N-CNT		1.62	0.84	0.78	[216]
Fe/N/C		1.59	0.81	0.78	[217]
Monometallic oxide					
MnO_x		1.77	0.73	1.04	[3]
CoO		1.56	0.85	0.71	[100]
Co_3O_4		1.52	0.78	0.74	[39]
Co_3O_4		1.54	0.82	0.72	
Bimetallic oxides					
Nonsupported oxide					
$NiMn_2O_4$		1.61	0.73	0.88	[165]
$NiCo_2O_4$		1.62	0.78	0.84	[218]
$Ni_{0.4}Co_{2.56}O_4$		1.75	0.79	0.96	[219]
$CoMn_2O_4$		1.83	0.75	1.08	[220]
$FeCo_2O_4$		1.71	0.75	0.96	[221]
$MnCo_2O_4$		1.65	0.76	0.89	[222]
Nonoxide supported					
$CoFe_2O_4$/G		1.69	0.72	0.97	[38]
$NiFe_2O_4$/MWCNT		1.56	0.54	1.02	[156]
$CoFe_2O_4$/G		0.54	0.62	0.08	[38]
Co_3O_4-$MnCo_2O_4$/N-rGO		1.68	0.77	0.91	[223]
$NiCo_2O_4$/C		1.67	0.70	0.97	[224]
Oxide supported					
NiO/$NiCo_2O_4$		1.49	0.72		[133]
$NiCo_2O_4$@MnO_x		1.5			[132]
MnO_x@$NiFeO_x$		1.52	0.94		[158]
Mn_3O_4@$CoMn_2O_4$		1.67	0.80	0.87	[225]
NiRu-LDH/Ti_4O_7			0.85		[190]
Chalcogenides					
CoS_2/N, S-GO		1.61	0.79	0.82	[226]
$CoSe_2$	320				[227]
$Ni_xFe_{1-x}Se_2$	195				[228]
$NiCo_2S_4$@N/S-rGO	210	1.70	0.72	0.98	[128]
$Co_{0.5}Fe_{0.5}S$@N-MC	410	1.57	0.81	0.76	[212]
Layered hydroxide-based catalysts					
NiFe-LDH-Fe-N-C	300	1.539	0.793	0.747	[229]
FeCo-LDH	279				[151]

(Continues)

TABLE 2 (Continued)

Bifunctional electrocatalysts	η (mV) at J = 10 mA/cm	E_{OER} (V) at J = 10 mA/cm	E_{ORR} (V) at J = −3 mA/cm	Oxygen electrode ΔE (V) = $E_{OER} - E_{ORR}$	Reference
CoNi-LDH/CoO	300				[230]
NiFeCo LDH		1.49	0.8	0.69	[185]
g-FeWCo	191				[151]

desirable advantages such as good conductivity and stability but they still possess issues such as limited surface areas, which is vital in this field.

4 | APPROACHES TO ENHANCING THE ACTIVITY

The effectiveness and efficiency of optimal electrocatalysts are determined based on the different properties of OER and ORR such as current density, onset potential, Tafel slope, electrochemical surface area, turnover frequency, half-wave potential, and potential gap (Figure 17). To modify the different basic properties of OER and ORR catalysts, different engineering approaches such as the introduction of doping, defects, and supports as well as the modification of facets, morphology, and composition are emerging as viable strategies. Here, the introduction of doping, defects, and conductive support materials can modify site activities, electronic structures, and conductivities, whereas the modification of facets, morphology, and composition can increase surface areas by exposing surfaces to electrolytes, which in turn can change the site populations of catalysts. In addition, the synergistic effects arising from the interactions between the dopant, the doped metal oxide, the catalyst, and the support can result in enhanced conductivities, increased site activities, changed electronic structures, and increased site populations in resulting catalysts,[164] all of which can enhance catalytic activity and stability.

4.1 | Doping engineering

The engineering of doping is one of the most effective methods to alter electronic structures and local structures to improve the site activity of electrocatalysts[231,232] in which the best strategy is the introduction of secondary metals (single or multiple metal doping) to oxides/hydroxides of TMs through nucleation doping and growth doping.[48,176] In nucleation doping, dopants are incorporated into all precursor molecules and serve as nucleation centers, allowing for the uniform doping of all NPs.[233] As for growth doping, dopants are introduced separately into the reaction mixture alongside precursor molecules, such as in the form of salts of the dopant element, resulting in the nonuniform doping of NPs due to its highly statistical nature. As for the formation of doped products, this depends on the reactivity of both the dopant precursor and the host material.[234] Furthermore, if the rates of reaction and the rates of dopant formation are unbalanced, the amount of dopant can become low, or new crystals mainly containing dopant elements can form. Favorable doping conditions of metal oxides depend on the ligand environment and the specific crystal facets,[235] which change as crystal growth continues. Because of this, most doping methods require careful trial and error selection of

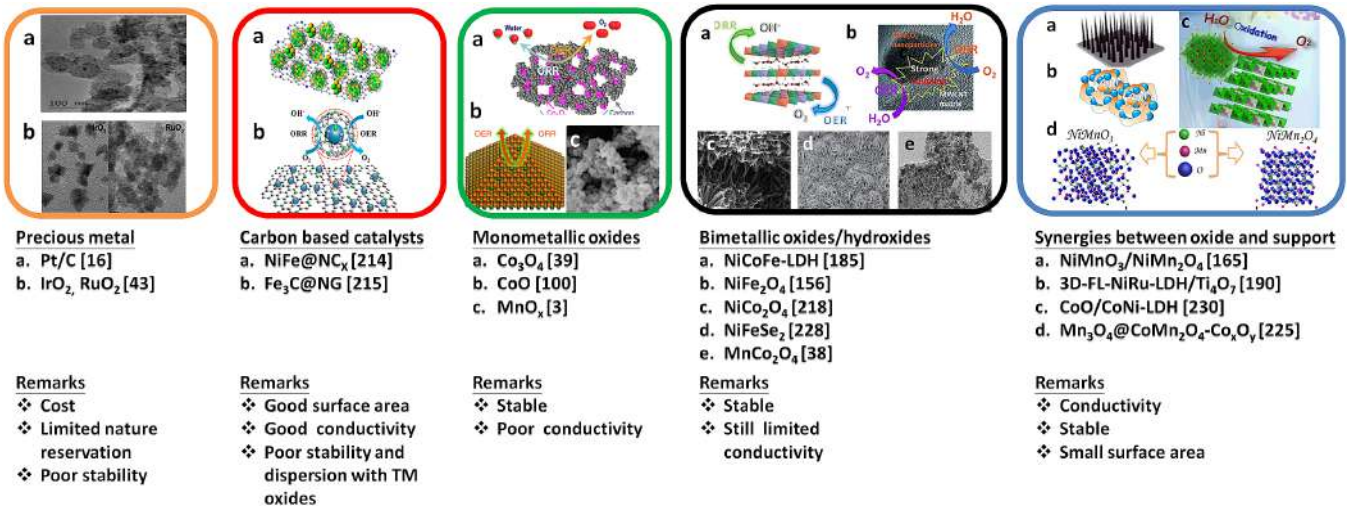

FIGURE 16 Summary of the development of OER and ORR electrocatalysts

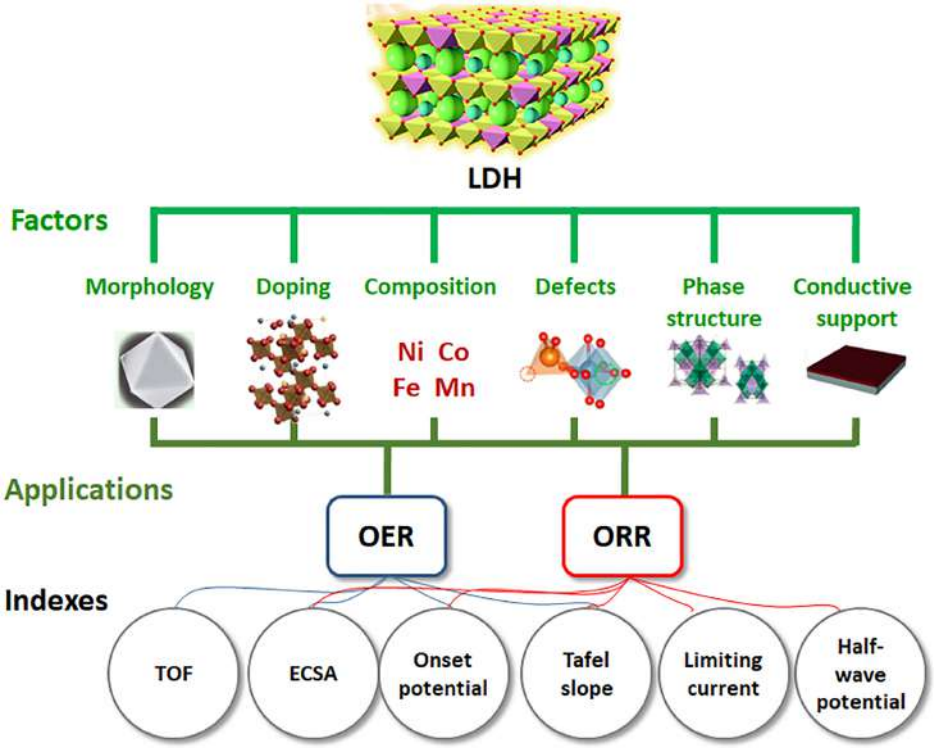

FIGURE 17 Summary of various properties used to evaluate ORR/OER electrocatalysts

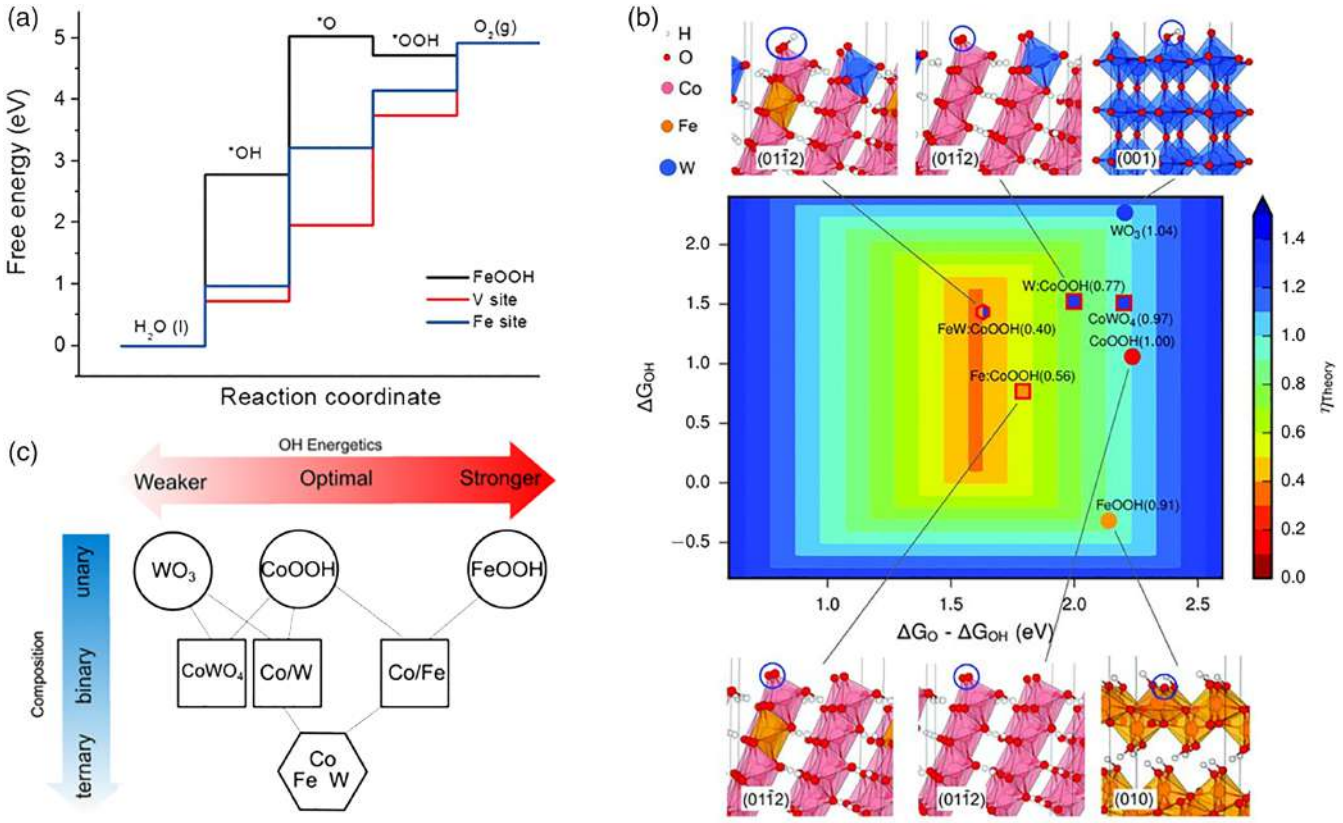

FIGURE 18 (a) Free energy landscape of V-doped FeOOH,[236] (b) DFT calculated OER activities for pure and W-doped CoFe OOH and W oxides,[151] and (c) the effect of doping on adsorption energy (ΔG_{OH})[151]

synthesis approaches and precursors. Fan et al.[236] complemented this approach by demonstrating the effects of V-doping into FeOOH and elucidated the synergistic effects between V and Fe (Figure 18a), in which the addition of vanadium into FeOOH enhances the electronic structure and conductivity of the material, resulting in the V-doped FeOOH demonstrating better OER activities than FeOOH by itself. Although Fe was identified as the active site for OER, site populations were not identified.

Researchers have reported that Fe can either significantly alter the electronic structure of NiOOH through the substitution of Ni with Fe or itself can act as an active site for OER.[61,237] In addition, researchers have examined the effects of Fe on Ni sites on the OER performance of NiOOH and reported that FeO_x produced very poor activity as compared with the composite material.[238] Recent evidence suggests that the NiOOH surface modified with the presence of Fe is the active site for OER.[239,240] $Ni_{1-x}Fe_xOOH$ has been reported to have a record low overpotential (η= 0.4 V) under alkaline conditions, where the metal-oxo bond is suggested to play a critical and catalytic role in the favorable O—O bond coupling.[241] Shin et al. suggested Co, Rh, and Ir among 17 TMs as promising dopants for NiOOH to further improve the OER activity based on in silico quantum-mechanical calculations.[242] However, in these studies, the OER mechanisms for the compounds with Fe impurities are still elusive and doubtful. Zhang et al.[151] studied the effects of dual-doping on catalytic activity and degree of adsorption energy in CoOOH and reported that the inclusion of Fe and W into CoOOH resulted in increased adsorption energies for OH (ΔG_{HO*}) as compared with the counter single atom doping in the reduction of energy barriers (Figure 18b,c).

In general, elemental doping can increase site activities through the formation of defect sites, the enhancement of electronic conductivities, and the modification of intrinsic electronic structures of catalysts, resulting in lowered energy barriers.[236,243]

4.2 | Defect engineering

Defects in crystalline materials arise for various reasons and from various sources. In the case of metal oxides, defects can be produced through high-temperature synthesis, exfoliation, and chemical etching, as well as doping atoms into crystal structures and decreasing thicknesses to atomic levels in which surface atoms can easily escape from lattices to form vacancy defects.[244] In high-temperature synthesis, metal oxides can shift to different crystalline phases driven by chemical potential, shifting from higher chemical potential phases at high temperatures to lower chemical potential phases as temperatures cool. Here, if cooling was conducted fast enough so that particles cannot fully complete the phase shift, defects can be created at the boundary of the different phases. Chemical etching agents can also be applied to particles to remove certain atoms on the surface of particles to create defects. Although this process destroys the crystalline structure of the material, defects created through this method are mostly on the surface.[245] Recent studies have also shown that the intrinsic site activity of catalyst active sites can significantly affect overall catalytic performances. Therefore, to improve the intrinsic site activity of metal oxides, surfaces need to be properly engineered,[246] and based on this, the formation of vacancy defects in catalysts is a promising strategy to adjust the electronic structure and surface property of metal oxides to enhance catalytic activity. In general, defect-rich metal oxide catalysts are characterized by lower coordination numbers, increased structure distortions, and dangling bonds on the surface.[247]

Although it is difficult to synthesize perfect crystal materials free of defects, defects can modify the surface electronic properties of electrocatalysts, in which different types of defects such as line defects, point defects, volume defects, and plane defects can form during material preparation. Furthermore, point defects; based on their location and composition, can be further divided into heteroatom dopants, impurities, and interstitial atoms and vacancies (Figure 19). Here, many researchers have reported that surface defects on electrocatalysts can enhance electrochemical reactions[51,52,54,55] in which many electrocatalysts possessing defects have been reported to exhibit much better OER/ORR activities than corresponding defect-free materials.

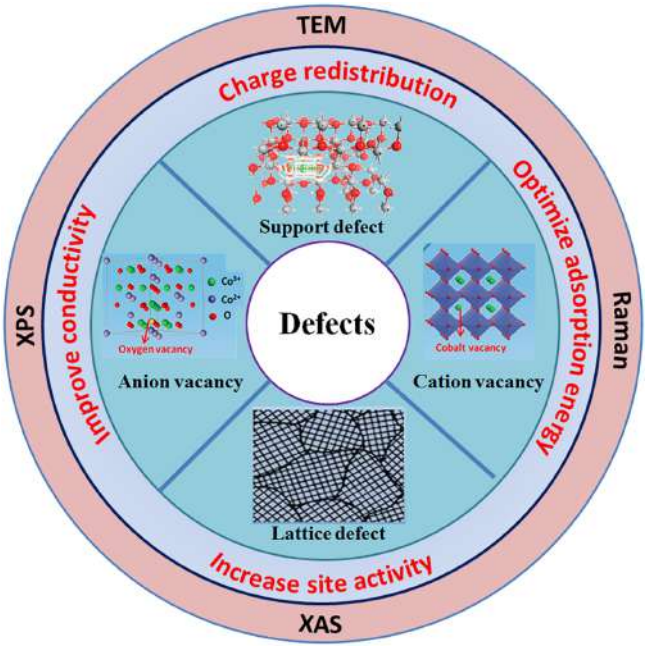

FIGURE 19 Schematic showing the various defects, their effects on OER/ORR electrocatalysts, and characterization techniques

As for defects in new materials, there has been rapid development in nanoscience and many novel materials with striking advantages have been discovered, providing interesting and meaningful research directions for the immediate future. In addition, researchers have reported that many of these advanced materials potentially possess numerous interior defects and oxygen vacancies, allowing for the publication of many satisfactory findings. However, the vacancies of other metal or nonmetal elements or defects in nonoxide compounds have rarely been discussed.[248,249] For example, graphyne is a star-shaped material similar to graphene[137,138] which can be considered to be a mixed hybridization of sp^n in which $1 < n < 2$. Here, researchers suggest that the existence of defects can have great impacts on performance such as in electrocatalysis.[139] With the emergence of conductive metal-organic frameworks (MOFs) as electrocatalysts for heterogeneous reactions,[250] defects on both the metal sites and organic sites should be further studied, in which coordinatively unsaturated metal atoms are thought to be the active sites.[23,107] Overall, the study of the defects of these novel materials can guide the creation of many effective catalysts and the discovery of interesting phenomena and the search and development of new effective methods to controllably prepare various defects is crucial.

Reviews concerning defects are common, the controllable preparation of electrocatalysts with various defects remains a great challenge. In addition, the control of defect concentrations can allow for the more systematic and clear understanding of the role of defects. Currently, most reported materials with defects are prepared using pyrolysis or template methods, but these methods cannot accurately control the generated defects, making the study of the actual relationship between the defect and activity difficult. However, plasma technology has emerged as a useful method to generate oxygen defects on the surface of hematite nanoflakes,[251] anatase TiO_2,[252] and In_2O_3.[253] For example, Xu et al.[254] created surface vacancies in Co_3O_4 using Ar plasma in the presence of P and noted that the in situ filling of P can effectively compensate coordination numbers and change the electronic property using heteroatoms. Overall, these newly developed strategies can guide the engineering of defects and allow for the study of interactive relationships between activity, stability, and defects.

Furthermore, the development of advanced methods to identify defects is also needed. This is because although there are already many advanced and effective techniques to characterize the various defect types, these techniques cannot quantitatively interpret defects. The development of theoretical tools such as hybrid functionals (e.g., B3LYP, HSE) in DFT to explore the effects of defects on performance is necessary.[255] Here, analytical tools such as in operando electrochemical impedance measurements, X-ray absorption spectroscopy (XAS),[256] and positron annihilation life spectroscopy[257] can be used to provide an understanding into the effects of defects on electrocatalysis in a clearer and more convincing manner.

Material stability is an important parameter for practical application. Furthermore, the stability of active defect sites to confirm whether defects change or recombine under working conditions also needs to be examined. To accomplish this, more accurate and high-end in situ measurement and characterization methods need to be developed.

The characterization of these above factors can affect site activities, and therefore, the understanding of active sites for catalysts is crucial to improve catalytic performances. Defects in TM catalysts can result in disordered structures, unsaturated bonds, lower coordination numbers, and dangling bonds. Here, researchers reported that lower coordination numbers of reactive sites can lead to more dangling bonds and result in higher catalytic activities, indicating that coordination numbers play a decisive role in identifying site activities.[247] Likewise, disordered structures can result in the formation of unsaturated bonds, leading to the formation of unsaturated atoms that can act as the activity sites in catalysts. Because of this, the number of unsaturated atoms plays a crucial role in the influence of catalytic properties, meaning that the increase of unsaturated atoms is an effective strategy to promote catalytic activity.[258] Furthermore, the introduction of vacancies can tailor the activity sites of electrocatalysts and the distortion of structure can enhance the structural stability of electrocatalysts by reducing surface energies. Overall, there are many types of defects (cation, anion, lattice, and intrinsic defects on supports, summarized in Figure 19) with different effects such as charge redistribution, conductivity enhancement, and adsorption energy optimization in OER electrocatalysts. Based on this, deeper investigations into defects need to be conducted and factors such as the type of defects as well as the effect of defects on electrocatalytic activity need to be studied. In addition, researchers should focus on defect–activity relationships as well as the identification, characterization, and manipulation of surface defects on catalysts.

4.2.1 | Characterization of defects

The positive effects of various defects have been widely studied through the use of different advanced tools and characterization techniques, and it is necessary to summarize these methods to provide guidance to researchers in the identification of defects. One of the most powerful tools used to determine the electronic structure and local geometry of catalysts is XAS.[259–261] For example, because defects can reduce coordination numbers and increase disordered structures and dangling bonds, Zhang et al. used extended X-ray

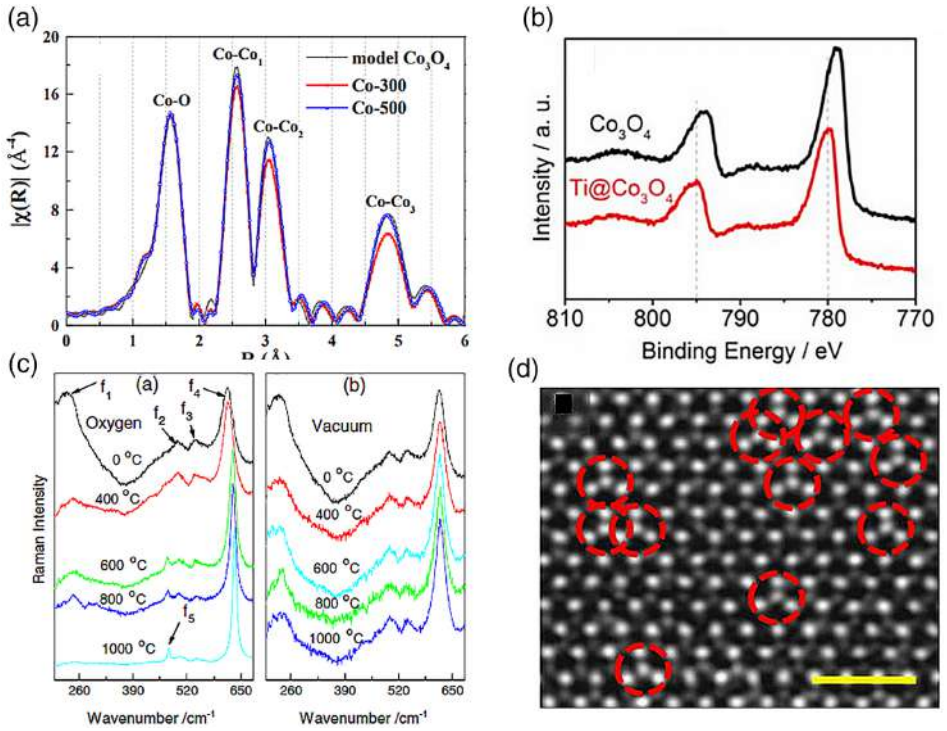

FIGURE 20 (a) Co K-edge FT-EXAFS of pristine and different temperature-treated Co_3O_4.[249] (b) The slight shift in Co 2p binding energy demonstrates the promotion of oxygen vacancy generation in the hybrid to accelerate OER.[262] (c) Raman spectra acquired from SnO_2 samples annealed at different temperatures under (i) oxygen and (ii) vacuum.[263] (d) Defects in the MoS_2 monolayer[264]

absorption fine structure (EXAFS) to study a model Co_3O_4, revealing that the existence of Co_3O_4-500 (Co-Co N = 8.00) and Co_3O_4-300 (Co-Co N = 7.50) can be attributed to the existence of V_{Co} (Figure 20a).[249] In addition, this technique (EXAFS) was also used by Liu et al.[265] to reveal that ultrathin CoFe LDH nanosheets possessed an octahedral coordination of Co-O_{OH} with a coordination number of N = 4.7, which is slightly less than that of pristine CoFe LDHs (N = 4.9) and can be attributed to the existence of oxygen vacancies. The researchers in this study also used this technique (EXAFS) to reveal that the bond distance of the exfoliated ultrathin CoFe LDH nanosheets was 3.148 Å, which is larger than that of pristine CoFe LDHs (3.136 Å). Furthermore, based on the obtained results, the N of Co-M was revealed to be only 4.4 in the exfoliated LDH, which is lower than that in pristine CoFe LDHs (N = 5.3), revealing the existence of metal vacancies (Co and Fe vacancies). Another important tool used to characterize defects is XPS, which is a surface-sensitive technique that can measure the chemical and electronic states of elements within a material. Here, defects are characterized by changing bonding energies through the appearance of new peaks and the slight shifting of peaks. Based on this, Zhang et al.[262] revealed strong shifts in binding energy for Co_3O_4 after coupling with Ti, suggesting strong electron transfer performances and the formation of oxygen vacancies in Co_3O_4/Ti (Figure 20b). Raman spectroscopy is another common and useful technique that can be used to characterize defects in materials, and especially in carbon materials. This is because defects in materials can change vibration modes in systems, resulting in the shifting or appearance of Raman peaks. For example, researchers have acquired representative Raman spectra from SnO_2 samples annealed under oxygen at different temperatures (Figure 20c) and obtained three weak peaks at 475.5 (f5), 540.5 (f3), and 498.5 cm^{-1} (f2) of the crystal SnO_2 with different peak positions, attributing the slight shifts to the OV-induced phonon confinement effect.[263,266] In addition, with the rapid development of electron microscopy, the direct imaging of atomic structures for samples is possible, in which the most advanced transmission electron microscopy (TEM) technologies can observe materials on the atomic scale, allowing for the direct observation and quantification of defects in materials (Figure 20d)[264]

Overall, these advanced methods can assist researchers in obtaining in-depth information about defects; even at the atomic level, and help to elucidate the positive effects of defects on electrocatalysts. However, challenges still remain for researchers to obtain more information about defects, in which there is still a lack of technologies; and especially in situ technologies, to further identify and quantify defects to evaluate the role of defects in electrocatalytic performance.

4.2.2 | Anion vacancies

Oxygen vacancies (V_O) are the dominant anion vacancies in TMOs because of low formation energies,[267] and in some solid metal oxides such as TiO_2, Nb_2O_5, and CeO_2 are the sole source of conduction electrons.[268] Here, the existence

of oxygen vacancies can influence the geometric and electronic structures of oxide surfaces[269] and alter their chemical reactivity, thus enhancing the conductivity and initial adsorption energy of water, as well as the performance of TMOs.[270,271] In addition, for the adsorption of inert molecules such as O_2, N_2, and CO_2, V_O can act as the direct coordinating site for enhanced substrate adsorption as well as the charge donor site, which is capable of activating these molecules due to the abundance of electrons localized at V_O.[100,254,272–276] Furthermore, surface V_O can improve the transfer of electrons from the metal d-band center to the O-vacancies and vice versa to further effectively tune the adsorption of surface species on catalysts.[277]

4.2.3 | Cation vacancies

Cation vacancies can also greatly affect the properties of oxide catalysts and metal cation vacancies can imbue surprising characteristics as a result of their various electronic and orbital distributions. Metal cation vacancies can also affect the site activity, active site density, and electrochemically active surface area (ECSA) of oxide catalysts[29] because cation defects can further decrease the coordination number of neighboring atoms, making them more reactive. In addition, cation defects can also strongly affect the electronic structure of metal oxide catalysts, which in turn can play an important role in increasing the valence state of nearby metal centers, tuning the activity of reactive sites and, therefore, improving their catalytic properties.[246] However, the large formation energy of metal cation vacancies relative to anion vacancies makes it more challenging to study the role of cation vacancies.

In general, oxygen and metal vacancies can not only decrease the coordination number of neighboring catalytic sites, but can also act as donors to narrow band gaps, minimize strains, and modify structures, and can simultaneously increase electrical conductivities and improve the adsorption of H_2O and electron density of materials, resulting in the improvement of intrinsic activity for active sites. In addition, the formation of multiple vacancies can improve ion exchange between electrolytes and catalytically active sites, and increase site activities for OER. Compared to oxygen vacancies, metal vacancies can provide better regulation of multifarious electron configurations and orbits, thus providing an efficient route for optimized water oxidation.[278] Furthermore, the stability of materials is another important parameter for practical application and various catalysts with defects have been reported to demonstrate desirable stabilities.[254,279] More studies are required to determine whether defects change or recombine under working conditions.

4.3 | Support engineering

To minimize the energy loss between electrodes and active sites where reactions take place, the electronic conductivity of catalysts and the interface between the catalyst and the electrolyte need to be optimized. Among the various approaches, the coupling with stable and conductive supports (Figure 21) has been reported to be an effective approach. Here, researchers report that carbonaceous materials as the metal oxide support is preferred in ORR/OER electrocatalysts due to their structural and chemical stability in harsh environments.[280]

Au nanostructure-decorated catalysts have been proposed to be able to enhance electrocatalytic activities through the formation of favorable local catalyst-gold interfacial interactions due to Au being the most active for ORR in alkaline media, despite poor performances in acidic media.[281,282] For example, Wang and coworkers[281] studied the influence of embedding NiFe-LDH electrocatalysts with polyatomic Au and reported that the polyatomic Au distribution on the surface of NiFe-LDH can exhibit higher activities with a current density of ~500 mA/cm and higher stability than pristine samples. Zhang et al.[282] synthesized single atom Au-decorated NiFe-LDHs as efficient OER catalysts and found that by downsizing the particles from the nanometer

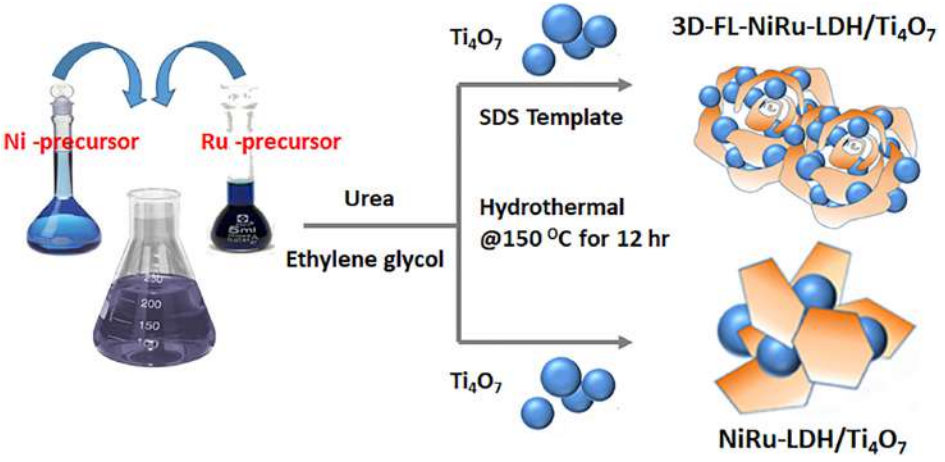

FIGURE 21 Coupling interaction between the catalyst and metal oxide support

scale to single atoms, Au usage can be effectively reduced and atomic utilization can be maximized. Gold is seen as a promising decorating material for catalysts with poor electronic conductivity, possessing the capacity to modify electronic structures and increase the conductivity and site activity of electrocatalysts. Similar to this concept, silver-decorated NiFe-LDHs have demonstrated their outstanding OER/ORR bifuncationality.[283] However, the main challenges of single atom chemistry are the control of mechanisms and characterization tools.

In the following subsections, highly ordered oxides such as TiO_x, CeO_x, WO_x, and $FeNiO_x$ are selected for detailed discussion.

4.3.1 | TiO_x support

TiO_2 is considered to be a potential support material for catalysts due to its environmental friendliness, high stability, moderate cost, large surface area (250 m^2/g), and its ability to alter the electronic properties of oxide catalysts, allowing for the control of oxide catalyst size, structure, and commercial availability. A known drawback of TiO_2 is its poor conductivity.[90] To resolve this, several studies have demonstrated that the conductivity of TiO_2 can be enhanced through the reduction of metal oxides to form oxygen vacancies,[190,284] which can be achieved through high-temperature annealing in reducing atmospheres to obtain Magnéli phased TiO_2 possessing conductivities several orders higher than TiO_2 (e.g., Ti_3O_5 [530 S/cm], Ti_4O_7 [1035 S/cm], Ti_5O_9 [631 S/cm], Ti_6O_{11} [63 S/cm], Ti_8O_{15} [25 S/cm], $Ti_3O_5 + Ti_4O_7$ [410 S/cm], $Ti_4O_7 + Ti_5O_9$ [330 S/cm], and $Ti_5O_9 + Ti_6O_{11}$ [500 S/cm]).[285,286] Here, researchers reported that the most conductive phase of titanium was Ti_4O_7, which reached its optimal conductivity at ca. 10^3 S/cm at room temperature.[87,190] However, researchers also reported that this method can lead to low surface areas and cause poor dispersion and increased aggregation of NPs during the blending of the catalyst with the support,[190,284] presenting a dilemma between the need for high conductivity and the need for high surface area for the electrocatalyst and support. Another method to enhance the conductivity of TiO_2 is through the introduction of appropriate donor dopants such as Nb,[65] Mo,[90] and W,[287] which can achieve relatively better conductivities as compared with bare TiO_2. To reduce the negative impact of particle growth during the doping treatment, researchers have proposed a template-based synthesis method using hexamethyldisilazane and tetra ethyl orthosilicate (TEOS), which may provide an alternative route to control particle sizes.[288] Yet, this approach also presents challenges such as the lack of controlled compositions, tedious preparation steps,[289] and the presence of liquid phases incorporated by capillary forces. But overall, supports that enhance conductivity coupled with supports that provide high surface areas can significantly improve the activity and stability of catalysts.[90,190]

4.3.2 | WO_x support

Tungsten oxide (WO_3) is robust in aggressive acidic and alkaline media and is known to enhance ORR.[290] Drawbacks such as poor electronic conductivity and small surface area hinder application as a catalyst support. Despite this, defective forms of tungsten oxide (WO_{3-x}) are currently attracting increasing attention as support materials due to comparable conductivities (1.76 S/cm) to graphitized carbon (3.0 S/cm).[291] In addition, these defective and reduced forms of tungsten oxide possess advantages such as moderate temperature preparation conditions (~600°C, whereas Ti_4O_7 is ~1,000°C), and relatively smooth and flat surfaces.[258] Furthermore, oxygen vacancy defects formed in these defective tungsten oxides can provide coordinatively unsaturated sites for molecular adsorption, and high-temperature treatment along with doping can further enhance conductivities. Overall speaking, through doping with foreign atoms and morphological variations (e.g., nanowire, ordered, and disordered core–shell structures), WO_x are not only promising oxygen electrocatalysts but are also good support materials for other catalysts.[292]

4.3.3 | CeO_x support

CeO_2 or ceria, a rare-earth metal oxide with a fluorite cubic structure that is widely regarded as a type of "oxygen-tank," can undergo surface hydration and carbonation and can be easily reduced. CeO_2 has been intensively studied as a promoter for many catalyst systems due to the existence of Ce^{4+}/Ce^{3+} redox couples.[293,294] If metal oxides are exposed to atmospheric H_2O and CO_2 at room temperature and pressure, bulk hydration and carbonation can occur,[295] producing important modifications to the reactivity of highly dispersed metals on the above supports. Furthermore, CeO_2 possesses reversible surface oxygen ion exchange, good electronic/ionic conductivity, and high oxygen storage capacity because of the flexible transition between the Ce^{3+} and Ce^{4+} oxidation states as a result of variations in oxygen concentration.[293,296,297] In addition, the multivalence of CeO_2 can generate strong electron interactions with other matrixes, and accordingly can enhance catalytic performances, in which the good electronic/ionic conductivity and high oxygen-storage capacity of CeO_2 are favorable factors for the enhancement of OER activity.[298,299]

Long et al.[176] recently designed and fabricated a novel catalyst of ceria film-supported metallic nickel NP-

decorated TMO nanosheets (ceria/Ni-TMO) to achieve efficient OER in alkaline electrolytes and reported that the presence of unique abundant oxygen species as well as the storage transfer property of the ceria film, which is favorable to the adsorption-desorption of intermediates during the water-splitting process, produced low onset potentials for both OER and HER. In addition to these promising results, the simple synthesis and earth abundance of the result material provides the exciting potential for commercial development in full electrocatalytic water splitting systems.[300]

4.3.4 | $NiFeO_x$ support

As-synthesized $NiFeO_x$ materials can also be used as supports or possess core@shell interactions with electrocatalysts. Here, core@shell systems involve the coating of one material with a thin layer of another material, and the functional properties of these resulting nanoscale materials depend on the size, composition, and structural order of the core and shell. For example, physical properties such as color are strongly dependent on the type of shell as well as the shell-to-core ratio in which the core and shell can be different materials or the same material with different structures, sizes, and morphologies.[301] In one study, Cheng et al.[302] recently designed a new class of TMO-based catalyst supports that are embedded into an amorphous MnO_x, and reported that in this NiFeO-MnO_x structure, the amorphous MnO_x shell can serve as an effective catalyst for OER and ORR, and the metal-oxide core can function as an outstanding structural confinement for the embedded metal-oxide core. As a result, the obtained core@shell structured bifunctional NiFeO@-MnO_x catalyst demonstrated a potential gap of 0.792 V for reversible OER and ORR in 0.1 M KOH solution. Similarly, Zhu et al.[303] provided evidence for enhanced OER activity and durability through the synergy of core–shell structure of NiFe/$NiFeO_x$. Likewise, hierarchically structured nanowires/nanosheets of CuO/$NiFeO_x$ show impressive activity and durability.[173] Here, the researchers suggested that the enhanced activity originates from the intrinsic activity of Ni as well as the synergistic effects between the defected $NiFeO_x$ support and catalyst. In addition, Zhu et al.[303] suggested that core can provide good bulk electron conduction and extend OER active sites to the whole oxide/hydroxide shell, allowing the shell to catalyze OER and protect the metal core from oxidation. Here, the researchers also suggested that the long-term stability of this catalyst originates from the degradation resistant nature of the metal oxide support.

4.4 | Facet, morphology, and composition engineering

4.4.1 | Morphology and composition engineering

Sabatier's principle states that adsorbate-catalyst interactions should be neither too weak or too strong in order for reactions to occur.[304] Here, the degree of interaction in electrocatalysts is mainly influenced by either the composition or morphology of the materials. To improve the degree of interaction, two main methods have been proposed involving the design of bimetallic catalysts and the development of porous nanostructures, in which the former can accelerate reaction kinetics and the latter can buffer stress from electrode swelling and shrinkage and provide more ion adsorption, site activity, and site population for charge transfer reactions, as well as shortened diffusion and transfer pathways for electrolyte ions (Figure 22).

To modify morphologies, researchers have used various reducing agents such as NaH_2PO_2 and $NaBH_4$ and templates such as sodium dodecyl sulfate, NaCl,[305] SiO_2, and MgO.[306] For example, $Co_xMn_{3-x}O_4$ catalysts were recently prepared using different reducing agents to control the crystallographic structure such as cubic and tetragonal phases (Figure 23a,b)[307,308] based on the report that crystallographic modification can accommodate the tuning of catalytic activity[309] in which the cubic phase reportedly displayed significantly improved ORR and OER activities as compared with the tetragonal phase. The chemical composition of the as-synthesized materials can also influence the coordination sites, surface structures, pore sizes, and surface areas of catalysts, and the composition of catalysts have a great impact on the oxidation/reduction potential of neighboring elements and the enhancement of the activity and selectivity of the product.[165,310]

To demonstrate this, Song et al. synthesized mesoporous cobalt oxide as well as Ni-/Mn-promoted cobaltite through a one-step wet chemical method and studied the effects of metal composition on OER and ORR performance through

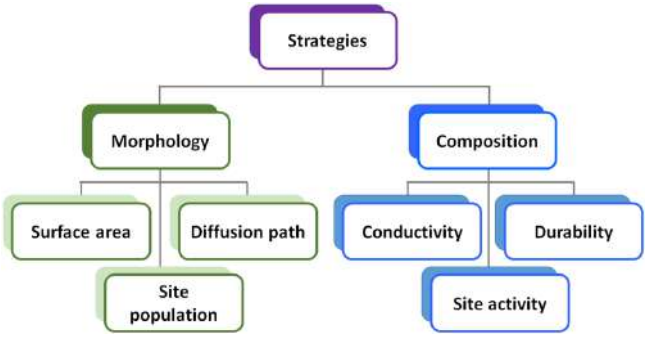

FIGURE 22 Strategies to enhance the performance of electrocatalysts

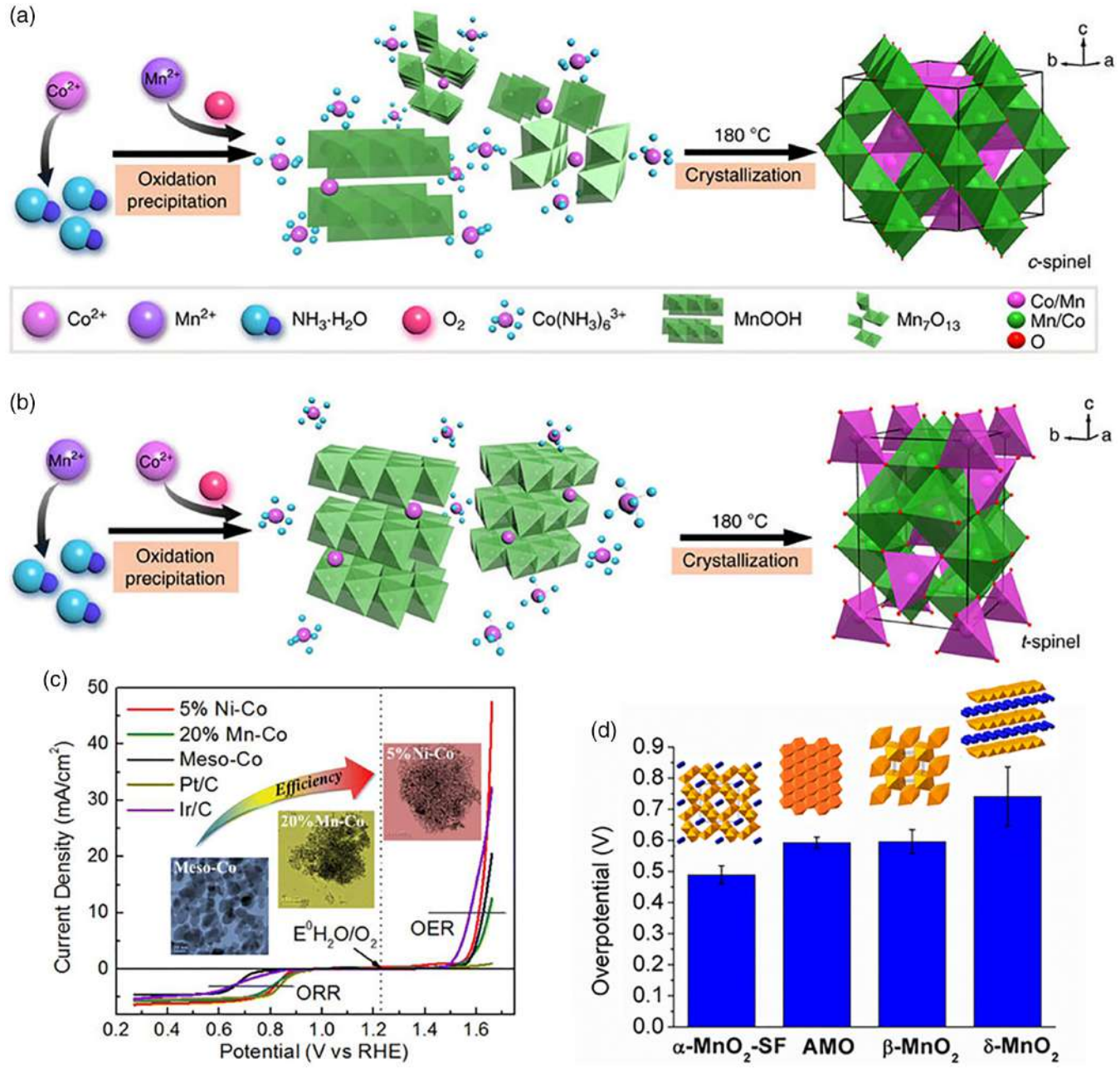

FIGURE 23 Schematics of the synthesis of (a) cubic and (b) tetragonal spinel phases.[166] (c) Polarization curves for the ORR and OER of 5% Ni-Co, 20%Mn-Co, Meso-Co, Pt/C, and Ir/C catalysts.[307] (d) Assessment of the overpotential required to reach 10 mA/cm for αMnO_2, βMnO_2, γMnO_2, and amorphous manganese oxides (AMO)[308]

the variation of Ni and Mn composition.[307] Here, the researchers reported that 5% Ni-Co demonstrated promising ORR and OER activities with an overpotential of 399 and 381 mV at −3 and 10 mA/cm^2, respectively (Figure 23c), and attributed the enhanced ORR activity to the incorporation of Ni and Mn, which resulted in an increase in surface oxygen defects and surface area. The researchers also attributed the enhanced OER performance to the oxidation of the surface from Co^{3+} to Co^{4+}. Thus, comprehensive investigation of surface structure–activity relationships for OER and ORR is crucial for the continuous improvement of future catalyst design for efficient bifunctional oxygen electrodes, in which the surface-sensitive nature of the oxygen electrode reactions and the engineering of morphologies and design of nanostructures such as nanoflower,[189] honeycomb,[311] needle-like,[312] nanowire array,[313] and dendrimer[314] structures can significantly influence the site activity and site population of catalysts.

In fact, the designated composition of catalysts can be deviated from its surface composition[260,315] and the material's morphology, composition, and phase could change during the course of utilization and vary from its pristine

state.[104,316] The interesting phenomenon deserves more investigation with the development of advanced analyzing tools (e.g., in situ/in operando spectroscopic measurement and apparatus design).

4.4.2 | Facet engineering

The atomic level engineering of surface structures and interfaces can be used to precisely manipulate the exposure of active sites and subsequently enhance the corresponding electrocatalytic activities.[99] Because of this, the modulation of material chemical and physical properties through selective facet engineering has become one of the most active research topics in this field, aimed at optimizing functional performance in different applications. In the interface application of heterogeneous catalysis, catalytic properties depend on the atomic arrangement of exposed surfaces and geometry sites, involving atom steps, corners, edges, coordination status, dangling bonds, and surface energies. Rational design of active and stable facets with favorable coordination and arrangement of atoms is the most promising route.[317] Here, different crystal planes exhibit different catalysis properties such as surface stability, oxygen vacancy formation energy, and interaction with surface molecules,[318] in which both octahedral and tetrahedral structures enclosed with all {111} facets possess larger surface area to volume ratios than cubic structures. Therefore, to design enhanced catalytic properties such as the thermal and structural stability of facets ({2kl} > {3kl} > {4kl}), a combination of thermodynamically favorable shapes such as {111} and {100} is vital.[101]

Furthermore, to obtain different facets composed of edges, etching is required in which two conventional synthesis methods are typically used.[319] One etching method commonly used is a template-assisted etching process in which metal is first deposited onto the edges of a well-controlled solid template particle, followed by the subsequent introduction of a proper etchant and the removal of the template, leaving behind the frame structure. The other etching method commonly used is a kinetic-controlled dissolution process in which stable or metastable particles are first generated. Following this, an etchant is added to remove internal atoms depending on the stability of the NPs.[320] In the design of electrocatalysts, catalysts that possess stable shapes may not be structurally or thermally stable.[321] Here, spherical particles possess better shape stability for different planes, and for polyhedra particles, shape stability is essentially determined by the average coordination number of surface atoms and their distribution.[322] Furthermore, a breakthrough was made by Lu and Cheng' team[317,323] in the understanding and control of crystal facets to dramatically increase the ratio of {001} to {101} in anatase TiO_2, in which metal oxides with variable compositions and crystallographic structures of {101}, {001}, and {010} facets and (α, β, γ) exhibit different activation barriers for O_2 desorption (Figure 24). Therefore, the engineering of surface

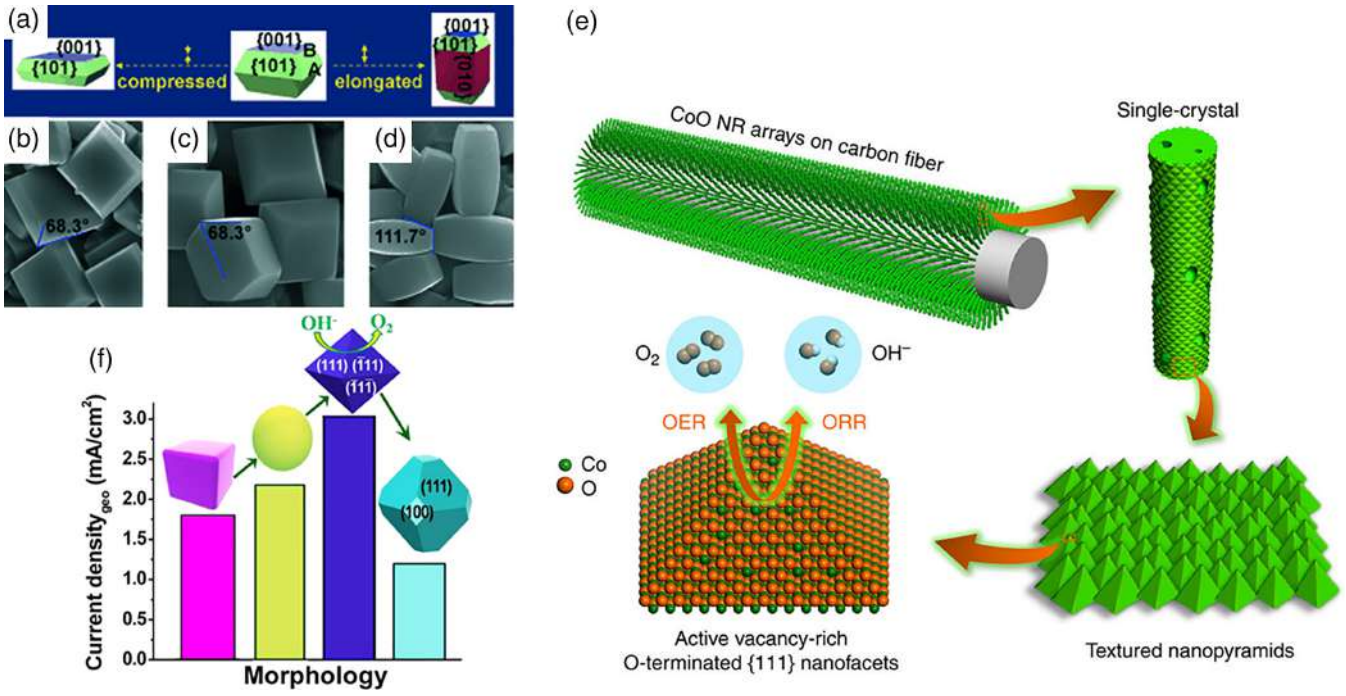

FIGURE 24 (a) Schematic representation of anatase TiO_2 with different crystal facets. (b–d) SEM images of anatase TiO_2 crystals synthesized with different aqueous solutions of HF containing different amounts of $TiOSO_4$ precursor at different times.[323] (e) Schematic representation of surface engineered CoO.[99] (f) Histogram expression for the shape-dependent electrocatalytic activity of spinel oxides[310]

structures of crystals with different facets can affect electrocatalytic performances and boost activity and stability.[310,324]

5 | CONCLUSIONS AND PERSPECTIVES

The ORR and OER are the two most vital reactions in RFC devices and rechargeable MABs, both of which are promising technologies to meet the demands of future renewable energy applications. Most of the time, the use of precious metal electrocatalysts such as Pt, RuO_2, and IrO_2 becomes unavoidable to improve kinetics in the aforementioned reactions. However, the high cost, limited abundance, poor stability, and poor bifunctional activity of Pt, Ir, and Ru are major hurdles to commercialization. Therefore, the development of low cost, highly efficient, and stable bifunctional electrocatalysts is important.

TM-based catalysts are inherently more stable than carbon materials in oxidizing environments, despite their average activities. Ni-based, Co-based, and Fe-based oxides and hydroxide such as NiFe oxides, NiFe-LDHs, and Co_3O_4 have demonstrated activity for OER, whereas Ni-based and Mn-based oxides such as NiMn-LDHs and different oxides of Mn (MnO_x) have demonstrated ORR activity. Therefore, composites of TMs can potentially be the best bifunctional electrocatalysts, but challenges such as intrinsically poor conductivity and low surface area remain in TM-based oxides.

In this review, selection criteria for adequate TM-based electrocatalysts and catalyst supports were first scrutinized. Following this, intrinsic and extrinsic factors affecting electrocatalytic activity were summarized. Furthermore, approaches to enhance the catalytic performance of OER/ORR were discussed, including (a) doping engineering, (b) defect engineering, (c) crystal facet engineering, (d) support engineering, and (e) morphology and composition engineering. Here, the composition, structure, and morphology are all factors responsible for the stability of water electrolysis catalysts. Advanced catalysts with outstanding stabilities can be obtained if all these factors are fully identified and carefully controlled. However, current design methods of electrocatalysts rely heavily on preacquired knowledge of existing materials and through trial-and-error, with few materials being developed based on the rational design and fundamental understanding of catalytic mechanisms of targeted electrochemical reactions, thus hindering further development of high-performance bifunctional catalysts. As an example, the perfect morphological control of catalysts can enable increased specific surface areas and more exposed catalytic active sites, thus shortening the distance for charge/mass transport and elevating conductivity and electrochemical performances. In addition, the innovative design and synthesis of unique nanostructures to significantly improve electrocatalytic performances is still challenging in energy conversion and storage devices. Furthermore, the total cost of the overall synthetic and electrochemical processes, including the control of waste and acid/base pollution, should be carefully taken into consideration and well optimized to realize the efficient and robust deployment of large-scale energy conversion and storage for sustainable global energy requirements. Overall, the design of electronic and phase structures, the creation and exposure of active sites, the elaborate control of morphology and dimension, and the regulation of lattice strain through means of alloying, compounding, heteroatom-doping, and synthetic procedure innovation/control are the most common methods to design novel bifunctional electrocatalysts.

The creation of defects in crystalline materials is one of the most important factors, which can affect site activity and site population in electrocatalysts, and can be created through high-temperature synthesis, exfoliation, and chemical etching. The origin of the advanced activity of these oxygen electrocatalysts is still unclear. To increase the OER/ORR activity of TM-based electrocatalysts, it is necessary to increase individual site activities and overall site populations, in which the activity of a catalyst is equal to the product of the site activity multiplied by the site population. Therefore, an in-depth understanding of active sites; such as the atomic-level interplay between active sites and site population, still requires deeper research, despite a large number of studies that have been conducted to investigate the elusive nature of active sites. Site activity is attributed to the electronic structure and local structure of an active site; therefore, any methods affecting the electronic structure and local structure of active sites, such as doping, defect, and decoration, can affect site activity as well. Furthermore, the site population of catalysts is associated with its exposed surface area as influenced by catalyst loading, electrode architecture, dispersion, size, and thickness. Here, morphological engineering can improve site population through the increase of surface area, whereas composition engineering can increase site activity through the enhancement of activity or the creation of defects. In addition to defects, the coupling between the catalyst and support can also have significant effects on site activity through the modification of catalyst conductivity. Although both site activity and site population are important to catalytic activity, the origin of catalytic activity can only be understood if they can be differentiated. Unfortunately, most factors impact site activity and site population simultaneously. Therefore, future research in this field should focus on the development of methodologies such as poisoning nonprecious transaction metal-based electrocatalysts with different anions such as chlorides to better

differentiate the difference between site activity and site population so that the origin of catalytic activity and stability in ORR/OER can be clarified.

Furthermore, the coupling effect between the catalyst and support is another prominent factor that can modify the conductivity, site activity, and site population of electrocatalysts, in which synergistic bifunctional activities between the catalyst and support can typically improve electrochemical activity and stability, resulting from the change in local and electronic structures of active sites through the creation of defective sites and exposure of more ECSA through the increase in catalytic surface area.

Finally, the long-term stability of ORR/OER electrocatalysts under real conditions (oxidation and reduction) still requires in-depth research. Researchers have been studying the stability of catalysts in OER and ORR individually, real bifunctional tests under successive oxidation-reduction (or charging–discharging) cycles are more challenging. Therefore, the investigation and identification of the origin of bifunctional catalytic activity as well as the fading and poison mechanisms of ORR/OER electrocatalysts are necessary. Future studies in this field should focus on the development of in situ TEM, Raman, and XAS characterization tools, as well as DFT calculations to understand the surface reactions of different sites during electrochemical processes.

ACKNOWLEDGMENTS

Financial support for this review was provided by the Ministry of Science and Technology (MOST) (105-3113-E-011-001, 104-2911-I-011-505-MY2, and 103-2923-E-011-004-MY3), the Ministry of Economic Affairs (MOEA) (101-EC-17-A-08-S1-183), the Top University Projects of the Ministry of Education (MOE) (100H451401), and Taiwan's Deep Decarbonization Pathways toward a Sustainable Society Project (106-0210-02-11-03). Research facilities were provided by the National Synchrotron Radiation Research Center (NSRRC) and the National Taiwan University of Science and Technology (NTUST).

CONFLICT OF INTEREST

The authors declare no potential conflict of interest.

REFERENCES

[1] T. R. Cook, D. K. Dogutan, S. Y. Reece, Y. Surendranath, T. S. Teets, D. G. Nocera, *Chem. Rev.* **2010**, *110*, 6474.
[2] M. K. Debe, *Nature* **2012**, *486*(7401), 43.
[3] Y. Gorlin, T. F. Jaramillo, *J. Am. Chem. Soc.* **2010**, *132*, 13612.
[4] J. Suntivich, H. A. Gasteiger, N. Yabuuchi, H. Nakanishi, J. B. Goodenough, Y. Shao-Horn, *Nat. Chem.* **2011**, *3*, 546.
[5] Y. Liang, Y. Li, H. Wang, J. Zhou, J. Wang, T. Regier, H. Dai, *Nat. Mater.* **2011**, *10*(10), 780.
[6] C. Tang, H.-S. Wang, H.-F. Wang, Q. Zhang, G.-L. Tian, J.-Q. Nie, F. Wei, *Adv. Mater.* **2015**, *27*, 4516.
[7] F. Cheng, J. Chen, *Chem. Soc. Rev.* **2012**, *41*, 2172.
[8] L. Grande, E. Paillard, J. Hassoun, J.-B. Park, Y.-J. Lee, Y.-K. Sun, S. Passerini, B. Scrosati, *Adv. Mater.* **2015**, *27*(5), 784.
[9] Y. Li, H. Dai, *Chem. Soc. Rev.* **2014**, *43*, 5257.
[10] Z. Peng, S. A. Freunberger, Y. Chen, P. G. Bruce, *Science (New York, N.Y.)* **2012**, *337*(6094), 563.
[11] G. Zhang, C. Li, J. Liu, L. Zhou, R. Liu, X. Han, H. Huang, H. Hu, Y. Liu, Z. Kang, *J. Mater. Chem. A* **2014**, *2*, 8184.
[12] M. Jahan, Z. Liu, K. P. Loh, *Adv. Funct. Mater.* **2013**, *23*, 5363.
[13] Y. Jiao, Y. Zheng, M. Jaroniec, S. Z. Qiao, *Chem. Soc. Rev.* **2015**, *44*, 2060.
[14] W. Zhou, X.-J. Wu, X. Cao, X. Huang, C. Tan, J. Tian, H. Liu, J. Wang, H. Zhang, *Energy Environ. Sci.* **2013**, *6*, 2921.
[15] F. Calle-Vallejo, M. T. M. Koper, A. S. Bandarenka, *Chem. Soc. Rev.* **2013**, *42*, 5210.
[16] A. Zadick, L. Dubau, N. Sergent, G. Berthomé, M. Chatenet, *ACS Catal.* **2015**, *5*, 4819.
[17] R. Borup, J. Meyers, B. Pivovar, Y. S. Kim, R. Mukundan, N. Garland, D. Myers, M. Wilson, F. Garzon, D. Wood, P. Zelenay, K. More, K. Stroh, T. Zawodzinski, J. Boncella, J. E. McGrath, M. Inaba, K. Miyatake, M. Hori, K. Ota, Z. Ogumi, S. Miyata, A. Nishikata, Z. Siroma, Y. Uchimoto, K. Yasuda, Kimijima, K.-i., Iwashita, N., *Chem. Rev.* **2007**, *107*, 3904.
[18] E. Casero, A. M. Parra-Alfambra, M. D. Petit-Domínguez, F. Pariente, E. Lorenzo, C. Alonso, *Electrochem. Commun.* **2012**, *20*, 63.
[19] Y. Zhang, H. Zhang, Y. Ma, J. Cheng, H. Zhong, S. Song, H. Ma, *J. Power Sources* **2010**, *195*(1), 142.
[20] G. Chen, S. R. Bare, T. E. Mallouk, *J. Electrochem. Soc.* **2002**, *149*, A1092.
[21] Y. Zheng, Y. Jiao, J. Chen, J. Liu, J. Liang, A. Du, W. Zhang, Z. Zhu, S. C. Smith, M. Jaroniec, G. Q. Lu, S. Z. Qiao, *J. Am. Chem. Soc.* **2011**, *133*, 20116.
[22] Y. Liang, Y. Li, H. Wang, H. Dai, *J. Am. Chem. Soc.* **2013**, *135*, 2013.
[23] T. Y. Ma, S. Dai, M. Jaroniec, S. Z. Qiao, *Angew. Chem. Int. Ed.* **2014**, *53*, 7281.
[24] S. Yang, Y. Sun, L. Chen, Y. Hernandez, X. Feng, K. Müllen, *Sci. Rep.* **2012**, *2*, 427.
[25] G. Wu, P. Zelenay, *Acc. Chem. Res.* **2013**, *46*, 1878.
[26] R. Bashyam, P. Zelenay, *Nature* **2006**, *443*(7107), 63.
[27] R. Li, Z. Wei, X. Gou, *ACS Catal.* **2015**, *5*, 4133.
[28] S. Zhuang, K. Huang, C. Huang, H. Huang, S. Liu, M. Fan, *J. Power Sources* **2011**, *196*, 4019.
[29] F. Cheng, J. Shen, B. Peng, Y. Pan, Z. Tao, J. Chen, *Nat. Chem.* **2011**, *3*(1), 79.
[30] D. U. Lee, J. Scott, H. W. Park, S. Abureden, J.-Y. Choi, Z. Chen, *Electrochem. Commun.* **2014**, *43*, 109.
[31] D. U. Lee, B. J. Kim, Z. Chen, *J. Mater. Chem. A* **2013**, *1*, 4754.
[32] M. Prabu, K. Ketpang, S. Shanmugam, *Nanoscale* **2014**, *6*, 3173.
[33] W. Yang, J. Salim, C. Ma, Z. Ma, C. Sun, J. Li, L. Chen, Y. Kim, *Electrochem. Commun.* **2013**, *28*, 13.

[34] Y. Wang, W. Ding, S. Chen, Y. Nie, K. Xiong, *Chem. Commun.* **2014**, *50*, 15529.
[35] T. Y. Ma, Y. Zheng, S. Dai, M. Jaroniec, S. Z. Qiao, *J. Mater. Chem. A* **2014**, *2*, 8676.
[36] H. W. Park, D. U. Lee, P. Zamani, M. H. Seo, L. F. Nazar, Z. Chen, *Nano Energy* **2014**, *10*, 192.
[37] H. Wang, Y. Yang, Y. Liang, G. Zheng, Y. Li, Y. Cui, H. Dai, *Energy Environ. Sci.* **2012**, *5*, 7931.
[38] W. Bian, Z. Yang, P. Strasser, R. Yang, *J. Power Sources* **2014**, *250*, 196.
[39] T. Y. Ma, S. Dai, M. Jaroniec, S. Z. Qiao, *J. Am. Chem. Soc.* **2014**, *136*, 13925.
[40] B. Zhang, Y. Niu, J. Xu, X. Pan, C.-M. Chen, W. Shi, M.-G. Willinger, R. Schlogl, D. S. Su, *Chem. Commun.* **2016**, *52*, 3927.
[41] X. Ge, A. Sumboja, D. Wuu, T. An, B. Li, F. W. T. Goh, T. S. A. Hor, Y. Zong, Z. Liu, *ACS Catal.* **2015**, *5*, 4643.
[42] R. Frydendal, E. A. Paoli, B. P. Knudsen, B. Wickman, P. Malacrida, I. E. L. Stephens, I. Chorkendorff, *ChemElectroChem* **2014**, *1*, 2075.
[43] Y. Lee, J. Suntivich, K. J. May, E. E. Perry, Y. Shao-Horn, *J. Phys. Chem. Lett.* **2012**, *3*(3), 399.
[44] S. Cherevko, S. Geiger, O. Kasian, N. Kulyk, J.-P. Grote, A. Savan, B. R. Shrestha, S. Merzlikin, B. Breitbach, A. Ludwig, K. J. J. Mayrhofer, *Catal. Today* **2016**, *262*, 170.
[45] R. Kötz, H. J. Lewerenz, S. Stucki, *J. Electrochem. Soc.* **1983**, *130*(4), 825.
[46] M. Ding, Q. He, G. Wang, H.-C. Cheng, Y. Huang, X. Duan, *Nat. Commun.* **2015**, *6*, 7867.
[47] R. L. Doyle, M. E. G. Lyons, *Phys. Chem. Chem. Phys.* **2013**, *15*, 5224.
[48] M. Gong, Y. Li, H. Wang, Y. Liang, J. Z. Wu, J. Zhou, J. Wang, T. Regier, F. Wei, H. Dai, *J. Am. Chem. Soc.* **2013**, *135*, 8452.
[49] H. Mistry, A. S. Varela, S. Kühl, P. Strasser, B. R. Cuenya, *Nat. Rev. Mater.* **2016**, *1*, 16009.
[50] S. F. Hung, Y. Y. Hsu, C. J. Chang, C. S. Hsu, N. T. Suen, T. S. Chan, H. M. Chen, *Adv. Energy Mater.* **2018**, *8*, 1701686.
[51] M. Favaro, C. Valero-Vidal, J. Eichhorn, F. M. Toma, P. N. Ross, Z. Liu, E. J. Crumlin, *J. Mater. Chem. A* **2017**, *5*, 11634.
[52] C. H. Lee, B. Jun, S. U. Lee, *ACS Sustain. Chem. Eng.* **2018**, *6*, 4973.
[53] D. A. García-Osorio, R. Jaimes, J. Vazquez-Arenas, R. H. Lara, J. Alvarez-Ramirez, *J. Electrochem. Soc.* **2017**, *164*, E3321.
[54] T. Shinagawa, A. T. Garcia-Esparza, K. Takanabe, *Sci. Rep.* **2015**, *5*, 13801.
[55] J. Suntivich, K. J. May, H. A. Gasteiger, J. B. Goodenough, Y. Shao-Horn, *Science (New York, N.Y.)* **2011**, *334*, 1383.
[56] A. Damjanovic, A. Dey, J. O. M. Bockris, *Electrochim. Acta* **1966**, *11*, 791.
[57] V. I. Birss, A. Damjanovic, *J. Electrochem. Soc.* **1987**, *134*, 113.
[58] Y. Wu, M. Chen, Y. Han, H. Luo, X. Su, M.-T. Zhang, X. Lin, J. Sun, L. Wang, L. Deng, W. Zhang, R. Cao, *Angew. Chem. Int. Ed.* **2015**, *54*, 4870.
[59] A. Indra, P. W. Menezes, N. R. Sahraie, A. Bergmann, C. Das, M. Tallarida, D. Schmeißer, P. Strasser, M. Driess, *J. Am. Chem. Soc.* **2014**, *136*, 17530.
[60] K. L. Pickrahn, S. W. Park, Y. Gorlin, H. B. R. Lee, T. F. Jaramillo, S. F. Bent, *Adv. Energy Mater.* **2012**, *2*, 1269.
[61] D. A. Corrigan, *J. Electrochem. Soc.* **1987**, *134*(2), 377.
[62] Y. Surendranath, M. W. Kanan, D. G. Nocera, *J. Am. Chem. Soc.* **2010**, *132*, 16501.
[63] A. Singh, L. Spiccia, *Coord. Chem. Rev.* **2013**, *257*, 2607.
[64] N. Ramaswamy, S. Mukerjee, *J. Phys. Chem. C* **2011**, *115*, 18015.
[65] B.-J. Hsieh, M.-C. Tsai, C.-J. Pan, W.-N. Su, J. Rick, H.-L. Chou, J.-F. Lee, B.-J. Hwang, *Electrochim. Acta* **2017**, *224*, 452.
[66] J. K. Nørskov, J. Rossmeisl, A. Logadottir, L. Lindqvist, J. R. Kitchin, T. Bligaard, H. Jónsson, *J. Phys. Chem. B* **2004**, *108*, 17886.
[67] Y. Zhang, F. Ding, C. Deng, S. Zhen, X. Li, Y. Xue, Y.-M. Yan, K. Sun, *Catal. Commun.* **2015**, *67*(Supplement C), 78.
[68] A. Vojvodic, J. K. Nørskov, *Natl. Sci. Rev.* **2015**, *2*(2), 140.
[69] S. Liu, M. G. White, P. Liu, *J. Phys. Chem. C* **2016**, *120*, 15288.
[70] G.-L. Chai, Z. Hou, T. Ikeda, K. Terakura, *J. Phys. Chem. C* **2017**, *121*, 14524.
[71] J. T. Mefford, X. Rong, A. M. Abakumov, W. G. Hardin, S. Dai, A. M. Kolpak, K. P. Johnston, K. J. Stevenson, *Nat. Commun.* **2016**, *7*, 11053.
[72] Y. Jiao, Y. Zheng, M. Jaroniec, S. Z. Qiao, *J. Am. Chem. Soc.* **2014**, *136*, 4394.
[73] L. Dai, Y. Xue, L. Qu, C. Hyun-Jung, J.-B. Baek, *Chem. Rev.* **2015**, *115*, 4823.
[74] W. Reitz, *Mater. Manuf. Process.* **2007**, *22*(6), 789.
[75] J. Greeley, N. M. Markovic, *Energy Environ. Sci.* **2012**, *5*, 9246.
[76] Y. J. Tong, *Chem. Soc. Rev.* **2012**, *41*, 8195.
[77] B. Lim, M. Jiang, P. H. C. Camargo, E. C. Cho, J. Tao, X. Lu, Y. Zhu, Y. Xia, *Science (New York, N.Y.)* **2009**, *324*, 1302.
[78] P. Strasser, S. Kühl, *Nano Energy* **2016**, *29*, 166.
[79] Y.-C. Lin, H.-L. Chou, M.-C. Tsai, B.-J. Hwang, L. S. Sarma, Y.-C. Lee, C.-I. Chen, *J. Phys. Chem. C* **2009**, *113*, 9197.
[80] J. Xu, P. Gao, T. S. Zhao, *Energy Environ. Sci.* **2012**, *5*, 5333.
[81] T. Reier, M. Oezaslan, P. Strasser, *ACS Catal.* **2012**, *2*, 1765.
[82] M. S. Burke, L. J. Enman, A. S. Batchellor, S. Zou, S. W. Boettcher, *Chem. Mater.* **2015**, *27*, 7549.
[83] L. Trotochaud, J. K. Ranney, K. N. Williams, S. W. Boettcher, *J. Am. Chem. Soc.* **2012**, *134*, 17253.
[84] R. D. L. Smith, M. S. Prévot, R. D. Fagan, Z. Zhang, P. A. Sedach, M. K. J. Siu, S. Trudel, C. P. Berlinguette, *Science (New York, N.Y.)* **2013**, *340*(6128), 60.
[85] J. O. Bockris, T. Otagawa, *J. Phys. Chem.* **1983**, *87*, 2960.
[86] P. J. Ferreira, G. J. la O', Y. Shao-Horn, D. Morgan, R. Makharia, S. Kocha, H. A. Gasteiger, *J. Electrochem. Soc.* **2005**, *152*, A2256.
[87] X. Li, A. L. Zhu, W. Qu, H. Wang, R. Hui, L. Zhang, J. Zhang, *Electrochim. Acta* **2010**, *55*, 5891.
[88] F. J. Lai, W. N. Su, L. S. Sarma, D. G. Liu, C. A. Hsieh, J. F. Lee, B. J. Hwang, *Chemistry* **2010**, *16*, 4602.
[89] B. J. Hwang, S. M. S. Kumar, C.-H. Chen, M.-Y. Cheng, D.-G. Liu, J.-F. Lee, *J. Phys. Chem. C* **2007**, *111*, 15267.
[90] V. T. T. Ho, C.-J. Pan, J. Rick, W.-N. Su, B.-J. Hwang, *J. Am. Chem. Soc.* **2011**, *133*, 11716.
[91] T. Ioroi, H. Senoh, S.-I. Yamazaki, Z. Siroma, N. Fujiwara, K. Yasuda, *J. Electrochem. Soc.* **2008**, *155*, B321.
[92] S. Trasatti, *Electrochim. Acta* **1984**, *29*, 1503.

[93] Y. Liang, H. Wang, J. Zhou, Y. Li, J. Wang, T. Regier, H. Dai, *J. Am. Chem. Soc.* **2012**, *134*, 3517.
[94] M. Hamdani, R. N. Singh, P. Chartier, *Int. J. Electrochem. Sci.* **2010**, *5*, 556.
[95] H. Wiame, M.-A. Centeno, S. Picard, P. Bastians, P. Grange, *J. Eur. Ceram. Soc.* **1998**, *18*, 1293.
[96] S. Shimada, M. Johnsson, S. Urbonaite, *Thermochim. Acta* **2004**, *419*(1), 143.
[97] N. Cheng, Q. Liu, J. Tian, X. Sun, Y. He, S. Zhai, A. M. Asiri, *Int. J. Hydrogen Energy* **2015**, *40*, 9866.
[98] J. Liu, L. Jiang, T. Zhang, J. Jin, Y. Lizhi, G. Sun, *Electrochim. Acta* **2016**, *205*, 38.
[99] K.-L. Yan, J.-Q. Chi, J.-Y. Xie, B. Dong, Z.-Z. Liu, W.-K. Gao, J.-H. Lin, Y.-M. Chai, C.-G. Liu, *Renew. Energy* **2018**, *119*, 54.
[100] T. Ling, D.-Y. Yan, Y. Jiao, H. Wang, Y. Zheng, X. Zheng, J. Mao, X.-W. Du, Z. Hu, M. Jaroniec, S.-Z. Qiao, *Nat. Commun.* **2016**, *7*, 12876.
[101] Z. Chen, C. X. Kronawitter, B. E. Koel, *Phys. Chem. Chem. Phys.* **2015**, *17*, 29387.
[102] D. Su, S. Dou, G. Wang, *Sci. Rep.* **2014**, *4*, 5767.
[103] R. Gao, J. Zhu, X. Xiao, Z. Hu, J. Liu, X. Liu, *J. Phys. Chem. C* **2015**, *119*, 4516.
[104] C.-W. Tung, Y.-Y. Hsu, Y.-P. Shen, Y. Zheng, T.-S. Chan, H.-S. Sheu, Y.-C. Cheng, H. M. Chen, *Nat. Commun.* **2015**, *6*, 8106.
[105] P.-C. Li, C.-C. Hu, H. Noda, H. Habazaki, *J. Power Sources* **2015**, *298*, 102.
[106] A. R. Mainar, L. C. Colmenares, O. Leonet, F. Alcaide, J. J. Iruin, S. Weinberger, V. Hacker, E. Iruin, I. Urdanpilleta, J. A. Blazquez, *Electrochim. Acta* **2016**, *217*, 80.
[107] J. P. Brenet, *J. Power Sources* **1979**, *4*(3), 183.
[108] Y. L. Cao, H. X. Yang, X. P. Ai, L. F. Xiao, *J. Electroanal. Chem.* **2003**, *557*, 127.
[109] F. H. B. Lima, M. L. Calegaro, E. A. Ticianelli, *J. Electroanal. Chem.* **2006**, *590*(2), 152.
[110] L. Mao, D. Zhang, T. Sotomura, K. Nakatsu, N. Koshiba, T. Ohsaka, *Electrochim. Acta* **2003**, *48*, 1015.
[111] M. Huynh, D. K. Bediako, D. G. Nocera, *J. Am. Chem. Soc.* **2014**, *136*, 6002.
[112] K. A. Stoerzinger, M. Risch, B. Han, Y. Shao-Horn, *ACS Catal.* **2015**, *5*, 6021.
[113] M. Huynh, C. Shi, S. J. L. Billinge, D. G. Nocera, *J. Am. Chem. Soc.* **2015**, *137*, 14887.
[114] Y. J. Lee, D. H. Kim, T.-G. Kang, Y. Ko, K. Kang, Y. J. Lee, *Chem. Mater.* **2017**, *29*, 10542.
[115] R. Zhou, Y. Zheng, D. Hulicova-Jurcakova, S. Z. Qiao, *J. Mater. Chem. A* **2013**, *1*, 13179.
[116] M. Sun, H. Liu, Y. Liu, J. Qu, J. Li, *Nanoscale* **2015**, *7*, 1250.
[117] J. Wang, K. Wang, F.-B. Wang, X.-H. Xia, *Nat. Commun.* **2014**, *5*, 5285.
[118] J. N. Song, W. Wang, F. X. Wang, Y. M. Kang, S. J. Liu, Z. Q. Lei, *Electrochim. Acta* **2017**, *258*, 1404.
[119] T. Hong, K. Brinkman, C. Xia, *J. Power Sources* **2016**, *329*, 281.
[120] A. Serov, N. I. Andersen, A. J. Roy, I. Matanovic, K. Artyushkova, P. Atanassov, *J. Electrochem. Soc.* **2015**, *162*, F449.
[121] L. Yang, J. Yu, Z. Wei, G. Li, L. Cao, W. Zhou, S. Chen, *Nano Energy* **2017**, *41*, 772.
[122] S. Chandrasekaran, E. J. Kim, J. S. Chung, C. R. Bowen, B. Rajagopalan, V. Adamaki, R. D. K. Misra, S. H. Hur, *J. Mater. Chem. A* **2016**, *4*, 13271.
[123] X. Liu, H. Wang, S. Chen, X. Qi, H. Gao, Y. Hui, Y. Bai, L. Guo, W. Ding, Z. Wei, *J. Energy Chem.* **2014**, *23*(3), 358.
[124] D. Cai, B. Liu, D. Wang, Y. Liu, L. Wang, H. Li, Y. Wang, C. Wang, Q. Li, T. Wang, *Electrochim. Acta* **2014**, *115*, 358.
[125] D. Cai, B. Liu, D. Wang, L. Wang, Y. Liu, H. Li, Y. Wang, Q. Li, T. Wang, *J. Mater. Chem. A* **2014**, *2*, 4954.
[126] V. Nikolova, P. Iliev, K. Petrov, T. Vitanov, E. Zhecheva, R. Stoyanova, I. Valov, D. Stoychev, *J. Power Sources* **2008**, *185*(2), 727.
[127] V. Rashkova, S. Kitova, I. Konstantinov, T. Vitanov, *Electrochim. Acta* **2002**, *47*, 1555.
[128] Q. Liu, J. Jin, J. Zhang, *ACS Appl. Mater. Interfaces* **2013**, *5*, 5002.
[129] T.-H. Ko, K. Devarayan, M.-K. Seo, H.-Y. Kim, B.-S. Kim, *Sci. Rep.* **2016**, *6*, 20313.
[130] Y. Xiao, C. Hu, L. Qu, C. Hu, M. Cao, *Chem Eur J* **2013**, *19*, 14271.
[131] Z.-Q. Liu, Q.-Z. Xu, J.-Y. Wang, N. Li, S.-H. Guo, Y.-Z. Su, H.-J. Wang, J.-H. Zhang, S. Chen, *Int. J. Hydrogen Energy* **2013**, *38*, 6657.
[132] L. Zeng, T. S. Zhao, R. H. Zhang, J. B. Xu, *Electrochem. Commun.* **2018**, *87*, 66.
[133] Z. Cui, S. Wang, Y. Zhang, M. Cao, *J. Power Sources* **2014**, *272*(Supplement C), 808.
[134] L.-K. Wu, W.-Y. Wu, J. Xia, H.-Z. Cao, G.-Y. Hou, Y.-P. Tang, G.-Q. Zheng, *Electrochim. Acta* **2017**, *254*(Supplement C), 337.
[135] B. Cui, H. Lin, J.-B. Li, X. Li, J. Yang, J. Tao, *Adv. Funct. Mater.* **2008**, *18*, 1440.
[136] S.-H. Bae, J.-E. Kim, H. Randriamahazaka, S.-Y. Moon, J.-Y. Park, I.-K. Oh, *Adv. Energy Mater.* **2017**, *7*, 1601492.
[137] R. P. Antony, A. K. Satpati, K. Bhattacharyya, B. N. Jagatap, *Adv. Mater. Interfaces* **2016**, *3*, 1600632.
[138] X. Lv, Y. Zhu, H. Jiang, X. Yang, Y. Liu, Y. Su, J. Huang, Y. Yao, C. Li, *Dalton Trans.* **2015**, *44*, 4148.
[139] N. Ma, Y. Jia, X. Yang, X. She, L. Zhang, Z. Peng, X. Yao, D. Yang, *J. Mater. Chem. A* **2016**, *4*, 6376.
[140] V. Tripkovic, H. A. Hansen, T. Vegge, *ACS Catal.* **2017**, *7*, 8558.
[141] C. N. Brodsky, R. G. Hadt, D. Hayes, B. J. Reinhart, N. Li, L. X. Chen, D. G. Nocera, *Proc. Natl. Acad. Sci. U. S. A.* **2017**, *114*, 3855.
[142] A. Restovic, E. Ríos, S. Barbato, J. Ortiz, J. L. Gautier, *J. Electroanal. Chem.* **2002**, *522*(2), 141.
[143] M. Li, Y. Xiong, X. Liu, X. Bo, Y. Zhang, C. Han, L. Guo, *Nanoscale* **2015**, *7*, 8920.
[144] M. De Koninck, S.-C. Poirier, B. Marsan, *J. Electrochem. Soc.* **2006**, *153*, A2103.
[145] C. Iwakura, A. Honji, H. Tamura, *Electrochim. Acta* **1981**, *26*, 1319.
[146] E. Laouini, M. Hamdani, M. I. S. Pereira, J. Douch, M. H. Mendonça, Y. Berghoute, R. N. Singh, *Int. J. Hydrogen Energy* **2008**, *33*, 4936.
[147] T. Grewe, X. Deng, H. Tüysüz, *Chem. Mater.* **2014**, *26*, 3162.
[148] C. Xiao, X. Lu, C. Zhao, *Chem. Commun.* **2014**, *50*, 10122.
[149] Q. Zhao, Z. Yan, C. Chen, J. Chen, *Chem. Rev.* **2017**, *117*, 10121.

[150] Y. Sheng, M. L. Botero, M. Y. Manuputty, M. Kraft, R. Xu, *ACS Appl. Energy Mater.* **2018**, *1*(2), 655.
[151] B. Zhang, X. Zheng, O. Voznyy, R. Comin, M. Bajdich, M. García-Melchor, L. Han, J. Xu, M. Liu, L. Zheng, F. P. García de Arquer, C. T. Dinh, F. Fan, M. Yuan, E. Yassitepe, N. Chen, T. Regier, P. Liu, Y. Li, P. De Luna, A. Janmohamed, H. L. Xin, H. Yang, A. Vojvodic, E. H. Sargent, *Science (New York, N.Y.)* **2016**, *352*(6283), 333.
[152] C. C. L. McCrory, S. Jung, J. C. Peters, T. F. Jaramillo, *J. Am. Chem. Soc.* **2013**, *135*, 16977.
[153] M. Görlin, P. Chernev, J. Ferreira de Araújo, T. Reier, S. Dresp, B. Paul, R. Krähnert, H. Dau, P. Strasser, *J. Am. Chem. Soc.* **2016**, *138*, 5603.
[154] R. N. Singh, J. P. Singh, B. Lal, M. J. K. Thomas, S. Bera, *Electrochim. Acta* **2006**, *51*, 5515.
[155] S. Anindita A., R. N. Singh, *Int. J. Hydrogen Energy* **2010**, *35*, 3243.
[156] P. Li, R. Ma, Y. Zhou, Y. Chen, Q. Liu, G. Peng, Z. Liang, J. Wang, *RSC Adv.* **2015**, *5*, 73834.
[157] X. Yan, L. Tian, K. Li, S. Atkins, H. Zhao, J. Murowchick, L. Liu, X. Chen, *Adv. Mater. Interfaces* **2016**, *3*, 1600368.
[158] Y. Cheng, S. Dou, M. Saunders, J. Zhang, J. Pan, S. Wang, S. P. Jiang, *J. Mater. Chem. A* **2016**, *4*, 13881.
[159] S.-A. Park, H. Lim, Y.-T. Kim, *ACS Catal.* **2015**, *5*, 3995.
[160] L. Han, S. Dong, E. Wang, *Adv. Mater.* **2016**, *28*, 9266.
[161] L. Dai, M. Liu, Y. Song, J. Liu, F. Wang, *Nano Energy* **2016**, *27*, 185.
[162] V. Maruthapandian, T. Pandiarajan, V. Saraswathy, S. Muralidharan, *RSC Adv.* **2016**, *6*, 48995.
[163] M.-R. Gao, Y.-F. Xu, J. Jiang, Y.-R. Zheng, S.-H. Yu, *J. Am. Chem. Soc.* **2012**, *134*, 2930.
[164] E. Rios, J. L. Gautier, G. Poillerat, P. Chartier, *Electrochim. Acta* **1998**, *44*, 1491.
[165] X. He, F. Yin, Y. Li, H. Wang, J. Chen, Y. Wang, B. Chen, *ACS Appl. Mater. Interfaces* **2016**, *8*, 26740.
[166] C. Li, X. Han, F. Cheng, Y. Hu, C. Chen, J. Chen, *Nat. Commun.* **2015**, *6*, 7345.
[167] R. L. Doyle, M. E. Lyons, *Photoelectrochemical Solar Fuel Production*, Springer, Girona, Spain **2016**, p. 41.
[168] I. C. Man, H. Y. Su, F. Calle-Vallejo, H. A. Hansen, J. I. Martínez, N. G. Inoglu, J. Kitchin, T. F. Jaramillo, J. K. Nørskov, J. Rossmeisl, *ChemCatChem* **2011**, *3*, 1159.
[169] K. S. Novoselov, A. K. Geim, S. V. Morozov, D. Jiang, Y. Zhang, S. V. Dubonos, I. V. Grigorieva, A. A. Firsov, *Science (New York, N.Y.)* **2004**, *306*(5696), 666.
[170] A. Ruban, H. L. Skriver, J. K. Nørskov, *Phys. Rev. B* **1999**, *59*, 15990.
[171] V. Stamenkovic, B. S. Mun, K. J. Mayrhofer, P. N. Ross, N. M. Markovic, J. Rossmeisl, J. Greeley, J. K. Nørskov, *Angew. Chem. Int. Ed.* **2006**, *45*, 2897.
[172] V. Viswanathan, H. A. Hansen, J. Rossmeisl, J. K. Nørskov, *ACS Catal.* **2012**, *2*, 1654.
[173] S. Czioska, J. Wang, S. Zuo, X. Teng, Z. Chen, *ChemCatChem* **2018**, *10*, 1005.
[174] Y. Wang, W. Qiu, E. Song, F. Gu, Z. Zheng, X. Zhao, Y. Zhao, J. Liu, W. Zhang, *Natl. Sci. Rev.* **1753**, *5*(3), 327.
[175] M. V. Makarova, J. Jirkovský, M. Klementová, I. Jirka, K. Macounová, P. Krtil, *Electrochim. Acta* **2008**, *53*, 2656.
[176] X. Long, Z. Wang, S. Xiao, Y. An, S. Yang, *Mater. Today* **2016**, *19*(4), 213.
[177] B. Sels, D. D. Vos, M. Buntinx, F. Pierard, A. Kirsch-De Mesmaeker, P. Jacobs, *Nature* **1999**, *400*(6747), 855.
[178] G. Fan, F. Li, D. G. Evans, X. Duan, *Chem. Soc. Rev.* **2014**, *43*, 7040.
[179] R.-R. Shan, L.-G. Yan, K. Yang, Y.-F. Hao, B. Du, *J. Hazard. Mater.* **2015**, *299*(Supplement C), 42.
[180] F. Ning, M. Shao, C. Zhang, S. Xu, M. Wei, X. Duan, *Nano Energy* **2014**, *7*(Supplement C), 134.
[181] Y. Dou, S. Zhang, T. Pan, S. Xu, A. Zhou, M. Pu, H. Yan, J. Han, M. Wei, D. G. Evans, X. Duan, *Adv. Funct. Mater.* **2015**, *25*, 2243.
[182] M. Gong, Y. Li, H. Wang, Y. Liang, J.Z. Wu, J. Zhou, J. Wang, T. Regier, F. Wei, H. Dai. arXiv preprint arXiv: 2013, 1303.3308.
[183] M. De Marco, R. Menzel, S. M. Bawaked, M. Mokhtar, A. Y. Obaid, S. N. Basahel, M. S. P. Shaffer, *Carbon* **2017**, *123*, 616.
[184] F. Wang, S. Sun, Y. Xu, T. Wang, R. Yu, H. Li, *Sci. Rep.* **2017**, *7*, 4707.
[185] L. Qian, Z. Lu, T. Xu, X. Wu, Y. Tian, Y. Li, Z. Huo, X. Sun, X. Duan, *Adv. Energy Mater.* **2015**, *5*, 1500245.
[186] A. Sumboja, J. Chen, Y. Zong, P. S. Lee, Z. Liu, *Nanoscale* **2017**, *9*(2), 774.
[187] Z. Lu, L. Qian, Y. Tian, Y. Li, X. Sun, X. Duan, *Chem. Commun.* **2016**, *52*(5), 908.
[188] Y. Zhao, B. Li, Q. Wang, W. Gao, C. J. Wang, M. Wei, D. G. Evans, X. Duan, D. O'Hare, *Chem. Sci.* **2014**, *5*(3), 951.
[189] K. Fan, H. Chen, Y. Ji, H. Huang, P. M. Claesson, Q. Daniel, B. Philippe, H. Rensmo, F. Li, Y. Luo, L. Sun, *Nat. Commun.* **2016**, *7*, 11981.
[190] K. B. Ibrahim, W.-N. Su, M.-C. Tsai, S. A. Chala, A. W. Kahsay, M.-H. Yeh, H.-M. Chen, A. D. Duma, H. Dai, B.-J. Hwang, *Nano Energy* **2018**, *47*, 309.
[191] D. Zhou, Z. Cai, X. Lei, W. Tian, Y. Bi, Y. Jia, N. Han, T. Gao, Q. Zhang, Y. Kuang, J. Pan, X. Sun, X. Duan, *Adv. Energy Mater.* **2018**, *8*, 1701905.
[192] M. F. P. Duarte, I. M. Rocha, J. L. Figueiredo, C. Freire, M. F. R. Pereira, *Catal. Today* **2018**, *301*, 17.
[193] K. Oda, T. Yoshio, K. Oda, *J. Mater. Sci.* **1987**, *22*, 2729.
[194] L. Yang, M. Gao, B. Dai, X. Guo, Z. Liu, B. Peng, *Electrochim. Acta* **2016**, *191*(Supplement C), 813.
[195] B. M. Jović, U. Č. Lačnjevac, V. D. Jović, N. V. Krstajić, *J. Electroanal. Chem.* **2015**, *754*(Supplement C), 100.
[196] B. Dong, X. Zhao, G.-Q. Han, X. Li, X. Shang, Y.-R. Liu, W.-H. Hu, Y.-M. Chai, H. Zhao, C.-G. Liu, *J. Mater. Chem. A* **2016**, *4*, 13499.
[197] X.-Y. Yu, Y. Feng, B. Guan, X. W. Lou, U. Paik, *Energy Environ. Sci.* **2016**, *9*, 1246.
[198] C. Tang, A. M. Asiri, X. Sun, *Chem. Commun.* **2016**, *52*, 4529.
[199] Y.-J. Tang, C.-H. Liu, W. Huang, X.-L. Wang, L.-Z. Dong, S.-L. Li, Y.-Q. Lan, *ACS Appl. Mater. Interfaces* **2017**, *9*, 16977.
[200] Y. Su, Y. Zhu, H. Jiang, J. Shen, X. Yang, W. Zou, J. Chen, C. Li, *Nanoscale* **2014**, *6*, 15080.
[201] H. Lin, N. Liu, Z. Shi, Y. Guo, Y. Tang, Q. Gao, Cobalt-Doping in Molybdenum-Carbide Nanowires Toward Efficient Electrocatalytic Hydrogen Evolution. *Adv. Funct. Mater.* **2016**, *26*, 5590–5598.

[202] K. Fominykh, P. Chernev, I. Zaharieva, J. Sicklinger, G. Stefanic, M. Döblinger, A. Müller, A. Pokharel, S. Böcklein, C. Scheu, T. Bein, D. Fattakhova-Rohlfing, *ACS Nano* **2015**, *9*, 5180.
[203] W. Zhou, J.-L. Zheng, Y.-H. Yue, L. Guo, *Nano Energy* **2015**, *11*, 428.
[204] Y. Feng, T. He, N. Alonso-Vante, *Chem. Mater.* **2008**, *20* (1), 26.
[205] X. Shang, X. Li, W.-H. Hu, B. Dong, Y.-R. Liu, G.-Q. Han, Y.-M. Chai, Y.-Q. Liu, C.-G. Liu, *Appl. Surf. Sci.* **2016**, *378*(Supplement C), 15.
[206] M. Liao, G. Zeng, T. Luo, Z. Jin, Y. Wang, X. Kou, D. Xiao, *Electrochim. Acta* **2016**, *194*(Supplement C), 59.
[207] D. Kong, H. Wang, Z. Lu, Y. Cui, *J. Am. Chem. Soc.* **2014**, *136*, 4897.
[208] D.-Y. Wang, M. Gong, H.-L. Chou, C.-J. Pan, H.-A. Chen, Y. Wu, M.-C. Lin, M. Guan, J. Yang, C.-W. Chen, Y.-L. Wang, B.-J. Hwang, C.-C. Chen, H. Dai, *J. Am. Chem. Soc.* **2015**, *137*, 1587.
[209] J.-Q. Chi, X. Shang, W.-K. Gao, B. Dong, K.-L. Yan, X. Li, Y.-R. Liu, Y.-M. Chai, C.-G. Liu, *Int. J. Hydrogen Energy* **2017**, *42*, 15189.
[210] L.-A. Stern, L. Feng, F. Song, X. Hu, *Energy Environ. Sci.* **2015**, *8*, 2347.
[211] J.-Q. Chi, X. Shang, F. Liang, B. Dong, X. Li, Y.-R. Liu, K.-L. Yan, W.-K. Gao, Y.-M. Chai, C.-G. Liu, *Appl. Surf. Sci.* **2017**, *401*(Supplement C), 17.
[212] M. Shen, C. Ruan, Y. Chen, C. Jiang, K. Ai, L. Lu, *ACS Appl. Mater. Interfaces* **2015**, *7*, 1207.
[213] X. Cui, P. Ren, D. Deng, J. Deng, X. Bao, *Energy Environ. Sci.* **2016**, *9*(1), 123.
[214] J. Zhu, M. Xiao, Y. Zhang, Z. Jin, Z. Peng, C. Liu, S. Chen, J. Ge, W. Xing, *ACS Catal.* **2016**, *6*, 6335.
[215] H. Jiang, Y. Yao, Y. Zhu, Y. Liu, Y. Su, X. Yang, C. Li, *ACS Appl. Mater. Interfaces* **2015**, *7*, 21511.
[216] Y. Liu, H. Jiang, Y. Zhu, X. Yang, C. Li, *J. Mater. Chem. A* **2016**, *4*, 1694.
[217] Y. Zhao, K. Kamiya, K. Hashimoto, S. Nakanishi, *J. Phys. Chem. C* **2015**, *119*, 2583.
[218] C. Jin, F. Lu, X. Cao, Z. Yang, R. Yang, *J. Mater. Chem. A* **2013**, *1*, 12170.
[219] T. N. Lambert, J. A. Vigil, S. E. White, D. J. Davis, S. J. Limmer, P. D. Burton, E. N. Coker, T. E. Beechem, M. T. Brumbach, *Chem. Commun.* **2015**, *51*, 9511.
[220] P. W. Menezes, A. Indra, N. R. Sahraie, A. Bergmann, P. Strasser, M. Driess, *ChemSusChem* **2015**, *8*(1), 164.
[221] W. Yan, Z. Yang, W. Bian, R. Yang, *Carbon* **2015**, *92*, 74.
[222] A. Zhao, J. Masa, W. Xia, A. Maljusch, M.-G. Willinger, G. Clavel, K. Xie, R. Schlögl, W. Schuhmann, M. Muhler, *J. Am. Chem. Soc.* **2014**, *136*, 7551.
[223] X. He, F. Yin, S. Yuan, N. Liu, X. Huang, *ChemElectroChem* **2016**, *3*, 1107.
[224] J. Wang, Z. Wu, L. Han, R. Lin, H. L. Xin, D. Wang, *ChemCatChem* **2016**, *8*(4), 736.
[225] Z. Luo, E. Irtem, M. Ibáñez, R. Nafria, S. Martí-Sánchez, A. Genç, M. de la Mata, Y. Liu, D. Cadavid, J. Llorca, J. Arbiol, T. Andreu, J. R. Morante, A. Cabot, *ACS Appl. Mater. Interfaces* **2016**, *8*, 17435.
[226] P. Ganesan, M. Prabu, J. Sanetuntikul, S. Shanmugam, *ACS Catal.* **2015**, *5*, 3625.
[227] Y. Liu, H. Cheng, M. Lyu, S. Fan, Q. Liu, W. Zhang, Y. Zhi, C. Wang, C. Xiao, S. Wei, B. Ye, Y. Xie, *J. Am. Chem. Soc.* **2014**, *136*, 15670.
[228] X. Xu, F. Song, X. Hu, *Nat. Commun.* **2016**, *7*, 12324.
[229] S. Dresp, F. Luo, R. Schmack, S. Kuhl, M. Gliech, P. Strasser, *Energy Environ. Sci.* **2016**, *9*, 2020.
[230] J. Wu, Z. Ren, S. Du, L. Kong, B. Liu, W. Xi, J. Zhu, H. Fu, *Nano Res.* **2016**, *9*(3), 713.
[231] B. Lu, D. Cao, P. Wang, G. Wang, Y. Gao, *Int. J. Hydrogen Energy* **2011**, *36*(1), 72.
[232] X. Zou, J. Su, R. Silva, A. Goswami, B. R. Sathe, T. Asefa, *Chem. Commun.* **2013**, *49*, 7522.
[233] P. Wu, X.-P. Yan, *Chem. Soc. Rev.* **2013**, *42*, 5489.
[234] R. Buonsanti, D. J. Milliron, *Chem. Mater.* **2013**, *25*, 1305.
[235] Y. Shen, J. Farquhar, H. Zhang, A. Masterson, T. Zhang, B. A. Wing, *Nat. Commun.* **2011**, *2*, 210.
[236] K. Fan, Y. Ji, H. Zou, J. Zhang, B. Zhu, H. Chen, Q. Daniel, Y. Luo, J. Yu, L. Sun, *Angew. Chem. Int. Ed.* **2017**, *56*, 3289.
[237] L. Trotochaud, S. L. Young, J. K. Ranney, S. W. Boettcher, *J. Am. Chem. Soc.* **2014**, *136*, 6744.
[238] J. W. Schultze Ed., *Ber. Bunsen. Phys. Chem.* **1981**, *85*(5), 461.
[239] M. W. Louie, A. T. Bell, *J. Am. Chem. Soc.* **2013**, *135*, 12329.
[240] D. A. Corrigan, R. S. Conell, C. A. Fierro, D. A. Scherson, *J. Phys. Chem.* **1987**, *91*, 5009.
[241] D. Friebel, M. W. Louie, M. Bajdich, K. E. Sanwald, Y. Cai, A. M. Wise, M.-J. Cheng, D. Sokaras, T.-C. Weng, R. Alonso-Mori, R. C. Davis, J. R. Bargar, J. K. Nørskov, A. Nilsson, A. T. Bell, *J. Am. Chem. Soc.* **2015**, *137*, 1305.
[242] H. Shin, H. Xiao, W. A. Goddard, *J. Am. Chem. Soc.* **2018**, *140*, 6745.
[243] Y. Pi, Q. Shao, P. Wang, F. Lv, S. Guo, J. Guo, X. Huang, *Angew. Chem. Int. Ed.* **2017**, *56*, 4502.
[244] Y. Sun, S. Gao, F. Lei, J. Liu, L. Liang, Y. Xie, *Chem. Sci.* **2014**, *5*, 3976.
[245] R. D. L. Smith, C. Pasquini, S. Loos, P. Chernev, K. Klingan, P. Kubella, M. R. Mohammadi, D. Gonzalez-Flores, H. Dau, *Nat. Commun.* **2017**, *8*, 2022.
[246] Y. Wang, Y. Zhang, Z. Liu, C. Xie, S. Feng, D. Liu, M. Shao, S. Wang, *Angew. Chem.* **2017**, *129*, 5961.
[247] Y. Sun, S. Gao, F. Lei, Y. Xie, *Chem. Soc. Rev.* **2015**, *44* (3), 623.
[248] M. Casas-Cabanas, G. Binotto, D. Larcher, A. Lecup, V. Giordani, J. M. Tarascon, *Chem. Mater.* **2009**, *21*, 1939.
[249] R. Zhang, Y.-C. Zhang, L. Pan, G.-Q. Shen, N. Mahmood, Y.-H. Ma, Y. Shi, W. Jia, L. Wang, X. Zhang, W. Xu, J.-J. Zou, *ACS Catal.* **2018**, *8*, 3803.
[250] C. A. Downes, S. C. Marinescu, *ChemSusChem* **2017**, *10*, 4374.
[251] C. Zhu, C. Li, M. Zheng, J.-J. Delaunay, *ACS Appl. Mater. Interfaces* **2015**, *7*, 22355.
[252] Q. Gan, H. He, K. Zhao, Z. He, S. Liu, S. Yang, *ACS Appl. Mater. Interfaces* **2018**, *10*, 7031.
[253] C. Shi, J. Liu, W. Li, X. Jiang, H. Yang, Q. Liu, *Ceram. Int.* **2018**, *44*, 22235.
[254] L. Xu, Q. Jiang, Z. Xiao, X. Li, J. Huo, S. Wang, L. Dai, *Angew. Chem.* **2016**, *128*, 5363.
[255] P. Deák, B. Aradi, T. Frauenheim, *Phys. Rev. B* **2012**, *86*, 195206.
[256] H.-Y. Wang, S.-F. Hung, H.-Y. Chen, T.-S. Chan, H. M. Chen, B. Liu, *J. Am. Chem. Soc.* **2016**, *138*(1), 36.

[257] X. Jiang, Y. Zhang, J. Jiang, Y. Rong, Y. Wang, Y. Wu, C. Pan, *J. Phys. Chem. C* **2012**, *116*, 22619.
[258] Y. Sun, Q. Liu, S. Gao, H. Cheng, F. Lei, Z. Sun, Y. Jiang, H. Su, S. Wei, Y. Xie, *Nat. Commun.* **2013**, *4*, 2899.
[259] V. T. Thanh Ho, K. C. Pillai, H.-L. Chou, C.-J. Pan, J. Rick, W.-N. Su, B.-J. Hwang, J.-F. Lee, H.-S. Sheu, W.-T. Chuang, *Energy Environ. Sci.* **2011**, *4*, 4194.
[260] C.-J. Pan, M.-C. Tsai, W.-N. Su, J. Rick, N. G. Akalework, A. K. Agegnehu, S.-Y. Cheng, B.-J. Hwang, *J. Taiwan Inst. Chem. Eng.* **2017**, *74*, 154.
[261] B.-J. Hwang, L. S. Sarma, J.-M. Chen, C.-H. Chen, S.-C. Shih, G.-R. Wang, D.-G. Liu, J.-F. Lee, M.-T. Tang, *J. Am. Chem. Soc.* **2005**, *127*, 11140.
[262] J. J. Zhang, H. H. Wang, T. J. Zhao, K. X. Zhang, X. Wei, Z. D. Jiang, S. I. Hirano, X. H. Li, J. S. Chen, *ChemSusChem* **2017**, *10*, 2875.
[263] L. Z. Liu, T. H. Li, X. L. Wu, J. C. Shen, P. K. Chu, *J. Raman Spectrosc.* **2012**, *43*, 1423.
[264] J. Hong, Z. Hu, M. Probert, K. Li, D. Lv, X. Yang, L. Gu, N. Mao, Q. Feng, L. Xie, J. Zhang, D. Wu, Z. Zhang, C. Jin, W. Ji, X. Zhang, J. Yuan, Z. Zhang, *Nat. Commun.* **2015**, *6*, 6293.
[265] R. Liu, Y. Wang, D. Liu, Y. Zou, S. Wang, *Adv. Mater.* **2017**, *29*(30), 1701546.
[266] C. Julien, M. Massot, S. Rangan, M. Lemal, D. Guyomard, *J. Raman Spectrosc.* **2002**, *33*(4), 223.
[267] J. Bao, X. Zhang, B. Fan, J. Zhang, M. Zhou, W. Yang, X. Hu, H. Wang, B. Pan, Y. Xie, *Angew. Chem. Int. Ed.* **2015**, *54*, 7399.
[268] C. J. Kevane, *Phys. Rev.* **1964**, *133*, A1431.
[269] J. Song, Z.-F. Huang, L. Pan, J.-J. Zou, X. Zhang, L. Wang, *ACS Catal.* **2015**, *5*, 6594.
[270] J. Paier, C. Penschke, J. Sauer, *Chem. Rev.* **2013**, *113*, 3949.
[271] J. Nowotny, M. A. Alim, T. Bak, M. A. Idris, M. Ionescu, K. Prince, M. Z. Sahdan, K. Sopian, M. A. Mat Teridi, W. Sigmund, *Chem. Soc. Rev.* **2015**, *44*, 8424.
[272] Y. Guo, Y. Tong, P. Chen, K. Xu, J. Zhao, Y. Lin, W. Chu, Z. Peng, C. Wu, Y. Xie, *Adv. Mater.* **2015**, *27*, 5989.
[273] U. Aschauer, J. Chen, A. Selloni, *Phys. Chem. Chem. Phys.* **2010**, *12*, 12956.
[274] J. Lee, D. C. Sorescu, X. Deng, *J. Am. Chem. Soc.* **2011**, *133*, 10066.
[275] L. Liu, C. Zhao, Y. Li, *J. Phys. Chem. C* **2012**, *116*, 7904.
[276] H. Li, J. Shang, J. Shi, K. Zhao, L. Zhang, *Nanoscale* **2016**, *8*, 1986.
[277] L. Zhuang, L. Ge, Y. Yang, M. Li, Y. Jia, X. Yao, Z. Zhu, *Adv. Mater.* **2017**, *29*, 1606793.
[278] M.-C. Tsai, T.-T. Nguyen, N. G. Akalework, C.-J. Pan, J. Rick, Y.-F. Liao, W.-N. Su, B.-J. Hwang, *ACS Catal.* **2016**, *6*, 6551.
[279] Y. Wang, T. Zhou, K. Jiang, P. Da, Z. Peng, J. Tang, B. Kong, W. B. Cai, Z. Yang, G. Zheng, *Adv. Energy Mater.* **2014**, *4*(16), 1400696.
[280] Z. Chen, D. Higgins, A. Yu, L. Zhang, J. Zhang, *Energy Environ. Sci.* **2011**, *4*, 3167.
[281] W. Zhu, L. Liu, Z. Yue, W. Zhang, X. Yue, J. Wang, S. Yu, L. Wang, J. Wang, *ACS Appl. Mater. Interfaces* **2017**, *9*, 19807.
[282] J. Zhang, J. Liu, L. Xi, Y. Yu, N. Chen, S. Sun, W. Wang, K. M. Lange, B. Zhang, *J. Am. Chem. Soc.* **2018**, *140*, 3876.
[283] S. A. Chala, M.-C. Tsai, W.-N. Su, K. B. Ibrahim, A. D. Duma, M.-H. Yeh, C.-Y. Wen, C.-H. Yu, T.-S. Chan, H. Dai, B.-J. Hwang, *ACS Catal.* **2019**, *9*(1), 117.
[284] A. D. Duma, Y. C. Wu, W. N. Su, C. J. Pan, M. C. Tsai, H. M. Chen, J. F. Lee, H. S. Sheu, V. T. T. Ho, B. J. Hwang, *ChemCatChem* **2018**, *10*, 1155.
[285] Z.-Y. Yuan, X.-B. Zhang, B.-L. Su, *Appl. Phys. A* **2004**, *78*, 1063.
[286] J. E. Graves, D. Pletcher, R. L. Clarke, F. C. Walsh, *J. Appl. Electrochem.* **1991**, *21*(10), 848.
[287] S. Sathasivam, D. S. Bhachu, Y. Lu, N. Chadwick, S. A. Althabaiti, A. O. Alyoubi, S. N. Basahel, C. J. Carmalt, I. P. Parkin, *Chem. Vap. Depos.* **2015**, *5*, 10952.
[288] R. E. Cochran, J.-J. Shyue, N. P. Padture, *Acta Mater.* **2007**, *55*, 3007.
[289] X. Wang, H. Wang, Y. Zhou, Y. Liu, B. Li, X. Zhou, H. Shen, *Sci. Rep.* **2015**, *5*, 8129.
[290] M. S. Saha, M. N. Banis, Y. Zhang, R. Li, X. Sun, M. Cai, F. T. Wagner, *J. Power Sources* **2009**, *192*(2), 330.
[291] E. Kang, S. An, S. Yoon, J. K. Kim, J. Lee, *J. Mater. Chem.* **2010**, *20*, 7416.
[292] K. Miecznikowski, *Arab. J. Chem.* **2017**.
[293] K. Liu, X. Huang, H. Wang, F. Li, Y. Tang, J. Li, M. Shao, *ACS Appl. Mater. Interfaces* **2016**, *8*, 34422.
[294] H. Li, S. Wu, C.-Y. Wu, J. Wang, L. Li, K. Shih, *Environ. Sci. Technol.* **2015**, *49*, 7373.
[295] P. Prins, K. Senthilkumar, F. C. Grozema, P. Jonkheijm, A. P. H. J. Schenning, E. W. Meijer, L. D. A. Siebbeles, *J. Phys. Chem. B* **2005**, *109*, 18267.
[296] Y. Zhu, S. Liu, C. Jin, S. Bie, R. Yang, J. Wu, *J. Mater. Chem. A* **2015**, *3*, 13563.
[297] J.-X. Feng, S.-H. Ye, H. Xu, Y.-X. Tong, G.-R. Li, *Adv. Mater.* **2016**, *28*, 4698.
[298] H. Xu, X. Hou, *Int. J. Hydrogen Energy* **2007**, *32*, 4397.
[299] Y.-R. Zheng, M.-R. Gao, Q. Gao, H.-H. Li, J. Xu, Z.-Y. Wu, S.-H. Yu, *Small* **2015**, *11*(2), 182.
[300] X. Long, H. Lin, D. Zhou, Y. An, S. Yang, *ACS Energy Lett.* **2018**, *3*(2), 290.
[301] A. Mirzaei, K. Janghorban, B. Hashemi, G. Neri, *J. Nanopart. Res.* **2015**, *17*(9), 371.
[302] Y. Cheng, S. Dou, J.-P. Veder, S. Wang, M. Saunders, S. P. Jiang, *ACS Appl. Mater. Interfaces* **2017**, *9*, 8121.
[303] K. Zhu, M. Li, X. Li, X. Zhu, J. Wang, W. Yang, *Chem. Commun.* **2016**, *52*, 11803.
[304] P. Sabatier, *Ber. Dtsch. Chem. Ges.* **1911**, *44*, 1984.
[305] C. N. He, N. Q. Zhao, *J. Mater. Chem.* **2012**, *22*, 1297.
[306] J. Kim, Y. Lee, S. Sun, *J. Am. Chem. Soc.* **2010**, *132*, 4996.
[307] W. Song, Z. Ren, S.-Y. Chen, Y. Meng, S. Biswas, P. Nandi, H. A. Elsen, P.-X. Gao, S. L. Suib, *ACS Appl. Mater. Interfaces* **2016**, *8*, 20802.
[308] Y. Meng, W. Song, H. Huang, Z. Ren, S.-Y. Chen, S. L. Suib, *J. Am. Chem. Soc.* **2014**, *136*, 11452.
[309] B. D. Chithrani, A. A. Ghazani, W. C. W. Chan, *Nano Lett.* **2006**, *6*(4), 662.
[310] T. Maiyalagan, K. R. Chemelewski, A. Manthiram, *ACS Catal.* **2014**, *4*(2), 421.

[311] S. J. Sitler, K. S. Raja, Z. Karmiol, D. Chidambaram, *J. Phys. D: Appl. Phys.* **2017**, *50*(3), 035502.
[312] W. P. S. L. Wijesinghe, M. M. M. G. P. G. Mantilaka, E. V. A. Premalal, H. M. T. U. Herath, S. Mahalingam, M. Edirisinghe, R. P. V. J. Rajapakse, R. M. G. Rajapakse, *Mater. Sci. Eng. C* **2014**, *42*, 83.
[313] J. Hou, Y. Sun, Y. Wu, S. Cao, L. Sun, *Adv. Funct. Mater.* **2018**, *28*, 1704447.
[314] B. Priyanka, E. N. Nasybulin, M. H. Engelhard, L. Kovarik, M. E. Bowden, X. S. Li, D. J. Gaspar, W. Xu, J.-. G. Zhang, *Adv. Funct. Mater.* **2014**, *24*, 7510.
[315] C. H. Chen, C. J. Pan, W. N. Su, L. S. Sarma, C. C. A. Andra, H. S. Sheu, D. G. Liu, J. F. Lee, B. J. Hwang, *ChemNanoMat* **2016**, *2*(2), 117.
[316] N.-T. Suen, S.-F. Hung, Q. Quan, N. Zhang, Y.-J. Xu, H. M. Chen, *Chem. Soc. Rev.* **2017**, *46*(2), 337.
[317] H. G. Yang, C. H. Sun, S. Z. Qiao, J. Zou, G. Liu, S. C. Smith, H. M. Cheng, G. Q. Lu, *Nature* **2008**, *453*, 638.
[318] L. Liu, Z. Jiang, L. Fang, H. Xu, H. Zhang, X. Gu, Y. Wang, *ACS Appl. Mater. Interfaces* **2017**, *9*, 27736.
[319] Z. P. Wei, M. Arredondo, H. Y. Peng, Z. Zhang, D. L. Guo, G. Z. Xing, Y. F. Li, L. M. Wong, S. J. Wang, N. Valanoor, T. Wu, *ACS Nano* **2010**, *4*, 4785.
[320] M. V. Kovalenko, L. Manna, A. Cabot, Z. Hens, D. V. Talapin, C. R. Kagan, V. I. Klimov, A. L. Rogach, P. Reiss, D. J. Milliron, P. Guyot-Sionnnest, G. Konstantatos, W. J. Parak, T. Hyeon, B. A. Korgel, C. B. Murray, W. Heiss, *ACS Nano* **2015**, *9*, 1012.
[321] F. Calle-Vallejo, D. Loffreda, T. M. KoperMarc, P. Sautet, *Nat. Chem.* **2015**, *7*(5), 403.
[322] X.-M. Zeng, R. Huang, G.-F. Shao, Y.-H. Wen, S.-G. Sun, *J. Mater. Chem. A* **2014**, *2*, 11480.
[323] J. Pan, G. Liu, G. Q. Lu, H.-M. Cheng, *Angew. Chem. Int. Ed.* **2011**, *50*, 2133.
[324] F. Cheng, Y. Su, J. Liang, Z. Tao, J. Chen, *Chem. Mater.* **2010**, *22*(3), 898.

How to cite this article: Ibrahim KB, Tsai M-C, Chala SA, et al. A review of transition metal-based bifunctional oxygen electrocatalysts. *J Chin Chem Soc*. 2019;1–37. https://doi.org/10.1002/jccs.201900001